UNIVERSIDADE DE SÃO PAULO
INSTITUTO DE FÍSICA DE SÃO CARLOS

LUANA CORSI ANTONIO

Polysaccharides as stabilizing and coating agents of polymeric nanocarriers for chemotherapeutics delivery

São Carlos
2023

LUANA CORSI ANTONIO

Polysaccharides as stabilizing and coating agents of polymeric nanocarriers for chemotherapeutics delivery

Dissertation presented to the Graduate Program in Physics at the Instituto de Física de São Carlos, Universidade de São Paulo to obtain the degree of Master of Science.

Concentration area: Applied Physics
Option: Biomolecular Physics
Advisor: Prof. Dr. Valtencir Zucolotto

Corrected Version

(Original version available on the Program Unit)

São Carlos
2023

Corsi Antonio, Luana
Polysaccharides as stabilizing and coating agents of polymeric nanocarriers for chemotherapeutics delivery / Luana Corsi Antonio; advisor Valtencir Zucolotto - corrected version -- São Carlos 2023.
112 p.

Dissertation (Master's degree - Graduate Program in Biomolecular Physics) -- Instituto de Física de São Carlos, Universidade de São Paulo - Brasil , 2023.

1. Nanomedicine. 2. Polymeric nanocarriers. 3. Polysaccharides. 4. Controlled drug delivery. 5. Cancer. I. Zucolotto, Valtencir, advisor. II. Title.

ACKNOWLEDGEMENTS

To my parents, Ronaldo and Márcia, I would like to thank you for encouraging me to study, for always providing me the best, and, most importantly, for all the love that you gave me. To my aunt, Adriana, and cousin, Ana Julia, I would like to thank for all the support, coffees, laughs and fun moments. To my boyfriend, Cauê, I would like to thank for being my life partner and for sharing with me all the moments. Thanks to all of you for putting up with my complaints when experiments went wrong. To all the family that I have not mentioned here, thank you for the love you gave me. You all were pivotal to my trajectory. I love you!

Thanks to all my college friends and "Pracodema" friends. You guys made my masters much more fun!

Special Thanks to Laís. Without your guidance I would not have completed my master's degree. Thank you for everything you taught me, since my first steps in the lab until writing this dissertation. Also, thank you for all our meetings and scientific discussions, they motivated and guided me to continue my research even when everything seemed to go wrong. You are a brilliant scientist and a great advisor!

I would like to thank my supervisor Zucolotto for all the thrust and freedom you gave through those many years.

Also, I would like to thank all the members of the Nanomedicine and Nanotoxicology Group (GNano).

I thank Fundação de Amparo a Pesquisa do Estado de São Paulo (FAPESP) for the fellowship during the master’s degree (2020/02386-7).

I would like to thank very much the University of São Paulo for guaranteeing all students an excellent education and for encouraging science.

ABSTRACT

ANTONIO, L. C. **Polysaccharides as stabilizing and coating agents of polymeric nanocarriers for chemotherapeutics delivery**. 2023. 112 p. Dissertation (Master in Science) - Instituto de Física de São Carlos, Universidade de São Paulo, São Carlos, 2023.

Polymeric nanocarriers (NCs) are efficient vehicles to delivery therapeutics to cancer, preventing drug unspecific biodistribution and increasing the drug amounts delivered to the tumor tissues. However, the NCs interaction with biological systems still lack a comprehensive assessment. In this dissertation we investigate how does polysaccharides affect the interactions between nanomaterials and cancer cells, as well as cancer-associated cells. In **Chapter 1** we studied the interaction of poly (lactic acid-co-glycolic acid) (PLGA) NCs prepared using Dex as stabilizing and caping agents with myocardial cells (H9C2), breast adenocarcinoma cells (MCF-7) and macrophages (RAW 264.7). By emulsion diffusion method, doxorubicin-loaded NCs were prepared with no Dex (PLGA-DOX), 1 %(w/v) (Dex1/PLGA-DOX) and 5 %(w/v) (Dex5/PLGA-DOX) NCs. Our results highlight that control over the amount of Dex added to the formulation of PLGA NCs impacts their interaction with non-phagocytic cells due to the decrease of protein adsorption (protein corona formation) with the increase of dextran amount. For doxorubicin-loaded formulations, the highest amount of Dex (5 %(w/v)) led to oxidative membrane damage and increase of early apoptotic events, suggesting that it may contribute to the long-term adverse effects more substantially than formulations with lower Dex concentrations or without Dex. In **Chapter 2** we explored the binding between hyaluronic acid (HA) and CD44, a receptor that mediates cell-cell and cell-matrix interactions, to transport a nanotherapeutic to the leukemic cells. To assess the macrophages' ability to effectively deliver NCs via CD44-targeting to acute myeloid leukemia (AML) cells, we studied their interaction with the NCs in co-cultures of macrophages (RAW 264.7) and AML cells (C1498). Three configurations of PLGA-based NCs were evaluated, namely: i) NCs modified with polyethylene glycol (PEG), to evade the immune system; ii) NCs modified with HA, CD44-HA binding and iii) non-modified NCs (carboxyl moiety). Macrophages previously exposed to NCs were co-cultured with AML cells and the uptake and delivery of NCs to AML cells were analyzed by flow cytometry. As a consequence of CD44 increased intensity, (PLGA)-PEG-HA NCs adhered to the membrane of pro-leukemic macrophages. Also, (PLGA)-PEG-HA NCs were delivered to AML blasts by cell-to-cell interaction, accumulating into the leukemic cell and increasing cancer cells' death. Overall, our results suggest that macrophage-based deliver

of (PLGA)PEG-HA NCs loaded with ATO is a promising platform to treat AML as (PLGA)PEG-HA NCs can improve targetability by adhering to AML-related macrophages and reduce AML blasts viability *in vitro*.
Keywords: Nanomedicine. Polymeric nanocarriers. Polysaccharides. Controlled drug delivery. Cancer.

RESUMO

ANTONIO, L. C. **Polissacarídeos como agentes estabilizantes e de revestimento em nanocarreadores poliméricos para entrega de quimioterápicos.** 2023. 112 p. Dissertação (Mestrado em Ciências) - Instituto de Física de São Carlos, Universidade de São Paulo, São Carlos, 2023.

Os nanocarreadores (NCs) poliméricos são veículos eficientes para a entrega de agentes terapêuticos ao câncer, evitando uma biodistribuição inespecífica e aumentando a quantidade de fármaco entregue a tecidos tumorais. No entanto, a interação dos NCs com sistemas biológicos ainda precisa ser avaliada de forma abrangente. Esta dissertação estuda o efeito de polissacarídeos na interação entre nanomateriais e células de câncer, assim como células associadas ao câncer. No **Capítulo 1**, estudamos a interação de NCs de poli (ácido láctico-co-ácido glicólico) (PLGA) preparados usando dextran (Dex) como agente estabilizante com células de miocárdio (H9C2), células de adenocarcinoma mamário (MCF-7) e macrófagos (RAW 264.7). NCs carregados com doxorrubicina (DOX) foram preparados sem Dex, com 1% (p/v) e 5% (p/v) de Dex. Nossos resultados destacam que o controle sobre a quantidade de Dex adicionada à formulação dos NCs impacta sua interação com células não fagocíticas devido à diminuição da adsorção de proteínas (formação de corona proteica) com o aumento da quantidade de Dex. Para formulações carregadas com DOX, a maior quantidade de Dex (5% (p/v)) levou a danos oxidativos na membrana e aumento de eventos apoptóticos precoces, sugerindo que pode contribuir para os efeitos adversos a longo prazo mais substancialmente do que formulações com menor concentrações de Dex ou sem Dex. No **Capítulo 2** exploramos a ligação entre o ácido hialurônico (AH) e o CD44, um receptor que medeia a interação célula-célula e célula-matriz, para transportar um nanoterapêutico a células leucêmicas. Para avaliar a capacidade dos macrófagos de efetivamente entregar NCs para células de leucemia mieloide aguda (LMA), estudamos a interação dos NCs em co-culturas de macrófagos (RAW 264.7) e células de LMA (C1498). Foram avaliadas três configurações de NCs de PLGA: i) NCs modificadas com polietileno glicol (PEG), para evadir o sistema imune; ii) NCs modificados com AH, para interação CD44-AH e iii) NCs não modificados (terminação carboxil). Macrófagos previamente expostos a NCs foram co-cultivados com células de LMA e a absorção e entrega de NCs para células AML foram analisadas por citometria de fluxo. Como consequência da superexpressão de CD44, NCs de (PLGA)-PEG-HA aderiram à membrana de

macrófagos pró-leucêmicos. Também, NCs de (PLGA)-PEG-HA foram entregues aos blastos de LMA por interação célula a célula, acumulando-se nas células leucêmicas e aumentando sua morte. No geral, nossos resultados sugerem que a entrega baseada em macrófagos é uma estratégia promissora para tratar LMA, pois pode melhorar a capacidade de direcionamento dos NCs modificados com AH e reduzir a viabilidade de blastos de LMA *in vitro*.

Palavras-chave: Nanomedicina. Nanocarreadores poliméricos. Polissacarídeos. Entrega controlada de fármacos. Câncer.

LIST OF FIGURE

LIST OF TABLE

CONTENTS

1 INTRODUCTION

Despite recent advances in cancer treatment, this disease remains a global public health problem, causing the death of over 10 million people worldwide in 2020.[1] The use of nanocarriers (NCs) as vehicles to delivery therapeutics to cancer cells has emerged as a promising strategy to advance cancer treatment by preventing drug unspecific biodistribution and increasing drug accumulation in the tumor tissues.[2] NCs loaded with chemotherapeutics were reported to overcome drug resistance in tumor cells and reduce drug dosage to treat cancer, reducing long term side effects, prolonging patient survival, as well as resulting in disease remission.[3-9] However, some aspects of this delivery system still lack a comprehensive assessment such as the NCs interaction with the biological systems. An in-depth investigation of how does NCs' physico-chemical properties affect their interaction with cells is pivotal to ensure the safety of the NCs. Furthermore, exploring the NCs properties and their effect in cancer cells, as well as in cancer-associated cells may guide the development of novel nanotherapeutics with boosted anti-cancer activities. This dissertation explores the polysaccharides effects in the interaction between nanomaterials and cells aiming to reduce the toxicity of the NCs to health cell while increasing drug accumulation into cancel cells.

1.1 Polymeric Nanocarriers

Since the 1960s, polymeric nanocarriers (NCs) gain ground on drug delivery to overcome high dosage and unspecific biodistribution.[10-11] The enhanced *in vivo* stability and versatility, occurring by different possibilities in base-polymers and cargo molecules including hydrophilic and hydrophobic drugs, as well as the promising preferential accumulation at tumor sites highlighted the polymeric NCs as promising platforms to delivery anti-cancer agents.[12] Several polymer based nanotherapeutics heve been used in the clinic or are in clinical trial phase such as Lupron Depot® and Trelstar®, both used to treat prostate cancer.[13] This delivery system can be synthesized from natural or synthetic polymers, with several different properties (e.g. size, shape, surface-charge, surface ligands and others) that can be optimized to boost NCs effectiveness in the cancer treatment.[14] The size of the NCs affects their blood half-life and polymeric NCs with hydrodynamic diameter between 20 to 300 nm have a longer blood circulation time than larger NCs. In addition, small NCs have often improved tumor

penetration.[15, 16] The NCs shape influences in the biodistribution, biological barrier-crossing and cellular uptake.[15-16] Anisotropically shaped particles can evade phagocytosis for prolonged durations while spherical NCs usually presents greater cellular uptake.[9] Surface charge also impacts cell uptake and positive surface charge maximize NCs interaction with cell membrane, increasing uptake by nonphagocytic cells.[17-18] A widely used strategy to prolong NC circulation and increase NC's targetability is the addition of ligands to the NCs' surface: the ligand type, position and density alter the NCs' bioactivity.[12] Premature drug release is the major cause of low accumulation of the cargo drugs into tumor sites, therefore, controlling the drug release rate is pivotal to effectively target tumor sites.[13] NCs prepared from hydrophobic polymers have slower degradation rate in physiologic conditions, resulting in extended drug release rates.[19] Polymeric NCs have simple formulation parameters and the commonly applied methods to synthesize polymeric NCs are physical entrapment methods such as nanoprecipitation and emulsification. Choosing a formulation method relies on cargo drug physicochemical properties as well as particle size, shape and drug load requirements. Depending on the preparation method and cargo drug physicochemical properties such as hydrophobicity, the drug can be encapsulated within the NP core, entrapped in the polymer matrix, covalently conjugated to the polymer backbone or grafted to the polymer surface.[22] Nanoprecipitation methods consist in the polymer precipitation from an organic solvent when water is added, self-assembling into core-shell-like structure to reduce system's free energy. Emulsification methods require an additional input of energy to form the NCs. Oil-in-water (O/W), water-in-oil (W/O), and water-in-oil-in-water (W/O/W) emulsions are prepared under intense shear stress from an organic water-immiscible phase containing the polymer and the aqueous phases containing surfactants.[20]

Poly(lactic-co-glycolic acid) (PLGA) is a co-polymer of poly lactic acid (PLA) and poly glycolic acid (PGA) widely used in biomedical applications because of its biocompatibility, biodegradability, as well as its metabolization into endogenous monomer PLA and PGA, ensuing minimal toxicity. Approved by US FDA and European Medicine Agency (EMA), PLGA nanoparticles can successfully carry hydrophilic and hydrophobic drugs providing protection from drug degradation, sustained release and an engineerable surface.[21] Several synthesis parameters such as solvent polarity, surfactant type, PLGA and surfactant concentration, organic/water phase ratio, drug affinity to external water phase and synthesis method affect drug loading capacity of the NCs and release kinetics, however it remains suboptimal.[22] Upon dispersing the PLGA polymer within a partially water-soluble organic solvent and preparing the NCs by double emulsion method, the encapsulation of hydrophilic

drugs into PLGA NCs was improved due to the formation of a temporary phase in which the polymer and hydrophilic are dissolved.[23] Desmopressin loading into PLGA NCs via the double emulsion was optimized by testing different stabilizers in the inner aqueous phase, as result Pluronic F-68 increased the encapsulation in 30% comparing to PVA.[24] Also, PLGA microparticles formulated by emulsifying the polymer in a Pluronic F127/dextran aqueous two-phase system vary drug loading of rhodamine B and coumarin-6 depending on Pluronic F127, dextran and PLGA amounts, showing increased drug loading for the hydrophobic coumaring-6 for the formulation with the highest PLGA content and reduced drug loading for the hydrophilic rhodamine B due to its affinity with the outer dextran phase.[25]

PLGA NCs generally have a biphasic or bimodal release profile. Initially, there is a fast and sharp release relative to solubilization of the drug adsorbed to the polymer surface or penetration of water in the nanocarriers, this phase is named as “burst release”. Then, a second phase occurs progressively as the water inside the NCs hydrolyzes the ester bonds in the polymer backbone, leading to release of lactic acid and glycolic acid monomers that are endogenous and easily metabolized by the body. In this stage, drug is released through diffusion and degradation until the nanoparticle is completely solubilized.[26] Control the drug release from the NCs is pivotal to properly deliver it to the targeted sites. Sustained, slow release over a period of time reduces repetitive dosing to maintain the drug concentration in the blood plasma and protect the drug from degradation and loss of activity prior to delivery, reducing the dosage necessary to achieve the therapeutic effects.[27] PLGA monomers content affects the degradation rate of the PLGA NCs. Since PLA is a hydrophobic molecule while PGA is hydrophilic, reduced PLA/PGA ratio results in an enhanced overall PLGA hydrophilicity, favoring PLGA hydrolysis.[19] Molecular weight (MW) also correlates with degradation rate as well as with resulting NCs hydrodynamic size, thus, increase in Mw results in reduction in the degradation rate and increase in the NCs diameter.[28-29]

Several chemotherapeutics have been encapsulated in PLGA-based nanocarriers and effectively delivered to various solid tumor.[3-9,22,31-33] Co-encapsulation of doxorubicin (DOX) and epoxomicin (Epo) into PLGA nanoparticles enhanced apoptosis in MCF-7 breast cancer cells (apoptosis index about 45%) while keeping HUVEC, a healthy cell line, apoptosis index below 10%.[66] PLGA NCs coated with 4T1 cell membrane reduced the tumor growth and metastasis of triple-negative breast cancer tumor in tumor-bearing mice by delivering 2-bromo-palmitate to 4T1 cells due to homotypic recognition, prolonging mice survival.[55] Besides, PLGA NCs were also used to treat leukemia. PLGA nanoparticles modified with transferring delivered anti-BCR/ABL antibodies to chronic myeloid leukemia, degrading the Abelson

murine leukemia viral oncoprotein (ABL) and hampering CML cells oncogenesis *in vivo*.[33] Also, ABL oncogene was knocked out by PLGA-PEG NCs carrying CRISPR/Cas9 plasmid expressing gRNA targeting the BCR/ABL and improved the survival of a CML mouse model.[34] Chemotherapeutics such as idarubicin, daunorubicin, cytarabine and doxorubicin were recently encapsulated into PLGA NCs to target leukemic cells, enhancing the performance of these conventional antileukemic drugs.[36-39]

The NCs enhance tissue specificity by passive or active targeting. Passive target was widely exploited in drug delivery to solid tumors because of an abnormal feature of the tumor tissue vascularization known as the Enhanced Permeability and Retention (EPR) effect.[39] Solid tumors produce larger concentrations of vascular permeability factors and vascular growth factors to increase nutrients and oxygen supply and favor tumor cells rapid growth.[40] Nonetheless, microvasculature formed at tumor tissue is heterogeneous and abnormal, with large gaps between endothelial cells that facilitate the extravasation of particulate material from the surrounding vessels into the tumor.[40-41] In addition, the lymphatic drainage system is inefficient at tumor tissue, favoring macromolecular accumulation in the tumor and delaying their clearance.[41] Although some studies attribute to EPR effect the NC accumulation of 10–15% of injected NPs at solid tumors compared with 0.1% of free drug, recent findings suggest that only a fraction of NC accumulation in tumors can be attributed to passive targeting.[2,42] A study in mouse tumor models (U87-MG 4T1, MMTV-PyMT) and patient-derived xenograft breast cancer showed that up to 97% of gold nanoparticles, with 15, 50 and 100nm core sizes, enter the tumor by active transport through endothelial cells rather than crossing gaps between cells.[42] The authors highlighted that other mechanisms such as immune cell interactions, protein coronas and molecular mechanisms have greater contribution on tumor targeting than EPR effect.[42] Supporting these findings, Wilhelm *et al*. reported that only 0.7% of the injected dose of NPs reaches solid tumors.[43] On the other hand, Price et al. questioned these generalized findings suggesting biased analysis due to quantifying NC distribution using non-standard calculations, which may have led to misleading results.[44] To fully understand the capacity of the NPs to passive target solid tumors, it is pivotal to perform extensive meta-analyses and statistical comparisons using pharmacokinetic datasets that include total, encapsulated, and released drug.[44] In solid tumors, interstitial fluid pressure and extracellular matrix density may contribute to EPR effect failure.[45] Therefore, the low efficiency in passive targeting tumor sites together with the fact that not all cancers form solid tumors substantiate the importance of developing new delivery and targeting strategies.

Active targeting NCs have been developed to enhance delivery compared to passive targeting. It involves modifying the NCs with affinity ligands that bind to antigens, extracellular matrix proteins or receptors overexpressed in the diseased tissue.[46-47] Different molecules can trigger specific and efficient NCs uptake through metabolic, adsorption or receptor targeting, endocytosis–enhancing treatment efficacy.[48] An example of active targeting is the use of hyaluronic acid (HA) decorated NCs to target the CD44 receptor overexpressed in some cancer cells, this strategy was reported to improved drug delivery to several cancer cells such as cancer stem cells, breast cancer cells, glioblastoma cells and ovarian cancer cells.[50-53] Active targeted PLGA NCs have also contributed to advances in cancer treatment, e.g. PLGA NCs conjugation with folic acid increased the uptake and cytotoxicity of the NCs in breast tumor *in vivo* by targeting the folate receptor over expressed in the breast cancer cells.[53-55] However, it is not clear how much active targeting increases NC accumulation in tumor tissue or affect biodistribution because most of the NCs are still retained by the liver and spleen, as these are clearance organs.[46] Besides, the receptor expression by tumor cells varies depending on the disease stage, providing an additional challenge for the use of receptor targeting.[56]

1.2 Polysaccharides

Polysaccharides are long chain polymeric carbohydrates abundant in nature.[57] Formed by O-glycosidic linkages between monosaccharides, [58] polysaccharides can be linear or branched, with a wide range of molecular weights and full of reactive groups, which contribute to their diversity in structure, property and code capacity. [59-60] In nature, polysaccharides have several important biological functions such as signaling, energy storage, cell structuring and modifications of protein properties.[60-61] Moreover, polysaccharides have a key role in cell-cell and cell-matrix recognition and adhesion.[61-62] Their importance in biological communication added to their hydrophilicity, stability and biodegradability make polysaccharides attractive to biomedical applications.

Many polysaccharides have been applied in nanomedicine as coating agents to increase systemic circulation times, since their branched structure and high hydrophilicity reduces opsonization avoiding NCs internalization and destruction by the mononuclear phagocyte system.[57,61] Most carbohydrates also have bioadhesive properties due to non-covalent interactions with biological tissues favored by their abundant hydroxyl, carboxyl and amino groups.[57,63] Polysaccharides can also actively target tissues by receptor-mediated endocytosis,[61,64] specifically binding to certain cell types through proteins expressed in cell

surface such as Lectins, carbohydrate specific receptors, which are overexpressed in some malignant cells.[65] NCs functionalization with lectins, anti-glycan antibodies, peptides and others polysaccharide binding molecules are also used to target aberrant polysaccharide expression on the surface of tumor and metastatic cells. [66]

Dextran (Dex) is a colloidal, hydrophilic and inert polysaccharide synthesized by bacteria from lactobacillus family.[57] Widely used for biomedical applications due to its biocompatibility, this polysaccharide is formed by of (1→6)-α-D-glucose monomers.[67] Several anti-cancer agents have been covalently coupled to dextran, showing lower systemic toxicity and lower drug resistance in P-glycoprotein overexpressing multiresistant cells.[68] Dex is also employed as coating agent to increase circulation time of nanomaterials since its hydrophilicity and branched structures reduce plasma protein absorption.[70-72] Dextran coating can trigger NCs uptake by scavenger receptors type 1 (SR-A1) and dextran-binding C-type lectins such as SIGN-R1 and mannose receptors (CD206), expressed in macrophages.[72-74] In addition, dextran based NCs have shown enhanced tumor penetration [74] as well as enzymatic hydrolysis through alpha amylase which is overexpressed in tumor cells, triggering NCs destruction and drug release into tumor environment. [72-73,75]

Another important polysaccharide is hyaluronic acid (HA), a negatively charged polysaccharide composed by repeated units of D-glucuronic acid and N-acetyl-D-glucosamine bounded by beta-linkages.[76] HA is abundant in the body and widely distributed in all tissues and body fluids, being an important component of extracellular matrix (ECM).[76] HA is overproduced in many cancers including pancreatic carcinoma, breast cancer, colorectal cancer, prostate cancer and brain tumors, being the major component of tumor-associated ECM.[77] HA accumulation in tumors correlates with poor prognosis, associated with HA role in epithelial-to-mesenchymal transition induction, leading to invasion and metastasis.[77-78] Depends on molecular weight, HA plays important role in cell motility, proliferation and cell–cell adhesion as well is a key component for embryonic development, wound healing repair, and inflammation.[60,67,79-80] Regulation of amount and length of HA molecules is pivotal in inflammation regulation, since low molecular weight HAs (6 to 20 kDa) have immunostimulatory properties while high molecular weight HAs (>500 kDa) are immunologic depressant.[79] This antagonistic effect may be related with HA polymer length implication in macrophages polarization as it was reported that low molecular weight HA polarizes macrophages to pro-inflammatory phenotype while high molecular weight HA induces an anti-inflammatory phenotype.[80] High molecular weight HA may also enhance cellular resistance to oxidative stress, while very low molecular weight HA (0.4 to 4.0 kDa) induces the expression

of heat shock proteins. Wound healing and embryotic development are associated with 20 to 200 kDa HA.[79-80] HA binds to the Custer determinant 44 (CD44), a transmembrane glycoprotein expressed in macrophages and in many types of cancer.[81] CD44 is overexpressed in several cancers including pancreatic, breast, ovarian, prostate, colorectal cancers, neuroblastomas as well as acute myeloid leukemic stem cells, becoming a promising target for cancer drug delivery systems.[51, 82-85] HA-CD44 interaction also regulates p53 gene expression in naked mole-rat and very high molecular weight HA (>6000 kDa) interaction with CD44 can partially attenuates p53 expression, protecting cells from stress.[79] Therefore, HA is applied in nanomedicine to target cancer cells and tumor associated macrophages via CD44-HA interaction as well as to explore its bioadhesive characteristics.[84, 86]

1.3 Protein corona

In physiological environments, the biodistribution of the NCs are affected by the adsorption of proteins on the NCs' surface, known as protein corona (PC) formation.[87] Some of these proteins, the opsonins, can initiate an immune response exposing the NCs to phagocytes, e.g., macrophages, reducing the NCs' blood half-life.[87] In addition, protein corona formation can mask surface functionalization of the NCs, leading to NCs' accumulation in the liver and spleen instead of in the target sites.[88-89] Transferrin-modified silica nanoparticles exposed to serum are shown to lose their targetability to transferrin receptor in A549 lung epithelial cells *in vitro*.[89] Also, *in vivo* PC formation in transferrin-modified polystyrene NCs hampered their blood-brain barrier crossing ability and, after transcytosis, PC amount and composition was changed.[88]
The amount and composition of the adsorbed proteins vary with the physicochemical properties of the NCs, e.g., charge, surface chemistry and stiffness, which impact the biological identity of the NCs.[90-96] Furthermore, protein exposure times may influence the protein composition of PC but not the protein amount, effect known as Vroman effect.[97-98] Vroman described that proteins with higher diffusion rates are first absorbed at a surface but then they are displaced by protein with greater affinity to the surface.[97] Proteins that are irreversible absorbed at the NCs surface form the hard corona while the replaceable proteins form a dynamic structure are called soft corona.[98] PC composition affects the NCs interaction and recognition by cells receptors, leading to uptake via different endocytosis pathways.[90] Polyethylene glycol (PEG) coating is standard used to provide a steric barrier to the surface of NCs reducing the opsonization and increasing the retention of the NCs in the blood.[99] In gold NPs, the size and PEG density at the surface modulates the protein corona content and amount, altering NPs'

uptake mechanism and efficiency in J774A.1 cells.[96] Also, polysaccharides such as Dex can be used as coatings to avoid NCs-protein interaction, reducing opsonization and fast blood clearance.[70-71] Dex hydrophilicity and branched chain provides a steric protection for NCs against plasma proteins interaction, reducing protein absorption.[69-71]

1.4 Bone marrow (BM) microenvironment in acute myeloid leukemia (AML)

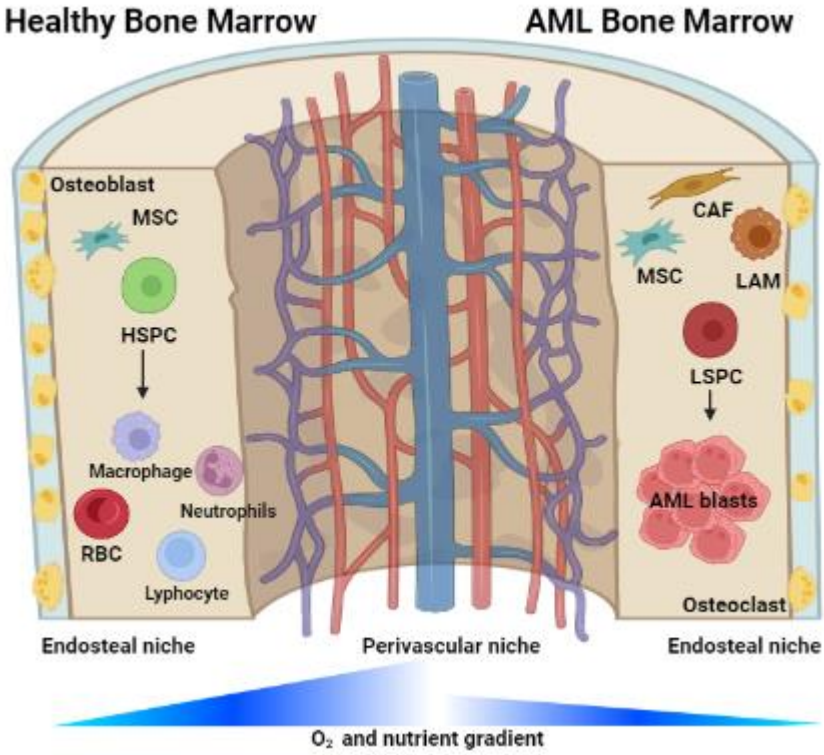

Figure 1 - The bone marrow microenvironment (BMME) in health and in acute myeloid leukemia (AML). The BMME is formed by the perivascular niche, rich in oxygen and nutrient, and the endosteal niche, shaped by osteoblasts and osteoclasts. In healthy BMME, hematopoietic stem and progenitor cells (HSPCs) differentiate into mature blood cells. In AML, some HSPCs accumulate genetic mutations giving rise to leukemic stem and progenitor cells (LSPCs) that differentiate into AML blasts. AML blasts accumulate into the BMME and compete with healthy hematopoietic cells for oxygen and nutrient, leading to expansion of the hypoxia regions and disruption of the oxygen and nutrient gradient that support HSPC function. Leukemic cells reprogram mesenchymal stem cells (MSC) and immune cells to leukemia supporting phenotypes such as cancer-associated fibroblasts (CAFs) and leukemia-associated macrophages (LAMs).

Source: By the author

The bone marrow microenvironment (BMME) is formed by the endosteal niche and the perivascular niche.[100] The endosteal niche, located at the bone marrow periphery, is defined by bone-producing osteoblasts and has reduced oxygen and nutrient levels.[101] The perivascular niche, the central region of the BM, is a region rich in oxygen and nutrients due to its closeness

to the vasculature.[101-102] The oxygen and nutrient gradients are pivotal for the maintenance of normal hematopoiesis.[102] The endosteal niche shelter hematopoietic stem and progenitor cells (HSPCs) and HPSCs interaction with BM stromal and immune cells support HSPSs survival and differentiation into mature blood cells.[100-101] The osteoblasts cells located at the endosteal niche form protective layers to the HSPCs and support HSPCs homing by cell-to-cell adhesion molecules.[101] Mesenchymal stem cells differentiate into adipocytes, chondrocytes, and fibroblasts within the perivascular niche and these cells contribute for hematopoiesis regulation by secreting factors such as C-X-C motif chemokine 12 (CXCL12), stem cell factor (SCF) and interleukin (IL) 7.[103-105] However, BMME dynamism makes BM niche separation slight since both niches are closely related and work in collaboration.[106]

Leukemia is a heterogeneous malignant disease that originates from aberrant regulation of transcription factors or clonal disorders that lead to a block in differentiation of hematopoietic stem and progenitor cells.[100] Leukemic cells accumulate into the BM and blood of patients disrupting normal hematopoiesis.[100] Leukemias are classified by the type of stem cells that originated the cancer, typically myeloid or lymphoid cells, and by the rate of disease progression, i.e. acute or chronic.[107] Acute myeloid leukemia (AML) is marked by the accumulation of immature myeloid blasts within the BM and blood of patients.[108] In AML, HSPCs cells accumulate genetic mutations giving rise to leukemic stem and progenitor cells (LSPCs) that initiate and maintain leukemic clonal hierarchy by differentiating to pre-leukemic cells and leukemic myeloblasts.[108] LSPCs take advantage of the BMME to ensure their endurance and proliferation. In addition, evidence suggests that changes in the BMME contribute to the selection and promotion of HSPCs malignant clones that do not grow under healthy BMME conditions.[100, 109-111] LSPCs also shifts the BMME equilibrium from the healthy state, that supports hematopoiesis, to an leukemic-supportive microenvironment that favors leukemogenesis and drug resistance. Leukemic cells population competes with HSPCs for oxygen and nutrients, leading to expansion of hypoxia regions and disruption of the oxygen and nutrient gradient that support normal hematopoiesis.[112-115] In addition, during AML development *in vivo*, leukemic cells reduce osteoblasts numbers, disturbing HSPCs hematopoietic activities and promoting AML progression.[116] The homing and engraftment of LSPCs within the BMME is mediated by interaction of CD44, overexpressed by LSPCs, with HA, highly concentrated in the extracellular matrix of the endosteal region.[117] The LSPCs are niche-dependent, and their interaction with the BMME is pivotal to provide pro-survival/anti-apoptotic signals, favoring chemotherapy resistance and AML relapse.[85, 118]

Leukemic cells also reprogram stromal and immune cells to leukemia supporting phenotypes within the BMME.[119] AML blasts recruit and induce polarization of macrophages into leukemia supporting phenotype either through direct cell-to-cell interactions or secreted factors (e.g., exosomes, cytokines, and chemokines).[102] In addition, stromal cells reprogramed by leukemic cells also promote growth, recruitment and polarization of macrophages towards leukemic supportive phenotypes.[120]

1.4.1 Leukemia-associated macrophages (LAMS)

Macrophages are highly plastic cells that respond to extracellular cues adopting different functional phenotypes that differ in terms of receptor expression, cytokine production, effector function, and repertoire of chemokines.(REF) AML induces infiltration and proliferation of macrophages into the BMME and spleen of patients and polarizes the macrophages toward pro-leukemic phenotypes.[121] Pro-inflammatory macrophages, are effector cells responsible for detection, phagocytosis and destruction of microorganisms and cancer cells. They are characterized by an increase in expression of markers such as antigen presentation molecules major histocompatibility complex class II (MHC-II), CD80, CD86 or CD38 and inflammatory mediators, such as interleukin 6 (IL-6), tumor necrosis factor-α (TNF-α), reactive oxygen species (ROS) and nitric oxide (NO). In leukemia, pro-inflammatory macrophages exhibit anti-leukemia and immunostimulatory functions, benefiting cancer drug sensitivity. Pro-inflammatory polarization of LAMs induced by targeting IRF7-JNK pathway with polyIC administration prolonged survival of AML and T cell acute lymphoblastic leukemia (T-AAL) mice.[121-122]

Anti-inflammatory macrophages express the hemoglobin/haptoglobin and mannose scavenging receptors CD163 and CD206 as well as secret arginase, metalloproteinases, transforming growth factor-β (TGFβ), interleukin 10 (IL-10) and other cytokines that induce immune suppression, angiogenesis and tissue repair.[123] In AML patients, an increased ratio of anti-inflammatory/pro-inflammatory macrophages within BM correlates with a worse prognosis rather than an elevated total number of infiltrated macrophage.[122, 124] In vitro, in vivo and clinical models, reported that macrophages polarized by AML blasts are anti-inflammatory macrophages characterized by upregulated CD206 expression and with leukemia-supporting and immunosuppressive properties.[121,125-126] Infiltration of anti-inflammatory macrophages into BM is related to drug resistance in AML patients due to its ability to upregulate pro-survival/anti-apoptotic pathways in AML blasts.[102,121] AML cells induce macrophage

polarization to anti-inflammatory leukemia-supporting phenotypes via cell-to-cell interaction as well as secreting factors, e.g., regulating growth factor independence 1 expression.[102, 121] Due to their role in AML progression and drug resistance, LAMs have become targets for leukemia therapy. Repolarizing anti-inflammatory LAMs towards pro-inflammatory phenotype by inducing IRF7 expression and consequent activation of SAPK/JNK pathway contributed to prolonged survival in AML mice model.[122] Another approach prevented AML signaling against macrophage phagocytosis by inhibiting SIRPa-CD47 interaction via monoclonal antibody blockage. SIRPα-antibody stimulated phagocytosis of AML cells and diminished primary patient-derived AML cells.[127]

1.4.2 Custer determinant 44 (CD44)

Custer determinant 44 (CD44) is a transmembrane adhesion molecule involved in the binding and metabolism of HA, an important component of the extracellular matrix.[81, 128] CD44 has been associated with homing efficiency, stemness, engraftment of AML cells, apoptosis and stress resistance in AML cells, besides, its expression is upregulated in the BM of AML patients.[85,117,129-130] In macrophages, CD44 expression levels are affected by macrophage phenotype.[131-132] CD44 is involved in the adhesion and homing to BM, and mobilization of leukemia-initiating cells. CD44 expression levels in BM correlates with a worse prognosis in leukemias.[117,133] CD44 is also expressed in leukemic stem cells (LSCs) and plays an important role in homing and engraftment of LSCs within the osteoblast-rich area of the bone marrow, retaining their ability to initiate and maintain the leukemic clonal hierarchy and favoring drug resistance and AML relapse.[85,118] Administration of monoclonal antibody directed to CD44 prevent AML-LSCs interaction with stem cell–supportive microenvironmental niches, leading to AML eradication.[85] In macrophages, CD44 regulates macrophage migration and $CD44^{-}$ macrophages are less sensitive to chemoattractants.[133]

1.5 Cell-based drug delivery systems

Despite great progress in nanocarrier-based drug delivery systems such as increased drugs solubility, bioavailability, retention time and cell uptake, some unsatisfactory physicochemical and biological properties have hampered their clinical use.[134] EPR effect showed not enough to guarantee NCs accumulation in tumor tissue and the increase in cell uptake due to active target

has not been translated into satisfactory accumulation within the targeted tissue.[43] The NCs fate continues to be mostly within the patient's liver and spleen.[43] Polyethylene glycol (PEG) coat in nanoparticles has been used to increase blood half-life, however, PEGylated NCs trigger immunogenicity after repeated doses, accelerating blood clearance through specific anti-PEG IgM.[135] In addition, despite advantages against free drugs, NCs organ and tissue barrier crossing remain suboptimal. Biomimeticing NCs coated with cell membrane were designed to overcome some of these shortcomings since cell membrane proteins "hide" the NCs from immune system, increasing blood half-life and reducing immunogenicity.[136] Retention of membrane proteins provide the NCs some properties from source cells, however, low yields hinders membrane-coated NCs clinical application.[136]

Cell-base delivery systems are promising strategies to effectively delivery drugs to targeted sites as they endow all the natural biological properties and functions of the carrier cells and have large drug loading capacity in the cytoplasmic compartment or on the cell membrane.[137-138] The cells are isolated from the patient, loaded with therapeutics and reinfused into patient's body, ensuring excellent biocompatibility, hypoimmunogenicity, long half-life in the blood, tissue-targeting and barrier crossing ability.[136] Depending on the targeted disease, the cell-based delivery strategy may use different cells types to take advantage of the carrier cell unique properties.[136-137]

Red blood cells (RBC) have a very long circulation time (about 120 days) associated with overexpression of cluster of differentiation 47 (CD47) receptor that interacts with signal-regulatory protein α (SIRPα) on macrophages inhibiting phagocytosis and mononuclear phagocyte system clearance.[139] Drug-loaded RBCs retain the long half-life property improving the pharmacokinetic properties of the loaded drug as well as increasing drug accumulation into the first organ after intra-arterial injection site, considering the blood stream direction..[139, 140] In addition, L-asparaginase delivered by RBC cells relapsed Acute Lymphoblastic Leukemia in phase III trial, indicating that RBC cell-based delivery is also effective for treating leukemia.[141] Other cell types also bring advantages to cell-based delivery by increasing specific targetability. Mesenchymal stromal cells (MSCs) and monocytes have an innate ability to home to BM and inflamed tissue, being applied to guide delivery of therapeutics to these sites. MSCs, carrying paclitaxel acquired a potent anti-leukemic activity, increasing the survival of BDF1-mice-bearing L1210.[142] Also, monocytes with flat polymeric particles attached to the membrane effectively delivered the particles to inflamed lungs and skin of BALB/c mice.[143] The particles attached did nothamper monocity transmigration through an endothelial monolayer and their differentiation into macrophages.[143] Otherwise, cancer cell-based carriers increase drug

targetability by due to homologous direction to source cancer cells. For example, cryo-shocked AML blast carrying doxorubicin remained able to BM homing, eliminating leukemia and prolonging the survival of tumor-bearing mice.[144]

1.5.1 Macrophage-based drug delivery systems

As present, different carrier cells were used to deliver free drugs and nanotherapeutics to cancer, improving cancer treatment. However, these cells have limited drug loading efficiency due to high cytotoxicity of the cargo, hindering their wide application as carriers.[136] Macrophages are immune cells with long half-life in the body involved in the mononuclear phagocytic system.[145] Macrophages' large phagocytic capacity and intrinsic tolerance of anticancer drugs allow high loading of free or nanoformulated drugs.[145-146] Cancer cells release cytokine and chemokine factors that recruit macrophages through chemotaxis, thus, macrophages may naturally target tumor sites.[146] In addition, macrophages have BM homing ability and interact via cell-to-cell contact with leukemic cells.[147] In metastatic cancer, RAW 264.7 macrophages interact with metastatic cells via α4 and β1 integrins that bind with vascular cell adhesion molecule 1 (VCAM-1) expressed by the malign cell.[146] Together, these properties make macrophages promising drug delivery vehicles to treat leukemias, metastatic and solid cancers.

Murine macrophage-like cells RAW 264.7 loaded with chemotherapeutics increased tumor-targeting and anti-cancer efficacy in 4T1 breast cancer and human breast tumor MCF-7 models.[145,148] RAW 264.7 macrophages loaded with free and nano-based paclitaxel (PTX) reduced the tumor volume by ~69% and ~93%, respectively, in Ehrlich ascites mice.[145] The authors associated the reduced efficacy of macrophages loaded with free PTX to the faster drug release from macrophages compared to macrophages loaded with nano-based PTX, leading to partial release of the drug before macrophages reach tumor sites.[145] Besides improving targeting, it was reported that macrophages can deeply penetrate tumors and murine bone-marrow-derived macrophages (BMDMs) carrying NCs encapsulating tirapazamine improved drug accumulation in hypoxic areas of 4T1 breast cancer.[7] Also macrophage-based carriers can cross the blood-brain barrier, as reported for PLGA nanoparticles that were effectively delivery by RAW264.7 macrophages into the brain of mice bearing intracranial U87 glioma.[149] The macrophages delivery of therapeutics to cancer cells occur through the cell-to-cell interaction, corroborated by Guo et al. study showing that doxorubicin delivered to human ovarian cancer

cell line SKOV by inflammatory RAW 264.7 macrophages via tunnelling nanotube pathways, resulting in ovarian carcinoma cell death.[150]

The aim of this dissertation is to explore the polysaccharides effects in PLGA-based NCs and to investigate their interaction with cancer cells as well as with cancer associated cells. Two different PLGA NCs were synthesized using polysaccharides as stabilizing, caping or coating agents. In **Chapter 1** we studied the interaction of PLGA NCs prepared using Dex as stabilizing and caping agents with myocardial cells (H9C2), breast adenocarcinoma cells (MCF-7) and macrophages (RAW 264.7) to address the effect of Dex in PLGA NCs formulations. In **Chapter 2** we explored the binding between HA and CD44, a receptor that mediates cell-cell and cell-matrix interaction, to transport a nanotherapeutic to the leukemic cells. To assess the macrophages' ability to effectively deliver NCs via CD44-targeting to AML cells, we studied their interaction with NCs in co-cultures of macrophages (RAW 264.7) and AML cells (C1498). Together, the chapters highlight the prospective use of PLGA NCs caped or coated with polysaccharides as vehicles to prevent chemotherapeutic unspecific biodistribution and increase the drug amounts delivered to the cancer cells.

2 CHAPTER I: THE AMOUNT OF DEXTRAN IN PLGA NANOCARRIERS MODULATES PROTEIN CORONA AND PROMOTES CELL MEMBRANE DAMAGE

2.1 Abstract

Polymeric nanocarriers (NCs) are efficient vehicles to prevent drug unspecific biodistribution and to increase the amount of drug delivered to the tumor tissues. However, some toxicological aspects of NCs still lack a comprehensive assessment, such as their effects on cellular processes that lead to toxicity. We evaluate the interaction of poly (lactic-co-glycolic acid) (PLGA) NCs prepared using dextran (Dex) and Pluronic®-F127 as stabilizing agents with myocardial cells (H9C2), breast adenocarcinoma cells (MCF-7) and macrophages (RAW 264.7) to address the effect of Dex in PLGA NCs formulations. By emulsion diffusion method, doxorubicin-loaded NCs were prepared with no Dex (PLGA-DOX), 1 %(w/v) (Dex1/PLGA-DOX) and 5 %(w/v) (Dex5/PLGA-DOX) NCs. Uptake analyses revealed a significant reduction in Dex5/PLGA-DOX NCs uptake by the H9C2 and MCF-7, which was also reduced for Dex1/PLGA-DOX NCs in the absence of *in vitro* protein corona, revealing an effect of dextran concentration on the formation of protein corona. RAW 264.7 cells presented a higher uptake of Dex5/PLGA-DOX NCs than the other NCs likely because of the receptor mediated endocytosis, since C-type lectins like SIGN-R1, mannose receptors and scavenger receptors type 1 that are expressed in RAW 264.7 can mediate Dex uptake. Despite the lower uptake, Dex5/PLGA-DOX NCs promote the generation of reactive oxygen species and oxidative membrane damage in MCF-7 and H9C2 even though cellular metabolic activity assessed by MTT was comparable between all the NCs. Our results highlight the importance of an in-depth investigation of the NCs-cell interaction considering additional mechanisms of damage apart from metabolic variations, as nanoparticle-induced damage is not limited to metabolic processes imbalance, but also other mechanisms, e.g., membrane and DNA damage.

2.2 Introduction

The anti-cancer activity of Doxorubicin (DOX) is widely known by the scientific community, however, its non-specific distribution in biological systems has limited its application.[151] In high doses, DOX can cause irreversible cardiomyopathy and even heart failure due to oxidative stress caused by increased production of reactive oxygen species (ROS).[152]

Polymeric nanocarriers (NCs) are efficient vehicles to prevent DOX unspecific biodistribution and to reduce long-term adverse effects.[30,152] Poly(lactic-co-glycolic acid) (PLGA) is a co-polymer widely used in biomedical applications because of its biocompatibility and biodegradability, besides, it is FDA-approved. Several chemotherapeutics have been encapsulated in PLGA-based NCs and evaluated for the treatment of various types of cancers.[21,30] However, some toxicological aspects of PLGA-based formulations still lack comprehensive studies on their effects on cellular processes that can lead to cell damage and death.

In the body, the biodistribution of the NCs is affected by the adsorption of proteins on the NCs' surface, known as protein corona.[87] Some of these proteins, the opsonins, can initiate an immune response exposing the NCs to phagocytes, e.g., macrophages, reducing the NCs' blood half-life.[87] Besides, macrophages are an important component of the tumor microenvironment. In addition, protein corona formation can mask surface functionalization of the NCs, leading to NCs' accumulation in the liver and spleen instead of in the target sites.[88-89] The amount and composition of the adsorbed proteins vary with the surface characteristics of the NCs, e.g., surface charge and surface chemistry, which impact the biological identity of the NCs.[91-93] Polyethylene glycol (PEG) coating is commonly used to provide a steric barrier to the surface of NCs reducing the opsonization and increasing the retention of the NCs in the blood.[99] However, PEGylation leads to poor NCs uptake by cells into tumor tissues, suggesting that PEG coatings may not always be the optimal choice for targeted drug delivery. [99, 153]

Another strategy applied to increase circulation time of nanomaterials is to use dextran (Dex) as coating agent due to its hydrophilicity and branched structure that reduce plasma protein adsorption.[69-71] Dextran coat can also trigger efficiently and selectively NCs uptake by scavenger receptors and dextran-binding C-type lectins. Dextran-based NCs have shown enhanced tumor penetration as well as enzymatic hydrolysis through alpha amylase which is overexpressed in tumor cells.[72-75]

Iron-oxide based NCs coated with dextran showed neurotoxicity and genotoxicity due to oxidative stress. [154-155] ROS imbalance is one of the frequently reported causes of NC-associated toxicities that can promote DNA and cell membrane ROS-mediated damage.[156-158] Oxidative stress induced by NCs is dependent on particle properties, e.g., surface chemistry, size and composition.[158] In-depth investigation of the NC-cell interaction is fundamental to ensure the safety of the NCs even at apparently non-toxic formulations, since effects including DNA damage, oxidative stress, and mitochondrial dysfunction can occur without detectable changes in cytotoxicity assessed by conventional colorimetric assays.[159]

We studied DOX loaded PLGA NCs prepared with 5 and 1 % (w/v) or without Dex as a stabilizing and capping agent. The uptake of PLGA NCs were evaluated in the presence and absence of serum by flow cytometry. Also, membrane damage, metabolic imbalance and ROS induction were assessed to study whether Dex content affects NC interaction with breast cancer cells (MCF-7), myocardium cells (H9C2) and macrophages (RAW 264.7).

2.3 Experimental

2.3.1 Materials

Poly(lactide-co-glycolide) (PLGA) (Resomer 503H 50:50 MW 24000-38000, acid terminated, #719870), Pluronic®-F127 (#P2443), Dextran 40 (Mr ~ 40 kDa, #31389), ethyl acetate (#319902), doxorubicin hydrochloride (#D2975000), deuterium oxide (#151882), tetrazolium blue thiazolyl bromide (MTT, #M2128), 2'-7'-dichlorodihydrofluorescein diacetate (CM-H2DCFDA, #D6883), ammonium persulfate (APS, #A3678), sodium dodecyl sulfate (SDS, #L3771), tetramethyl ethylenediamine (TEMED, #T9281), glycine, 2-mercaptoethanol (2-ME, #M6250), glycerol (#G9012), bromophenol blue (#114391), KCl (#C2010.0.AH), NaCl (#C1060.01.AH), KH_2PO_4 (#P9791) and Na_2HPO_4 (#S5136) were obtained from Sigma-Aldrich. Trypan Blue Stain (0.4%(w/v)) for use with the Countess™ Automated Cell Counter was purchased from Invitrogen™. Dimethyl sulfoxide (DMSO, #D1011.01.BJ) was obtained from Synth. Dulbecco's Modified Eagle Medium (DMEM) culture media with (#00074) and without phenol, 0.25% trypsin-EDTA solution (#T2500), Fetal Bovine Serum (FBS, #S0011) and L-Glutamine 200 mmol ml^{-1} (#G0209) were obtained from Vitrocell. FITC Annexin V Apoptosis Detection Kit I (#556547) was obtained from BD Pharmingen™. Pierce™ BCA Protein Assay Kit (#23225) and GelCode™ Blue Stain Reagent (#24590) were obtained from Thermo Scientific™. 30% Acrylamide/BIS solution (#161-0156) was obtained from Bio-Rad Laboratories.

2.3.2 Syntheses of the PLGA-DOX, Dex1/PLGA-DOX and Dex5/PLGA NCs

The nanocarriers were prepared by the emulsion diffusion method.[160] 200 µl of 10 mg ml^{-1} aqueous doxorubicin solution was emulsified in 2.5 ml of ethyl acetate containing 2.5% (w/v) of 50:50 PLGA and 5 ml of a 2.5% (w/v) aqueous solution of Pluronic®-F127. The emulsion was prepared on ice bath by sonication in a Delta Ultrasound sonicator, model

Sonifier 450D, with power equal to 550 W and 20% amplitude for 90 s. To the resulting emulsion was added 5 ml of 0.01 M phosphate buffer pH 8.6 containing 2.5 %(w/v) of Pluronic®-F127 and kept under moderate stirring for 1 h. Ethyl acetate was removed by evaporation under low pressure in a desiccator. For the synthesis of blank NCs, 200 µl of Milli-Q water (resistivity 18.2 MΩ cm) was sonicated with the organic phase and the surfactant solution for the formation of the first emulsion. The synthesis of the NCs in the presence of Dex was carried out by the same procedure, however, the ethyl acetate containing 2.5% (w/v) of 50:50 PLGA was emulsified with 5 ml of Milli-Q water containing 2.5% (w/v) of Pluronic®-F127 and 1 or 5 %(w/v) dextran. Pluronic®-F127-stabilized NCs were also synthesized (without Dex).

2.3.3 Characterization of the PLGA-DOX, Dex1/PLGA-DOX and Dex5/PLGA NCs

Zeta potential and size distribution (DLS) of all nanoparticles (NPs) were performed using Zetasizer Nano ZS, Malvern. The concentrations of the NCs were evaluated by Nanoparticle Tracking Analysis (NTA), Nanosight NS300, Malvern, besides size assessment. NTA analyses were performed with 50-100 particles/frame and Camera Level of 12 (shutter: 1200; gain: 146). Each formulation was diluted 10 times (10 NCs per ml) and 1000 times prior to DLS and NTA analyses, respectively.

Infrared analyses were performed using an Infrared spectrometer Nicolet 6700/GRAMS Suite, with 128 scans per sample with 4 cm^{-1} resolution from 4000 to 400 cm^{-1}. The samples were prepared by drop-casting 20 µL of the formulations in silicon wafer and dried under reduced atmosphere. UV-visible spectra were obtained using a Hitachi U-2900 spectrophotometer, in a Quartz cuvette (10 mm path length). Fluorescence spectroscopy was performed using the SpectraMax M3 Multi-Mode Microplate (Molecular Devices) controlled by SoftMax Pro software, in a four-sided polished Quartz cuvette (10 mm path length).

Transmission electron microscopy (TEM) images were obtained in a JEM-2100 Transmission Electron Microscope. 3 or 10 µl of the samples at the concentration of 10^{11} NCs per ml were deposited on copper grids for 60 s and dried with filter paper. Samples were stained with 3 µl of 2% uranyl acetate for 30 s and again dried with filter paper. Staining followed by drying step with paper filter was repeated one more time. TEM images were analyzed using Fiji (ImageJ) to measure the diameter of 50 NCs per sample.

Proton nuclear magnetic resonance (1H NMR) spectra were recorded on an Agilent technologies 400/54 Premium Shielded NMR Magnet at 400 MHz. Approximately 1.5 mg of

freeze-dried Dex5/PLGA-DOX, Dex1/PLGA-DOX, and PLGA-DOX NCs were diluted with 600 µL of D_2O and transferred to a 5 mm NMR tube. The molar ration of (1→6)-α-D-glucose monomers from dextran (δ 4.98 ppm) and polylactic acid (PLA) monomers of PLGA (δ 1.2 ppm) was calculated by the equation (1)

$$\frac{M_{\alpha-\mathrm{D}-\mathrm{glucose}}}{M_{PLA}} = \frac{N_{\alpha-\mathrm{D}-\mathrm{glucose}}}{N_{PLA}} \cdot \frac{A_{\alpha-\mathrm{D}-\mathrm{glucose}}}{A_{PLA}} \quad (1)$$

where A is the peak area, and N is the number of nuclei giving rise to the signal.

2.3.4 Encapsulation efficiency (EE) and cumulative release of DOX

Doxorubicin encapsulation efficiency was determined by UV-visible spectroscopy. 1 ml of each nanocarrier formulation – PLGA-DOX, Dex1/PLGA-DOX and Dex5/PLGA-DOX NCs was centrifuged (10,000 g, 30 min, 20 °C) and the pellets containing the NCs were resuspended in Milli-Q water. Absorbance was measured before and after centrifugation. The encapsulation efficiency values were obtained according to equation (2).

$$\%EE = \frac{ABS_{\max\, after\ centrifugation}}{ABS_{\max\, before\ centrifugation}} \quad (2)$$

To obtain the release profile of PLGA-DOX, Dex1/PLGA-DOX and Dex5/PLGA-DOX NCs, 250 µl of each formulation were centrifuged (10,000 g, 20 min, 20 °C) and resuspended in 1.5 ml of 1X PBS buffer, pH 7.4. The samples were incubated at a microtube shaker under constant agitation, at 37 °C and protected from light.

At defined times, the samples were centrifuged (10,000 g, 20 min, 20 °C) and supernatants collected. The pellets were resuspended in fresh buffer and incubated again at the microtube shaker under the same conditions. The cumulative release (CR) values were obtained according to equation (3), with the percentage released DOX (% released(t)) calculated by equation (4)

$$\%\, CR = \%\, released(t-1) + \%\, released(t) \quad (3)$$

$$\%\, released = \frac{[\mathrm{DOX}]_t \cdot (\mathrm{Volume})}{DOX_{Total}} \cdot 100 \quad (4)$$

where $[DOX]_t$ is the concentration of DOX at time t determined by the equation of the calibration curve in Fig. S2 (Supplementary Information) obtained by linear regression (R^2 = 0.987), Volume is 1.5 ml representing the supernatant collect after centrifugation at each time point, and DOX_{total} is the amount of DOX in 250 µl of each NC formulation.

2.3.5 Protein corona characterization

First, the amount of adsorbed protein to the NCs was measured by the bicinchoninic acid (BCA) assay. PLGA-DOX, Dex1/PLGA-DOX and Dex5/PLGA-DOX NCs were incubated with medium containing 10% (v/v) of FBS and medium without FBS for 2 h at 37 °C. After incubation, the NCs were centrifuged once to remove unbound serum (10,000 g, 20 min, 20 °C) and resuspended in the same volume of ddH_2O. Aliquots of 10 µl were transferred to 96-well plate with 40 µl of 2% (w/v) sodium dodecyl sulfate and 200 µl of freshly prepared BCA working reagent was added to each well and the plate was incubated at 37 °C for 1 h. Absorbance was measured on a SpectraMax® M3 plate reader (Molecular Devices), controlled by SoftMax Pro software at 562 nm. Bovine serum albumin (BSA) was used as protein standard to determine the amount of adsorbed protein on the NCs. Protein concentration was calculated by discounting the absorbance of the NCs incubated with medium without FBS, followed also by one centrifugation (10,000 g, 20 min, 20 °C), from each respective formulation incubated with medium containing 10%(v/v) FBS. Assay was repeated three times for the same batches of NCs but exposed separately to FBS for protein adsorption.

For the sodium dodecyl sulfate–polyacrylamide gel electrophoresis (SDS-PAGE), the NCs were incubated with media containing 10% (v/v) of FBS for 2 h at 37 °C, centrifugated (10,000 g, 20 min, 20 °C) and resuspended in 20 µl of 2x Laemmli buffer (4% (w/v) SDS, 10% (w/v) 2-mercaptoethanol (2-ME), 20% (v/v) glycerol, 0.004% (w/v) bromophenol blue, 0.125 M Tris HCl pH 6.8). The samples were then incubated at 96 °C for 10 min to denature the adsorbed proteins. The NCs were pelleted by centrifugation (10,000 g, 20 min, 20 °C) and 10 µl of the supernatant containing the isolated proteins were loaded to 10% (v/v) polyacrylamide gel. The gel was resolved at 100 V for 1.5 h and stained with GelCode™ Blue Stain Reagent following the manufacturer's instructions.

2.3.6 Cell culture

Myocardium cells from rat heart (H9C2, ATCC) human breast adenocarcinoma from mammary gland (MCF-7, ATCC), and mouse monocyte/macrophage-like cells from ascites (RAW 264.7, ATCC) were cultured in DMEM supplemented with 10 %(v/v) FBS in 75 cm^2 flasks at 37 °C in humidified atmosphere with 5% CO_2. Cells were subculture at 70-80%

confluency. DMEM medium already contains gentamicin sulfate (50 mg l^{-1}) and amphotericin B (25 µg ml^{-1}).

2.3.7 Cell viability and cell damage

Cell viability, early apoptotic cells detection and cell membrane damage were assayed by the tetrazolium reduction colorimetric method, FITC Annexin V Apoptosis Detection Kit I (#556547) and trypan blue exclusion method, respectively. In tetrazolium reduction colorimetric assay, (3-(4,5-dimethylthiazol-2-yl)-2,5-diphenyltetrazolium bromide) (MTT, #M2128) is reduced to formazan by the action of NAD(P)H dependent oxidoreductases. Assays were performed in 96-well clear plates with flat bottom and $5 \cdot 10^3$ cells were seeded per well and grown for 24 h before being exposed to the NCs. PLGA-DOX, Dex1/PLGA-DOX and Dex5/PLGA-DOX NCs were tested at range of DOX concentrations from 1.6 to 50 µg ml^{-1}. Absorbance was measured on a SpectraMax® M3 plate reader (Molecular Devices), controlled by SoftMax Pro software at 570 and 630 nm.

Annexin V is a Ca^{2+}-dependent phospholipid-binding protein that binds to membrane phosphatidylserine (PS) exposed on early apoptotic cells. The analyses were performed using the FITC Annexin V Apoptosis Detection Kit I. In a 24-well plate, 10^5 cells of each strain were seeded in each well and grown for 24 h. The cells were exposed to the nanocarriers at 1 µg ml^{-1} of DOX for 24 h. The culture medium was removed, the cells were detached from the plate with 0.25 % trypsin-EDTA solution, washed by centrifugation (4 °C, 500 g, 10 min) and resuspended in 1X Annexin V Binding Buffer provided by the kit. The cells were stained with 5 µl of Annexin V-FITC conjugate provided in the kit and incubated in dark for 15 min. The measurements were performed immediately in a BD FACS Callibur™ Flow Cytometer equipped with one laser (488 nm). Emission was measured using FL1 (530/30) and data analysis was performed using FlowJo v10. Trypan blue is a large negatively charged dye that is excluded by viable cell with intact cell membranes while dead cells are stained, due to their damaged membranes. Trypan blue exclusion assays were performed in 48-well clear plates with flat bottom and 10^5 cells were seeded per well and grown for 24 h before being exposed to the NCs. PLGA-DOX and Dex5/PLGA-DOX NCs were tested at range of DOX concentrations from 0.01 to 10 µg ml^{-1}. After incubation with treatment, the cells were detached from the plate with 0.25% trypsin-EDTA solution and 10 µl aliquots of sample were mixed with 10 µl of Trypan blue 0.4 %(w/v). The viable cells were counted using a Countess II Automated Cell Counter (Invitrogen).

2.3.8 Internalization assays

Flow cytometry experiments were performed with a BD FACS Calibur™ Flow Cytometer, equipped with an air-cooled argon-ion laser (488 nm). For the experiment, cells were seeded in 24-well plates, at 10^5 cells per well and grown for 24 h. Cells were exposed to DOX loaded NCs for 2 or 4 h at 37 °C, 5% CO_2. Following incubation, the medium containing the NCs was removed, cells were washed with 1X PBS (pH 7.4) and detached from the plate with 0.25% trypsin-EDTA solution. Samples were centrifuged (4 °C, 500 g, 10 min) and washed with Sheath Fluid (BD Bioscience) supplemented with 0.5 %(w/v) bovine serum albumin. Emission was measured using FL2 (585/42) and data analysis was performed using FlowJo v10. For the inhibition studies, cells were incubated for 30 min with amiloride (100 µg ml^{-1}), nystatin (40 µg ml^{-1}), nocodazole (10 µg ml^{-1}), hydroxi-dynasore (100 µmol l^{-1}), dansyl-cadaverine (100 µmol l^{-1}), heparin (10 units ml^{-1}), dextran (2 mg ml^{-1}) and dextran sulfate (5 µg ml^{-1}) prior incubation with the NCs for 2h.

2.3.9 Reactive oxygen species (ROS)

ROS Detection was performed by oxidation of 2'-7'-dichlorodihydrofluorescein diacetate (CM-H_2DCFDA). Cells were seeded in a 24-well plate, 10^5 cells of each strain per well, and grown for 24 h. The cells were exposed to nanocarriers at 12.5 µg ml^{-1} of DOX for 2 h, washed with PBS (pH 7.4) and incubated with 10 µmol l^{-1} CM-H_2DCFDA in DMEM culture medium without phenol for 30 minutes. The culture medium was removed, the cells were detached from the plate with 0.25% trypsin-EDTA solution or cell scraper, washed by centrifugation (4 °C, 500 g, 10 min) and resuspended in Sheath Fluid (BD Bioscience) supplemented with 0.5 %(w/v) bovine serum albumin. All measurements were performed in a BD FACS Calibur™ Flow Cytometer equipped with one laser (488 nm). Excitation was measured using FL1 (530/30) and data analysis was performed using FlowJo v10.

2.3.10 Statistics

Statistical analyses were performed using ANOVA with Tukey's post hoc test using the software Origin Pro 8. Significance level was 0.05. *p-value < 0.05, ** p-value < 0.01 and *** p-value < 0.001.

2.4 Results and discussion

2.4.1 Effect of dextran on the properties of DOX loaded PLGA NCs

The size distributions of DOX-loaded PLGA nanocarriers prepared in the absence or presence of dextran were measured by DLS, NTA and transmission electron microscopy (TEM) (Fig. 2a-f). The NCs sizes are homogeneously distributed (PdI < 0.2, Table 1) and size populations are represented in Fig. 2a (PLGA-DOX NCs), Fig. 2b (Dex1/PLGA-DOX NCs) and Fig. 2c (Dex5/PLGA-DOX NCs), and corroborated by TEM images (Fig. 2d, 2e and 2f). Zeta potential (ζ-potential) was also determined for all formulations and confirmed the negative surface charge (Table 1) due to carboxyl end groups in PLGA. Analysis of the dextran content in the NCs was performed by NMR spectroscopy and showed that the molar ratio of (1→6)-α-D-glucose monomers from dextran and PLA monomers was 8,2 and 1,7 % for Dex5/PLGA-DOX and Dex1/PLGA-DOX NCs, respectively (Fig. S8).

The NCs concentration – particles number per mL - was estimated using NTA and Dex1/PLGA-DOX NCs exhibited a higher particle yield (Table 1 and Fig. 2g). Above a certain concentration, dextran/Pluronic solution separates in two phases, with Pluronic F127 partitioning into a dextran continuous phase.[25] PLGA preferably partition into the Pluronic F127 phase due to the amphiphilic properties of Pluronic F127 and the partial solubility of ethyl acetate in water, but it can also form multiple emulsions.[25] The rate of a Pluronic®-F127/dextran aqueous two-phase system affects PLGA emulsion and particle structure, forming core-shell or composite particles.[25] Our results indicated that NCs prepared by the emulsion of PLGA into an aqueous two-phase system containing 1 %(w/v) of dextran and 2.5 %(w/v) Pluronic®-F127 increase particle yield.

Table 1 - Characterization of DOX-loaded PLGA nanocarriers with and without dextran. NTA size (diameter), Z-average (PdI), TEM size (diameter), ζ potential, particle concentration and encapsulation efficiency of the NCs synthesized with and without dextran. Statistical analysis was performed using ANOVA with Tukey's post hoc test. Values represented are mean ± SD of independent syntheses (n=4). *Significantly different from PLGA-DOX NCs with p-value < 0.05, #significantly different from Dex1/PLGA-DOX NCs with p-value < 0.05.

Nanocarrier	NTA size (nm) (D90)	Z-average (nm) (PdI)	TEM size (nm)	Zeta potential (mV)	Concentration (10^{12} NCs/ml)	Encapsulation efficiency (EE) (%)
Dex5/PLGA-DOX NCs	101 ± 30 (129 ± 6)	127 ± 26 (0.19)	115 ± 29	-38 ± 4	1.3 ± 0.2$^{\#}$	67 ± 3$^{*,\#}$
Dex1/PLGA-DOX NCs	102 ± 28 (129 ± 3)	111 ± 13 (0.11)	66 ± 17	-35 ± 3	6 ± 1*	52 ± 4
PLGA-DOX NCs	107 ± 28 (132 ± 11)	114 ± 10 (0.07)	83 ± 27	-36 ± 7	1.3 ± 0.2$^{\#}$	54 ± 4

Source: By the author

Loading and release of DOX were evaluated with UV-visible and fluorescence spectroscopies. For Dex5/PLGA-DOX NCs, a significant increase in the encapsulation efficiency (EE) was observed when compared to Dex1/PLGA-DOX and PLGA-DOX NCs (Table 1 and Fig. 2h). Encapsulation efficiency (EE) is affected by changing the type and concentration of the stabilizing agent in emulsions.[161] The use of surfactants in drug encapsulation by double emulsion is critical as a barrier to drug release at the internal interface, and, at the external interface, as a steric stabilizer.[162] By adding Tween 20 or Tween 60 to the external aqueous phase of polybutyl adipate (PBA) nanocapsules prepared by double emulsion, Khoee and Yaghoobian reported that the higher viscosity of the external aqueous phase and reduced diffusion of the hydrophilic cargo increased the encapsulation efficiency of penicillin-G.[162] PLGA NPs formed by the emulsion of 0.0625% PLGA in 2% Pluronic®-F127/10% dextran aqueous two-phase system have a core-shell morphology with Pluronic®-F127 concentrated in the core and dextran concentrated in the shell, as reported by Yeredla et al.[25] The increase of EE for Dex5/PLGA-DOX NCs may be a consequence of the dextran arrangement at the NCs shell preventing DOX diffusion to the external aqueous phase during emulsion preparation.

Cumulative release (Fig. 2i) revealed higher release rates for Dex1/PLGA-DOX and Dex5/PLGA-DOX NCs compared to PLGA-DOX NCs at 2.5, 4 and 12 h, indicating an increase in the burst release for the dextran-containing formulations. Dextran solubility in water may maximize the interactions of NCs with water molecules, favoring the penetration of the solvent in the nanocarrier hydrophobic core, intensifying the release.[163-165]

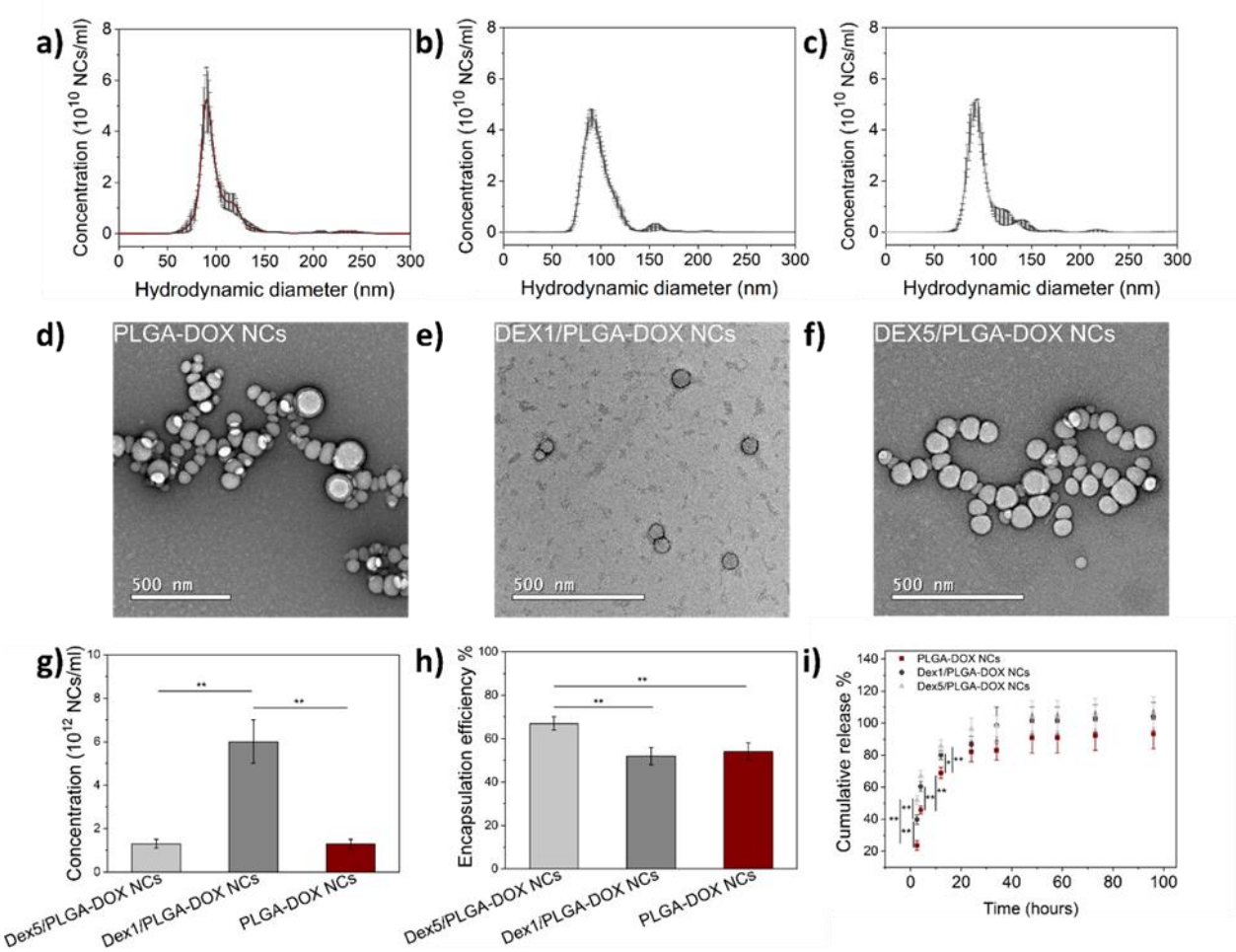

Figure 2 - Characterization of the PLGA-DOX, Dex1/PLGA-DOX and Dex5/PLGA NCs. NTA size distribution of a) PLGA-DOX NCs, b) Dex1/PLGA-DOX NCs and c) Dex5/PLGA-DOX NCs with respective representative TEM images in d), e) and f). g) Particle yield (number of NCs per ml), h) encapsulation efficiency and i) cumulative release profile in 1xPBS at pH 7.4 and 37 °C of PLGA-DOX, Dex1/PLGA-DOX and Dex5/PLGA NCs. Statistical analysis was performed using ANOVA with Tukey's post hoc test. Values represented are mean ± SD (n=4). *p-value < 0.05, ** p-value < 0.01.

Source: By the author

2.4.2 Dextran modulates protein corona formation and hinders uptake by non-phagocytic cells

In vitro cellular uptake studies were performed with H9C2, MCF-7 and RAW 264.7 by flow cytometry. H9C2 and MCF-7 were incubated for 4 h at 37 °C with free DOX, PLGA-DOX, Dex1/PLGA-DOX and Dex5/PLGA NCs. RAW 264.7 cells were exposed to the same samples for 2 and 4 h at 37 °C. Initial DOX dosage was equivalent for all groups (12.5 µg ml^{-1}).

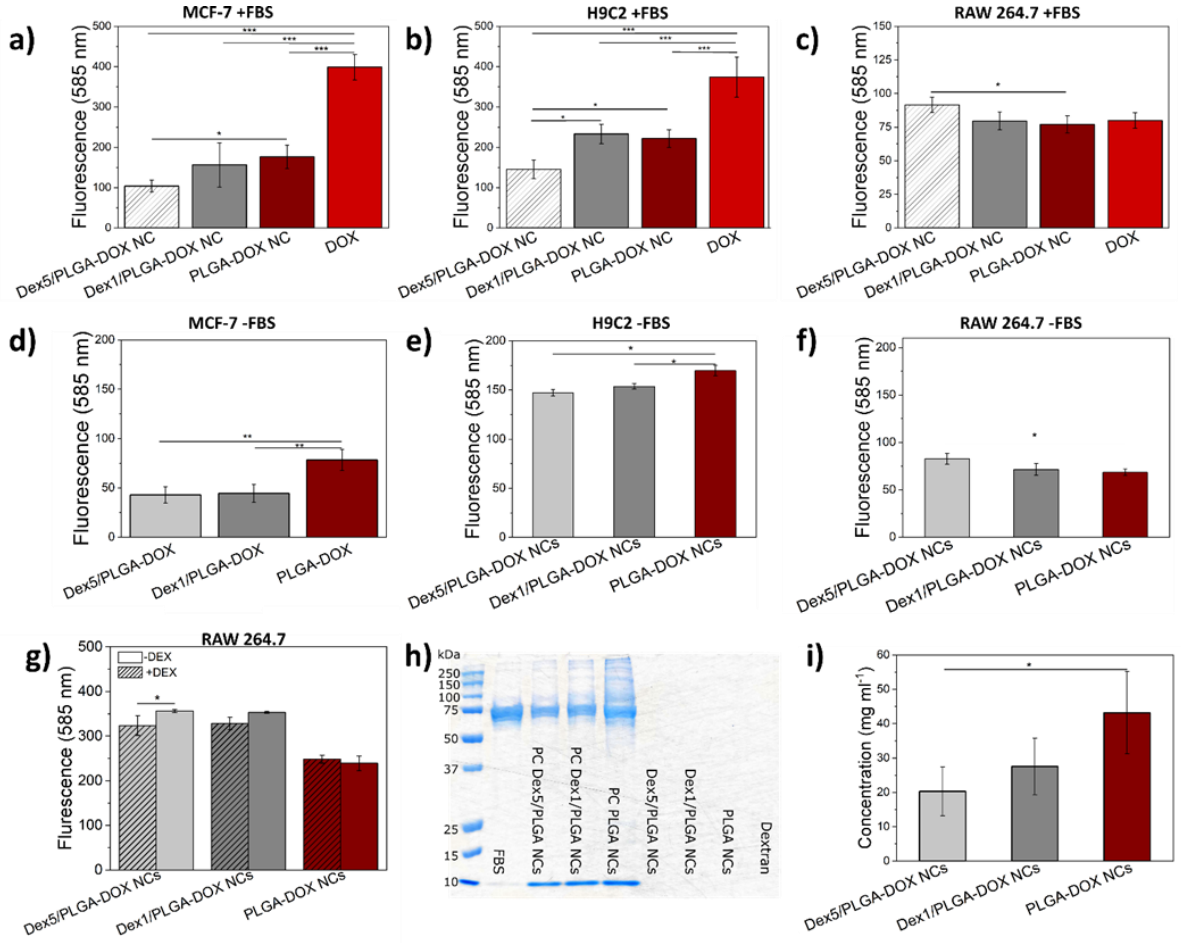

Figure 3 - In vitro cellular uptake of PLGA-DOX, Dex1/PLGA-DOX and Dex5/PLGA NCs by flow cytometry analysis. Comparison of cell fluorescence of a) MCF-7 and b) H9C2 incubated for 4 h and c) RAW 264.7 incubated for 2 h at 37 °C with DOX, PLGA-DOX, Dex1/PLGA-DOX and Dex5/PLGA-DOX NCs. Uptake by d) MCF-7, e) H9C2 and f) RAW 264.7 in the absence FBS. MCF-7, H9C2 and RAW 264.7 were incubated for 2 h at 37 °C with PLGA-DOX, Dex1/PLGA-DOX and Dex5/PLGA-DOX NCs in medium without FBS. DOX dosage was 12.5 μg ml^{-1} for all analyses. g) Uptake of Dex5/PLGA-DOX, Dex1/PLGA-DOX and PLGA-DOX NCs by RAW 264.7 with Dex excess (2 mg ml^{-1}). Characterization of protein corona formed on PLGA-DOX, Dex1/PLGA-DOX and Dex5/PLGA-DOX NCs incubated for 2 h with media containing 10 %(v/v) of FBS at 37°C. h) Adsorbed protein amount measured by the bicinchoninic acid (BCA) assay. i) SDS-PAGE gel image of the proteins recovered from protein corona formed on PLGA-DOX, Dex1/PLGA-DOX and Dex5/PLGA-DOX NCs (FBS concentration was 1 %(v/v)). Statistical analysis was performed using ANOVA with Tukey's post hoc test. Values represented are mean ± SD (n=3, n=4). *p-value < 0.05, ** p-value < 0.01, *** p-value < 0.001.

Source: By the author

A comparison of the fluorescence intensities in Fig. 3 indicated a significant reduction in Dex5/PLGA-DOX NCs uptake by MCF-7 (Fig. 3a) and H9C2 (Fig. 3b), non-phagocytic cells, when compared to PLGA-DOX NCs and Dex1/PLGA-DOX NCs. In contrast, RAW 264.7, a phagocytic cell, showed higher uptake for Dex5/PLGA-DOX NCs in 2 h (Fig. 3c). It has been shown that dextran-coated NCs efficiently target macrophages[166-167] and recently, Q. Chen et al. demonstrated that dextran-coated PLGA NCs have increased uptake in macrophages due to

receptor mediated endocytosis.[32] C-type lectins like SIGN-R1 and mannose receptors (CD206) are expressed in macrophages and mediate Dex uptake, as well as scavenger receptors type 1 (SR-A1), highly expressed in RAW 264.7. These biomolecules may be responsible for triggering the Dex5/PLGA-DOX NCs internalization in RAW 264.7 cells.[168-173] Competition with free Dex (2 mg ml^{-1}) reduced the uptake of Dex5/PLGA-DOX NCs (Fig 3g), corroborating with receptor mediated endocytosis of these NCs. However, Dex1/PLGA-DOX NCs uptake was not significantly different from PLGA-DOX NCs in 2 h as well as no significative difference was observed in the uptake of Dex1/PLGA-DOX NCs in the presence and absence of free Dex (Fig. 3g). In addition, no significant difference was observed between any of the tested formulations after 4 h of incubation with the NCs (Fig. S5a, Supplementary Information).

In biological environments (mimicked *in vitro* by FBS rich medium), proteins bind to the NCs forming protein corona (PC) affecting cell uptake.[91-93, 96, 174] To study the PC influence on the NCs uptake, MCF-7, H9C2 and RAW 264.7 cells were incubated for 2 h at 37 °C with PLGA-DOX, Dex1/PLGA-DOX and Dex5/PLGA-DOX NCs in medium without FBS. Dex1/PLGA-DOX NCs uptake by MCF-7 and H9C2 is reduced in the absence of FBS compared to PLGA-DOX NCs (Fig. 3d and 3e), which is not observed in the presence of serum. However, RAW 264.7 showed higher uptake for Dex5/PLGA-DOX NCs in medium without FBS (Fig 3f), the same uptake pattern shown in the presence of serum (Fig. 3c). To characterize the protein corona (PC) formed on PLGA-DOX, Dex1/PLGA-DOX and Dex5/PLGA-DOX NCs, we incubated the NCs with media containing 10% of FBS for 2 h at 37 °C. The absorbed protein amount was measured by BCA assay (Fig. 3h) and the PC molecular composition was studied by SDS-PAGE (Fig. 3f). SDS-PAGE gel image (Fig. 3i) showed that the NCs' PC are formed by proteins with a range of densities. Increases in Dex amount led to decreases in the lane intensity, corroborating the results from the BCA assay. Two band sizes are very distinct to the protein corona, one relative to serum albumin and globulins, major components of FBS, with sizes around 55-70 kDa, and the other, most likely relative to apolipoprotein C (~ 10 kDa).

Surface modifications influence the composition and thickness of protein corona, affecting the uptake of NCs.[90, 96] Dextran can reduce the interaction of NPs with serum proteins and higher amounts of dextran on chitosan-based NPs diminished the hard corona around them.[92] In addition, the Dex ability of preventing protein adsorption is well known to the scientific community.[57, 61, 175-176] Sakulkhu et al. reported that the serum proteins adsorb to a greater extent onto PVA-coated superparamagnetic iron oxide nanoparticles (SPIONs) than onto dextran-coated SPIONs, and that negatively charged dextran-coated SPIONs protein corona was formed specifically by alpha-1-antiproteinase, thyroxine-binding globulin, endopin-1, fetuin-B,

transthyretin, hemoglobin subunit alpha, and apolipoprotein A-II.[177] Thus, the protein adsorption onto NCs prepared with 5 %(w/v) Dex is reduced compared to the Dex1/PLGA-DOX NCs, which exhibit higher intracellular accumulation attributed to PC formation, suggesting that protein adsorption is dependent on the dextran amount. Such dependence has already been reported by Tekie et al. that showed that higher amounts of dextran decreased the hard corona formation in chitosan-based nanoparticles.[92] Corona formation may also mask ligand-functionalization on particle surface, limiting its targeting abilities.[88-89,178-179] The surface functionalization masking effect may be observed for the Dex1/PLGA-DOX NCs when uptake studies are performed in the presence of FBS (Fig. 3a).

To elucidate the differences in the NCs uptake, the main endocytic pathways were assessed by pharmacological inhibitors for PLGA-DOX NCs (Fig. S5b, Supplementary Information) and Dex5/PLGA-DOX NCs (Fig. S5c, Supplementary Information) in MCF-7 cells. Uptake was decreased by amiloride, hydroxi-dynasore and dansyl-cadaverine inhibition of macropinocytosis and clathrin-mediated endocytosis, respectively, for both NCs with and without Dex. Non-targeted spherical nanoparticles with ~100 nm are mainly internalized by clathrin-dependent endocytosis[180] while dextran is used as a macropinocytosis marker.[181] However, dextran endocytic pathway may vary with molecular weight.[182] In HeLa cells, dextran 70 kDa enter the cells by clathrin and dynamin-independent micropinocytosis while dextran 10 kDa is internalized by clathrin and dynamin-dependent endocytosis in addition to macropinocytosis.[182] Nevertheless, inhibition of clathrin-dependent and independent endocytosis and macropinocytosis had no effect on dextran-based doxorubicin nanocarriers uptake.[183] Some authors suggested that dextran-coated NCs are mainly internalized by fluid phase endocytosis pathways, without the mediation of a receptor.[184-185] Noteworthily, aldehyde-functionalized dextran-based nanocarrier systems are not affected by inhibition of clathrin-dependent and independent endocytosis, micropinocytosis and membrane cholesterol depletion in SK-N-BE cells, a human neuroblastoma cell line, but they are affected by glucose content in the medium, as well as concanavalin A, while MRC-5 cells seem indifferent to both treatments.[186] The latter highlights the fact that nanoparticles internalization depends not only on the particles properties, e.g., size and surface, but also on the cell type.[57, 176]

We investigate if heparan sulfate proteoglycan (HSPG) acts as receptor for the NCs, by competitive inhibition with free heparin. HSPG is a cell-surface receptor that is involved in the uptake of diverse macromolecular cargo and play a role in various diseases such as cancer.[187, 188] Incubation of MCF-7 with the NCs in the presence of heparin did not diminished NCs uptake compared to incubation in the absence of heparin, indicating that HSPG does not participate in

NCs uptake. Also, competitive inhibition with free Dex did not affect the uptake of NCs capped with the polysaccharide, which indicates that the uptake is not receptor-mediated in MCF-7. Dextran interaction with the cellular membrane of non-phagocytic cells may limit NCs-cell adhesion and affect non-receptor mediated endocytosis, which is supported by competitive assay in the presence of free Dex.[170, 184-185, 189] In addition, dextran coatings are shown to avoid non-specific hydrophobic interactions and reduce cell adhesion between dextran coating and cell membrane,[175, 190] which supports the hypothesis that the uptake is not receptor-mediated in MCF-7. Similar results were reported for the uptake of superparamagnetic NPs coated with dextran by HeLa cells.[185]

2.4.3 Dextran-containing formulations induce cell membrane damage

All NCs formulations presented a sustained-release profile with most of the DOX being released during the first 30 h. It correlates with the cell viability of MCF-7 (Fig. 4a, 4c and Fig. S3a), H9C2 (Fig. 4b, 4d and Fig. S3b) and RAW 264.7 (Fig. S3c, Supplementary Information) assessed by MTT and Trypan Blue exclusion assays. The cells were incubated with PLGA-DOX, Dex1/PLGA-DOX and Dex5/PLGA-DOX NCs at 37 °C for 24 and 48 h. Viability is clearly lower after 48 h incubation, if compared to 24 h (Fig. S3, Supplementary Information), which agrees with the release of DOX showed in the release profile (Fig. 2i) and the half-life of DOX–DNA covalent lesions, known to be 5-40 h.[191-192] Also, all formulations have shown to be more effective against the breast cancer cells, MCF-7, if compared to their effect on myoblast from heart tissue, H9C2, and macrophages, RAW 264.7.

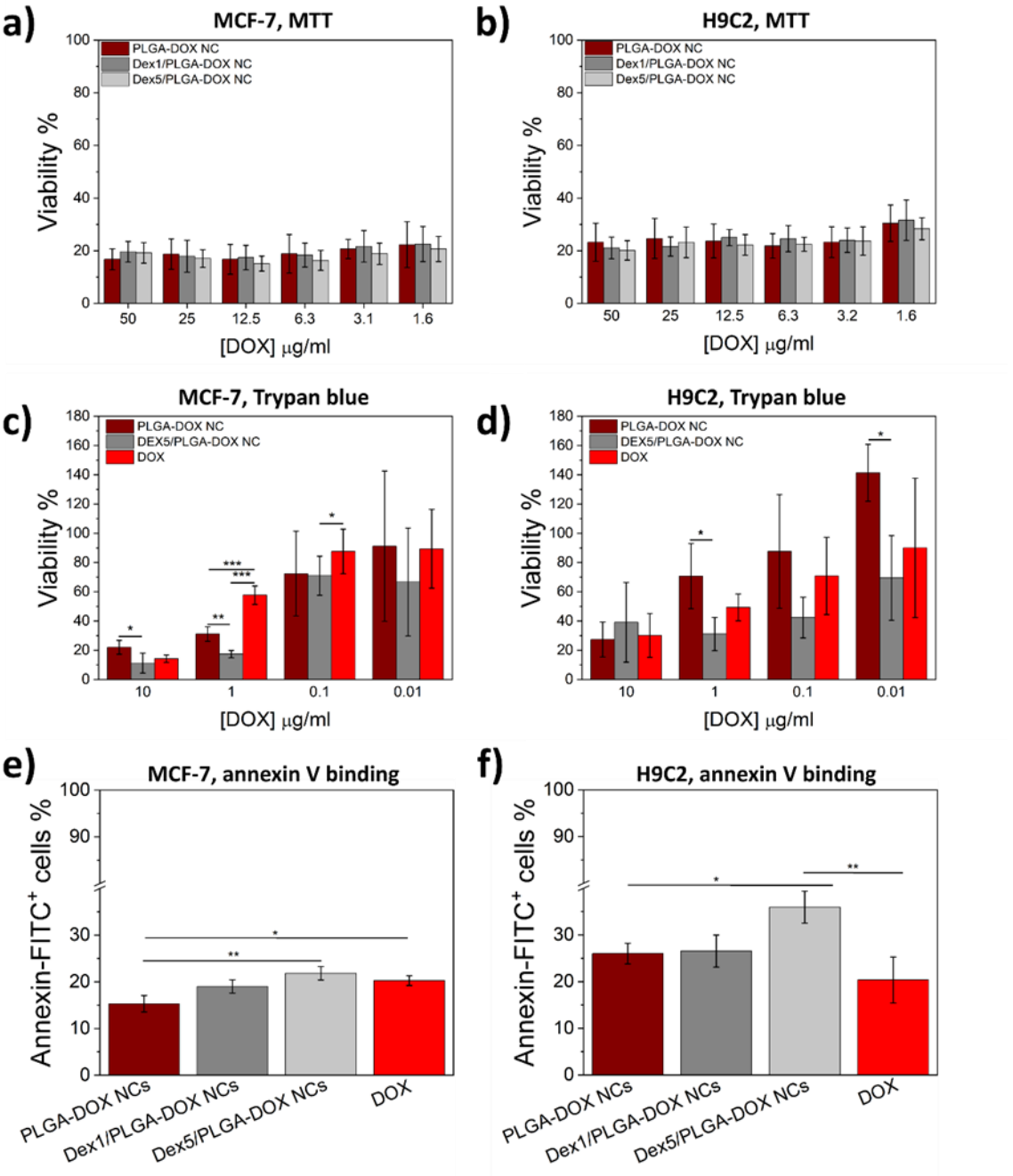

Figure 4 - Evaluation of cellular viability by MTT, Trypan Blue and annexin V binding assay for NCs prepared in the presence and absence of dextran 40. Viability of a) MCF-7 and b) H9C2 incubated for 48 h at 37 °C with PLGA-DOX, Dex1/PLGA-DOX and Dex5/PLGA NCs by MTT assay. Viability of c) MCF-7 and d) H9C2 incubated for 48 h at 37 °C with PLGA-DOX, Dex1/PLGA-DOX and DOX by trypan blue assay. Viability of e) MCF-7 and f) H9C2 incubated for 24 h at 37 °C with PLGA-DOX, Dex1/PLGA-DOX and DOX by annexin V binding assay. Statistical analysis was performed using ANOVA with Tukey's post-hoc test. Values represented are mean ± SD (n=4). *p-value < 0.05, ** p-value < 0.01, *** p-value < 0.001.

Source: By the author

Non-significant difference on cellular viability was observed between NCs formulations as assessed by MTT (Fig. 4a and 4b). However, by trypan blue exclusion assay (Fig 4c and 4d)

and annexin V binding assay (Fig. 4e and 4f) it was possible to observe a reduced viability of MCF-7 and H9C2 treated with Dex5/PLGA-DOX NCs in comparison with PLGA-DOX NCs. The choice of the best method to assess cell damage caused by drug carrier formulations depends on the mechanism of damage and location of its direct target.[193-194] MTT assay assesses the mitochondrial function by measuring activity of mitochondrial dehydrogenase enzymes while annexin V specifically binds to exposed phosphatidylserine (PS) in early apoptotic cells.[195-196] Trypan blue exclusion assay evaluates cell membrane integrity by accounting dead cells that took up trypan blue, a negatively charged dye excluded by live cells.[196] Apoptosis is a normal genetically programmed process for removal of unwanted cells.[195,197] However, cancer cells express anti-apoptotic genes that allow them to survive longer, favoring tumor growth and drug resistance.[197-198] One of the earliest features of apoptosis is the loss of membrane asymmetry and translocation of phosphatidylserine (PS) from the inner side of the plasma membrane to the surface. Annexin V specifically binds to exposed PS in early apoptotic cells.[195] Annexin V binding assay showed that Dex5/PLGA-DOX NCs treatment leads to higher amounts of early apoptotic cells than PLGA-DOX and Dex1/PLGA-DOX NCs.

PS translocation precedes the loss of membrane integrity, which occurs in later stages of cell death both in apoptotic or necrotic process.[61] It is common to stain the cells with annexin V together with 7-Aminoactinomycin D (7-AAD) or propidium iodide (PI), fluorescent compounds that intercalate in DNA and can only pass through damage cell membranes.[195, 199] However, the fluorescence spectrum of DOX overlaps with the spectra of both dyes and, only staining with annexin V was evaluated.[200] Therefore, we assessed the membrane integrity by the trypan blue exclusion assay. Despite both Dex5/PLGA-DOX and PLGA-DOX NCs have decreased cell viability after 48 h exposure, the NCs prepared with 5%(w/v) of Dex may have induced greater membrane damage levels, corroborating with annexin V apoptosis detection. Although MTT assay is commonly used to verify cytotoxicity *in vitro*, this test has known limitations to assess nanomaterials toxicity.[201-207] MTT assay can misled cell viability due to optical interference.[208-210] For example, MTT assay is reported to overestimate the viability of CHO-K1 cells treated with nanoscale TiO_2 when compared to trypan blue exclusion assay because nanoscale TiO_2 induces O_2^{-2} formation and reduces MTT.[204] The viability of bovine peripheral blood mononuclear cells exposed to $K_2Cr_2O_7$ evaluated by MTT did not match trypan blue exclusion assay due to ROS interference in the MTT results.[211] Superoxide ions can reduce tetrazolium salts and produce the absorbent formazan, therefore MTT assay may not be representative for toxicity of nanomaterial for which induction of oxidative stress is as a key toxicity mechanism.[204, 211-212]

2.4.4 Dex5/PLGA-DOX NCs induces oxidative stress in MCF-7 and H9C2

To evaluate ROS production, free DOX, Dex5/PLGA-DOX, Dex1/PLGA-DOX and PLGA-DOX NCs were incubated 2 h at 37°C with MCF-7, H9C2 and RAW 264.7 cells, and ROS generation was detected by oxidation of 2'-7'-dichlorohydrofluorescein diacetate (CM-H_2DCFDA) using flow cytometry. DOX dosage was the same for all experimental groups (12.5 µg ml^{-1}). Although free dextran 40 exhibits hydrogen peroxide scavenging activity,[213] Dex5/PLGA-DOX NCs induced higher generation of reactive oxygen species (ROS) in MCF-7 (Fig. 5a) and H9C2 (Fig 5b) compared with Dex1/PLGA-DOX, PLGA-DOX NCs and free DOX. Oxidative stress is one of the main DOX toxicity mechanisms,[151] which might explain the increased generation of ROS associated with the larger amount of DOX per particle. thus, the increased ROS generation after 2 h of incubation, besides the larger amount of DOX per particle. It has been reported that faster iron ion release by dextran-coated iron oxide nanoparticles (IONs) may contribute to the generation of ROS compared to PEG-coated IONs, as observed for Dex5/PLGA-DOX NCs (Fig. 2i) where dextran favors water infiltration accelerating NC degradation.[214-215]

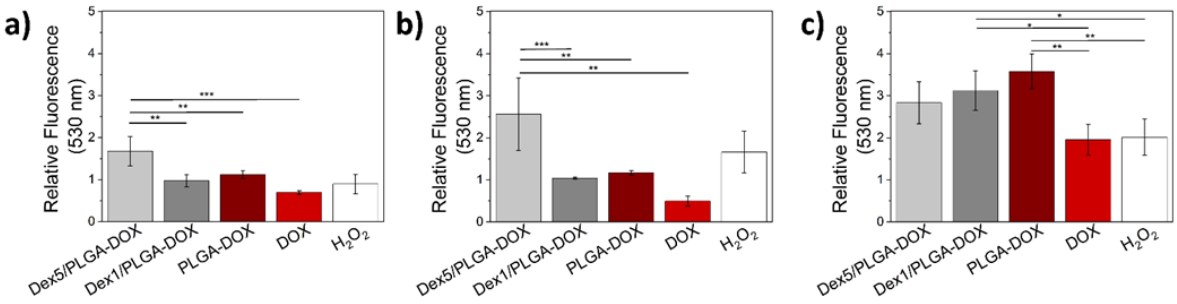

Figure 5 - ROS studies to evaluate oxidative stress induced by free DOX, Dex5/PLGA-DOX, Dex1/PLGA-DOX, PLGA-DOX NCs. Flow cytometry detection of ROS by oxidation 2'-7'-dichlorodihydrofluorescein diacetate (CM-H_2DCFDA) in a) MCF-7, b) H9C2 and c) RAW 264.7 cell lines after incubation for 2 h at 37 °C with the NCs. Statistical analysis was performed using ANOVA with Tukey's post-hoc test. Values represented are mean±SD (n=4). *p-value < 0.05, ** p-value < 0.01, *** p-value < 0.001.

Source: By the author

RAW 264.7 presented similar ROS generation for the NCs with and without dextran (Fig 5c). It was also observed higher ROS levels induced by the NCs than by free DOX, which may be due to inflammation-induced oxidative stress.[158] Macrophages, as professional phagocytic cells, can induce ROS upon NP uptake via the NADPH oxidase enzyme system.[216]

Despite the reduced uptake, Dex5/PLGA-DOX NCs showed higher ROS levels in heart cells indicating that it may cause long-term adverse effects such as irreversible cardiomyopathy and

heart failure, induced by oxidative stress.[151-152, 214] Dextran-coated IONs formerly reported to be safe for stem and other non-neuronal cell types were found to be toxic in neurons, mainly due to oxidative stress.[154] In addition, dextran-coated SPIONs showed genotoxicity caused by oxidative stress at non-cytotoxic concentrations in HepG2 cells.[155]

Oxidative stress effects include DNA damage, mitochondrial dysfunction and membrane damage due to lipid peroxidation.[156] Lipid peroxidation inhibits membrane functions by modifying the dielectric constant and contributing to the depolarization of the membrane potential, which lead to loss of membrane barrier properties and cell death. Also, lipid peroxidation products are highly reactive and can change structure and function of membrane proteins, cytoplasmic enzymes and nucleic acids.[157] Therefore, ROS studies indicate that oxidative membrane damage may be the main cause of the increased toxicity of Dex5/PLGA-DOX NCs assessed by trypan blue exclusion assays and annexin V binding assay.

Besides increasing the circulation time of nanomaterials, dextran can improve drug delivery to tumor tissues due to enzymatic hydrolysis through alpha amylase which is overexpressed in tumor cells. [72-73, 75] In addition, aldehyde dextran nanocarriers loaded with DOX showed poor efficacy in cells monolayers but overperformed free DOX in three-dimensional SK-N-BE(2) tumor spheroids due to improved tumor pemetration.[74] Overall results suggest that 5 %(w/v) of dextran applied as a stabilizing and capping agent in PLGA NCS loaded with DOX may induce ROS imbalance and oxidative membrane damage, collaborating with aggravation adverse effects such as irreversible cardiomyopathy and heart failure, caused by oxidative stress.[151-152, 214] The addition of 1 %(w/v) of dextran in the NCs synthesis did not increase their toxic effect in myocardium cells when compared with PLGA-DOX NCs. Thus, Dex1/PLGA-DOX NCs may be a promising formulation for further investigation as they may improve breast cancer treatment without favoring severe adverse effects.

These results highlight the importance of an in-depth investigation of the NCs-cell interaction considering the mechanisms of damage. The specificity of the toxicity tests must also be considered, since effects including DNA and membrane damage, oxidative stress, and mitochondrial dysfunction can be posed without detectable changes in cytotoxicity assessed by MTT assays.[155,158]

2.5 Conclusions

The DOX-loaded PLGA NCs were prepared by the emulsion diffusion method using Pluronic®-F127 and 0, 1 and 5 %(w/v) of dextran (Dex) as stabilizing agents. The Dex5/PLGA-

DOX NCS showed an increased encapsulation efficiency when compared with Dex1/PLGA-DOX and PLGA-DOX NCs attributed to the Dex arrangement at the NCs shell preventing DOX diffusion to the external aqueous phase during emulsion preparation. Dex5/PLGA-NCs revealed a reduced uptake by myocardium and breast adenocarcinoma cells, which was also reduced for Dex1/PLGA-DOX NCs in the absence of serum, suggesting that protein corona formation is modulated by the amount of dextran in the formulation which was supported by BCA assay and SDS-PAGE of the NCs in the presence of serum. Competitive inhibition with free dextran did not affect the uptake of NCs capped with the polysaccharide in breast adenocarcinoma cells, supporting the hypothesis that the uptake is not receptor-mediated in non-phagocytic cells. Otherwise, RAW 264.7 expresses C-type lectins and scavenger receptors that can mediate Dex uptake, justifying the enhanced uptake of Dex5/PLGA-DOX NCs by this cell line.

All the NCs affect cell viability to the same extent when assessed by MTT, however, Dex5/PLGA-DOX NCs induced greater membrane damage in MCF-7 and H9C2. Nanoparticle-induced damage is not limited to mitochondrial dysfunction, but other mechanisms, e.g., membrane and DNA damage, also correlates with cell death. The higher percentage of early apoptotic cells and membrane-damaged cells triggered by Dex5/PLGA-DOX NCs is correlated with their greater induction of ROS, revealing that membrane damage may be posed by oxidative stress. Since irreversible cardiomyopathy and heart failure are mainly induced by oxidative stress, Dex5/PLGA-DOX may contribute more to the long-term adverse effects than formulations with lower Dex concentrations or without Dex.

3 CHAPTER II: PRO-LEUKEMIC MACROPHAGE-BASED DELIVERY OF NANOTHERAPEUTICS TO ACUTE MYELOID LEUKEMIA

3.1 Abstract

Acute myeloid leukemia (AML) cells recruit macrophages and induce pro-leukemic phenotypes. Known as leukemic-associated macrophages (LAMs), the macrophages promote cancer progression and drug resistance, correlated with poor prognosis. Nevertheless, LAMs intrinsic targeting to cancer cells also allows them to act as transporters of nanocarriers (NCs). We explored the binding between hyaluronic acid (HA) and CD44, a receptor that mediates cell-cell and cell-matrix interaction, to transport a nanotherapeutic to the leukemic cells. To assess the macrophages' ability to effectively deliver NCs via CD44-targeting to AML cells, we studied their interaction with NCs in co-cultures of macrophages and AML cells. Three configurations of NCs based on poly (lactic acid-co-glycolic acid) (PLGA) were evaluated: i) NCs modified with polyethylene glycol (PEG), to evade the immune system; ii) NCs modified with HA, CD44-HA binding and iii) non-modified NCs (carboxyl moiety). Macrophages previously exposed to NCs were co-cultured with AML cells and the uptake and delivery of NCs to AML cells were analyzed by flow cytometry. (PLGA)PEG-HA NCs were more internalized by pro-leukemic macrophages than non-induced or LPS-induced phenotypes, indicating specificity and in agreement with the upregulation of CD44 in pro-leukemic macrophages. (PLGA)PEG-HA NCs interaction with macrophages occurs mostly through adhesion to cell surface, preventing the NCs from lysosomal destruction. In co-culture model, AML-supporting macrophages delivered a greater amount of (PLGA)PEG-HA NCs to C1498 cells than non-induced macrophages. Corroborating, viability assays indicated that (PLGA)PEG-HA NCs loaded with arsenic trioxide (ATO) increase leukemic cell death as a result of the pro-leukemic macrophages acting as bearer of the NCs. Overall, the results provide evidence that macrophage-based delivery of (PLGA)PEG-HA NCs loaded with ATO is a promising strategy to treat AML.

3.2 Introduction

Acute myeloid leukemia (AML) is a severe hematological malignancy marked by the accumulation of undifferentiated myeloid blasts in the bone marrow (BM) and the disruption of normal hematopoiesis.[108] Although it starts in the BM, cells are also often found in the peripheral blood. The disease is caused by genetic mutations and aberrant epigenetic regulation

in hematopoietic stem and progenitor cells, leading to a block in differentiation, increased self-renewal, and dysregulated proliferation.[85] Besides, bone marrow microenvironment (BMME) cues and interaction with resident cells modulate leukemia progression.[103, 121] AML cells are able to re-educate the BMME stromal cells to leukemia-supporting phenotypes via cell-to-cell interaction, secreted factors and signal transduction modulation of transcription factors.[121, 217] Upregulation of mannose scavenging receptors (CD206) expression demonstrates that AML blasts recruit and induce macrophages polarization to anti-inflammatory phenotype with leukemia-supporting and immunosuppressive properties.[126,218] Infiltration of leukemia-associated macrophages (LAMs) into the bone marrow and spleen of AML patients correlates with therapy resistance and inferior patient outcomes.[102,121] Custer determinant 44 (CD44) is a transmembrane adhesion molecule involved in the binding and the metabolism of hyaluronic acid (HA), an important component of the extracellular matrix.[81, 128] HA participates in the regulation of the inflammatory response of macrophages, and low molecular weight HA polarizes macrophages to a pro-inflammatory phenotype while high molecular weight HA induces an anti-inflammatory phenotype.[219] CD44 has been associated to homing efficiency, stemness, engraftment of AML cell, apoptosis and stress resistance in AML cells, and its expression is upregulated in the BM of AML patients.[85,117,129-130] In macrophages, CD44 is highly expressed and its expression levels are affected by macrophage phenotype.[131-132]

Macrophages are a crucial element of the cancer microenvironment due to their role in cancer progression, which also make them suitable targets for targeted cancer treatment. Common therapeutic strategies are: inhibiting the recruitment of monocytes and macrophages, [220] specific LAM depletion, [147] phenotypic reprogramming to M1-like anti-cancer macrophages, [9] and blocking of the CD47-SIRPα pathway [127, 221] Furthermore, as macrophages have long half-lives in the body and natural targeting to cancer cells due to chemotactic mobility, they can be promising tools for drug delivery to cancer cells.[146] Macrophages have a high loading capacity for nanotherapeutics since they can directly phagocytose nanocarriers in the bloodstream.[7] Murine macrophage-like cells RAW 264.7 loaded with free or nano-based doxorubicin (DOX) increased tumor-targeting and anti-cancer efficacy in mice bearing intracranial U87 glioma, 4T1 breast cancer and human breast tumor MCF-7 models.[145,148-149] In addition, murine bone-marrow-derived macrophages (BMDMs) carrying NCs encapsulating tirapazamine improved tumor penetration and drug accumulation in hypoxic areas of 4T1 breast cancer.[7] Solid tumor formation is uncommon in leukemia but the interaction of leukemic cells with macrophages also occurs either through contact-dependent effects (direct cell-to-cell

interactions) or contact-independent effects (via cancer or macrophage-secreted factors).[102, 123] Thus, nanocarriers (NCs) decorated with HA can be used in macrophage-based cancer therapies, exploiting the macrophages as carriers of the NCs.[131,222-226] To assess the macrophages' ability to effectively deliver nanotherapeutics to leukemic cells, we employed co-cultures of macrophages and leukemic cells to better resemble the microenvironment and cell-cell interaction. Three configurations of NCs based on poly (lactic acid-co-glycolic acid) (PLGA) were evaluated: i) NCs modified with polyethylene glycol (PEG), for evasion of the immune system; ii) NCs modified with hyaluronic acid, for interaction with macrophages via the CD44 receptor and iii) non-modified NCs.

3.3 Experimental

3.3.1 Materials

Poly(lactide-co-glycolide) (PLGA) (Resomer 503H 50:50 MW 24000-38000, acid terminated, #719870), Pluronic®-F127 (#P2443), poly(ethylene glycol) bis(amine) (NH_2-PEG-NH_2, Mw 3000, #14502), arsenic trioxide (ATO, #202673), rhodamine B (RhB, #83689), deuterium oxide (D_2O, #151882), chloroform-d (CDCl3, #151823), lipopolysaccharide (LPS, #L4391), hyaluronic acid sodium salt (1500-1800 kDa, #53747), tetrazolium blue thiazolyl bromide (MTT, #M2128), glycine (#G8898), KCl (#C2010.0.AH), NaCl (#C1060.01.AH), KH_2PO_4 (#P9791), Na_2HPO_4 (#S5136), N-hydroxusuccinimide (NHS, #56480), N-(3-dimethylaminopropyl)-N'-ethylcarbodiimide hydrochloride (EDC, #03450), triethylamine (TEA, #T0886), 2-(N-Morpholino) ethanesulfonic acid (MES monohydrate, #69892), dichloromethane anhydrous (DCM, #270997), diethyl ether (#E1017) , methanol (#A1085), acetone (#A1017) and ethylenediaminetetraacetic acid disodium salt dihydrate (EDTA, #E5134) were obtained from Sigma-Aldrich. Trypan Blue Stain (0.4%(w/v)) for use with the Countess™ Automated Cell Counter, Anti-Mo CD80 (B7-1) eBioscience PE-cyanine5 (#15-0801-82), Anti-Mo CD86 (B7-2) eBioscience PE-cyanine5 (#15-0862-82), Anti-Mo CD206 (MMR) eBioscience PerCP-eFluor 710 (#46-2061-82), Anti-Hu/Mo Arginase-1 eBioscience PerCP-eFluor 710 (#46-3697-82), CellTracker Green CMFDA (#C7025) and CellMask Green plasma membrane stain (#C37608), were purchased from Invitrogen™. Dimethyl sulfoxide (DMSO, #D1011.01.BJ) was obtained from Synth. Dulbecco's Modified Eagle Medium (DMEM) culture media with (#D0072) and without phenol (#000394), Fetal Bovine Serum (FBS, #S0011) and L-Glutamine 200 mmol ml^{-1} (#G0209) were obtained from Vitrocell. FITC

Annexin V Apoptosis Detection Kit I (#556547) and PE-Cy7 Mouse Anti-Human CD44 (#560533) were obtained from BD Pharmingen™.

3.3.2 Synthesis of the PLGA-PEG-NH_2 copolymer

The synthesis of PLGA-PEG-NH2 was adapted from Saneja et al.[227] 250 mg of PLGA (Resomer 503H 50:50, MW 24000-38000, carboxylic acid terminated), 42 mg of EDC and 42 mg of NHS were added to 5 ml of DCM anhydrous. The reaction was maintained for 24 h at room temperature under nitrogen atmosphere. The resulting solution was filtered through a syringe filter with a 0.45 µm pore size. The activated PLGA was precipitated with cold diethyl ether and dried under reduced pressure. 200 mg of activated PLGA in DCM were added dropwise to 200 mg of poly(ethylene glycol) bis(amine) (NH2-PEG-NH_2, Mw 3000) in DCM. After, 50 µl of TEA was added to the reaction. The reaction was purged with N_2 for 1 h and then maintained in a closed flask for 24 h under mild stirring at room temperature PLGA-PEG-NH_2 was precipitated with cold diethyl ether, washed three times with cold methanol, and dried under reduced pressure.

Conjugation of NH_2-PEG-NH_2 with PLGA-COOH was confirmed by using Fourier-transform infrared (FTIR) and proton nuclear magnetic resonance (^{1}H NMR) spectroscopy. FTIR spectroscopy was performed in an Infrared spectrometer Nicolet 6700/GRAMS Suite at 128 scans per sample with 4 cm^{-1} resolution from 4000 to 400 cm^{-1}. The samples were prepared by drop-casting 20 µl of the formulations in silicon wafer and dried under reduced. ^{1}H NMR were recorded on an Agilent technologies 400/54 Premium Shielded NMR Magnet at 400 MHz. Approximately 15 mg of PLGA-COOH or PLGA-PEG-NH_2 copolymers were dissolved in 750 µl of chloroform-d (CDCl3) and transferred to a 5 mm NMR tube.

3.3.3 Syntheses of PLGA and PLGA-PEG-NH_2 NCs loaded with RhB or ATO

500 µl of 2.5% (w/v) PLGA-PEG-NH_2 solution was prepared in acetone and kept under stirring for 10 minutes. Then, 1 mL of 2.5% (w/v) Pluronic®-F127 in deionized water (diH_2O)

containing 300 µg of RhB (0.3 mg/ml) or ATO (0.2 mg/ml) was poured onto the organic phase under constant stirring. Acetone was evaporated under reduced pressure in a desiccator.

3.3.4 Conjugation of hyaluronic acid or polyethylene glycol carboxylic acid terminated to (PLGA)PEG-NH_2 NCs

Conjugation of HA with (PLGA)PEG-NH_2 NCs was by EDC/NHS coupling adapted from Saneja *et al*.[227] The carboxylic groups of 5 µg HA in the form of hyaluronic acid sodium salt were activated with 5 µg of EDC and 5 µg of NHS in 300 µl of 10 mM MES monohydrate buffer (pH 5.5) for 30 min. The pH of the solution containing the activated HA was adjusted to 7.0 with 1 M sodium bicarbonate solution and (PLGA)PEG-NH_2 NCs were subsequently added dropwise to the solution. The reaction was kept for another 2 h under mild magnetic stirring and then centrifuged (10000 g, 25 min, 20 °C) and resuspended in 50 mM Tris buffer, pH 8.0, containing 0.1% (w/v) glycine to neutralize the reaction medium. The (PLGA)PEG-HA NCs were recovered by centrifugation (10000 g, 30 min, 20°C). Polyethylene glycol carboxylic acid (PEG(COOH)) terminated conjugation to (PLGA)PEG-NH_2 NCs followed the same protocol as HA conjugation where 5 µg of PEG(COOH) were also activated with EDC and NHS.

3.3.5 Indirect determination of hyaluronic acid conjugation to the PLGA(PEG)-NH_2 NCs

To assess the conjugated amount of HA on the surface of the NCs, the concentration of unconjugated HA present in the supernatant was estimated using the turbidimetric method of hexadecyltrimethylammonium bromide (CTAB).[228] Standard solutions of HA (50 µl, 0.005 – 1 mg ml^{-1}) were prepared in deionized water and added to a 96-well plate in triplicate. After, sodium acetate buffer (50 µl, 0.2 M, pH 5.5) were added and the plate was incubated for 10 min at 37 °C. 100 µl of CTAB solution (10 mM) was added to the wells and the absorbance was measured at 570 nm using the SpectraMax® M3 plate reader (Molecular Devices) controlled by SoftMax Pro software. Calibration curve was obtained by linear regression (Supp Fig. S5). The unconjugated HA was obtained by centrifuging the PLGA(PEG)-HA NCs (10000 g, 30 min, 20 °C) and collecting the supernatant. Measurements were performed in triplicate of independent syntheses. The mass of HA conjugated to the surface of the NCs was estimated by

subtracting the amount of HA present in the supernatant from the initial amount of HA added to the reaction.

3.3.6 Characterization of the NCs

Zeta potential and size distribution of all the nanoparticles (NPs) were measured using Zetasizer Nano ZS, Malvern. The NCs' yield ans size were evaluated by nanotracking analysis (NTA), Nanosight NS300, Malvern. NTA analyses were performed with 50-100 particles/frame and Camera Level of 12 (shutter: 1200; gain: 146).

The (PLGA)PEG-NH_2 NCs conjugation with HA or PEG(COOH) was confirmed by FTIR and ^{1}H NMR. After centrifugation (10000 g, 25 min, 20 °C), the NCs were resuspended in deionized water and added to silicon wafers by drop-casting 20 µl of each sample on its surface. The samples were dried under reduced atmosphere. ^{1}H NMR spectra were recorded on an Agilent technologies 400/54 Premium Shielded NMR Magnet at 400 MHz. (PLGA)COOH, (PLGA)PEG, and (PLGA)PEG-HA NCs were freeze-dried and 2.5 mg of each formulation were dispersed in 600 µL of D2O and transferred to a 5 mm NMR tube prior to analysis.

Cryogenic Transmission Electron Microscopy (Cryo-EM) images were obtained in a JEM-2100 Transmission Electron Microscope. The formulations – (PLGA)COOH, (PLGA)PEG, and (PLGA)PEG-HA NCs – were centrifugated (10000 g, 25 min, 20 °C) and resuspended in deionized water at the concentration of 10^{11} NCs/ml. The samples were prepared by depositing 3 µL of each formulation on a copper grid, the excess was dried for 3 s with filter paper and the grid was dipped in liquid ethane. The samples were vitrified using Vitrobot Mark.

Arsenic trioxide (ATO) encapsulation efficiency was determined by Inductively coupled plasma mass spectrometry (ICP-MS). 1 ml of each nanocarrier formulation – (PLGA)COOH, (PLGA)PEG-NH2, (PLGA)PEG, and (PLGA)PEG-HA NCs – was centrifuged (10000 g, 25 min, 20 °C), the pellets containing the NCs were digested by adding 0.5 mL of HNO_3 and 0.2 mL of 30% (w/v) H_2O_2 to each sample. The samples were heated at 100 °C for at least 2 h within a closed vessel and then diluted to 10 ml with diH_2O. ICP-MS was performed by LabExata using a PerkinElmer's NexION® 2000 instrument. The encapsulation efficiency values were obtained according to equation (1).

$$\%EE = \frac{[ATO]_{in\ the\ NCs}}{[ATO]_{in\ the\ synthesis}} \times 100 \quad (1)$$

3.3.7 Cell culture

Monocyte/macrophage-like cell (RAW 264.7, ATCC) and lymphoblasts from acute myeloid leukemia (C1498, ATCC) of *Mus musculus* were cultured in DMEM supplemented with 10 %(v/v) FBS in 75 cm^2 flasks (Greiner) at 37 °C in humidified atmosphere with 5% CO_2 and cultured to 70% of confluence prior to experiments. C1498 cells, non-adherent cells, were cultured in suspension while RAW 264.7 cells, adherent cells, were cultured in adhered to the surface of the flasks.

3.3.8 Induction of RAW 264.7 macrophages and polarization study

In a 12-well plate, 1 x 10^5 non-activated RAW 264.7 macrophages (MØ) were seeded per well. The macrophages were stimulated for 48 h with 100 ng ml^{-1} of liposaccharides (LPS) (M(LPS)) or conditioned medium from C1498 cells (M(C1498)) and incubated at 37 °C, 5% CO_2 in a humidified atmosphere. 1 x 10^5 C1498 cells were cultured in 10 ml of fresh medium and after 48h the conditioned medium was collected by centrifugation. The macrophages were detached from the plate with a cell scraper. To study the pro-inflammatory phenotype induced by LPS (M(LPS)), cells were centrifuged (500 g, 10 min, 4°C) and resuspended in 200 µl of PBS (pH 7.4) containing 5 mM of ethylenediaminetetraacetic acid (EDTA), 2% FBS, 1 %(w/v) BSA and the antibody anti-CD80 (0.06 µg/ml) or anti-CD86 (2.5 µg/ml) labeled with PE-Cy5 (extracellular staining protocol). To study the anti-inflammatory phenotype induced on macrophages by conditioned medium from C1498 culture, both CD206 and Arg1 intensity were evaluated. Arg1 is a marker predominantly expressed in the cytosol while CD206, despite being present on the surface of macrophages, it is found largely unassociated with the membrane. Thus, for intracellular staining, the cells were washed with PFE buffer, fixed with 3.7% paraformaldehyde (PFA) for 15 minutes, washed again with PFE buffer, centrifuged (500 g, 10 min, 4°C) and resuspended in 200 µl of PBS (pH 7.4) containing 5 mM of EDTA, 2% (v/v) FBS, 1% (w/v) BSA, 0.2% (v/v) Triton X-100 and the antibodies anti-CD206 (0.2 µg/ml) or anti-Arg1 (0.3 µg/ml) labeled with PerCP-eFluor710. During the antibody extra and intracellular staining, the cells were kept at 4 °C for 40 minutes. Then, the cells were washed by centrifugation (500 g, 10 min, 4 °C), resuspended in PFE buffer and kept on ice until the measurement was performed. CD44 intensity was also evaluated in M(LPS), M(C1498) and MØ phenotypes using the extracellular staining protocol with anti-CD44 (2.4 µg/ml) labeled with PE-Cy7. Measurements were performed using the FL3 filter (650/30 nm) of the BD FACS

CalliburTM Flow Cytometer equipped with a laser at 488 nm. Data was analyzed using FlowJo software V10.

3.3.9 Internalization assays

NCs internalization by macrophages and leukemic cells were studied in mono- and cocultures. For the experiment in monocultures, C1498 cells were seeded in 12-well plates, at 1 x 10^5 cells per well and grown for 24 h. 1 x 10^5 MØ macrophages were seeded per well in 12-well plates, stimulated for 48 h with LPS (M(LPS)), conditioned medium from C1498 cells (M(C1498)) or non-stimulated. C1498 cells and the macrophages were exposed to RhB-loaded NCs for 0.5, 1, 2 or 4 h at 37 °C, 5% CO_2. Following incubation, the medium containing the NCs was removed, cells were washed with 1X PBS (pH 7.4) and detached from the plate using a cell scrapper. Samples were centrifuged (4 °C, 500 g, 10 min) and washed with PFE buffer.

To distinguish between the NCs adhered to the cell surface and internalized, the cells were also exposed to the NCs at 4 °C. Before adding the NCs, the cells were incubated for 30 min at 4 °C. Following, cells were exposed to ice-cold NCs for 2 h at low temperature (4 °C). Also, to assess the binding ability of the (PLGA)PEG-HA NCs to HA receptors, CD44, (PLGA)PEG-HA NCs were co-incubated with 50 µg ml^{-1} HA for 2 h at 37 °C. HA was incubated with the cells for 30 min before adding the NCs.

For coculture experiments, 1 x 10^5 MØ macrophages were seeded per well in 12-well plates and stimulated for 48 h with LPS, conditioned medium from C1498 cells or non-stimulated. To distinguish MØ macrophages and C1498 cell in the co-culture experiments, C1498 cells were stained with CellTracker™ Green prior to each incubation with MØ macrophages. Thus, C1498 cells were centrifuged and resuspended in a 2 nM CellTracker™ Green solution prepared in serum free medium at 1 x 10^5 C1498 cells/ml and incubated for 10 min at 37 °C, protected from light. The stained C1498 cells were centrifuged twice (25 °C, 300 g, 5 min) to remove CellTracker™ Green excess and stored at 37 °C in humidified atmosphere with 5% CO_2 until the experiment's next steps.

After induction, the macrophages were exposed to RhB-loaded NCs for 2 h. The medium was removed and the non-interacting NCs were removed by washing the macrophages with PBS pH 7.4. Then, 2.5 x 10^5 C1498 cells prior stained with CellTracker™ Green were added to each well together with the NC-loaded RAW264.7 cells and the plate was incubated for 4 h at 37 °C in humidified atmosphere with 5% CO_2. The cells were detached from the plate with a cell scraper, washed by centrifugation (4 °C, 500 g, 10 min) and resuspended in PFE

buffer. Experiments were performed with a BD FACS Callibur™ Flow Cytometer, equipped with an air-cooled argon-ion laser (488 nm). Emission was measured using FL2 (590/30) and data analysis was performed using FlowJo v10.

3.3.10 Confocal microscopy

Confocal microscopy experiments were performed using a Zeiss LSM900 laser-scanning confocal microscope. For the experiment in monocultures, cells were seeded on coverslips in 12-well plates at 10^4 cells per well. Macrophages phenotypes were induced for 48 h by exposure to LPS and conditioned medium as previously described. Following 48 h induction, cells were incubated with 1 ml of $1x10^{10}$ RhB-loaded NCs per ml for 2 h at 37 °C, 5% CO_2. Following incubation, the media containing the NCs were removed, cells were washed three times with 1X PBS (pH 7.4) and incubated with 5 µg/ml of CellMask™ Green plasma membrane stain for 5 min. At the end of the incubation period, cells were washed three times with 1X PBS (pH 7.4), fixed with 3.7% paraformaldehyde for 10 min, rewashed with PBS and blocked with 2 %(w/v) BSA for 15 min. The cells were rinsed three times with PBS prior to incubation with anti-CD44 (2.4 µg/ml) labeled with PE-Cy7 for 45 min at room temperature, washed again, stained with 0.1 µg/ml Hoechst 33342 for 10 min, washed three times with PBS and one time with ddH_2O. The coverslips were mounted with Fluoroshield medium. At least 3 images were collected per sample from three independent experiments. After acquisition, the Pearson's coefficient of anti-CD44 labeled with PE-Cy7 and RhB-loaded NCs was calculated for 3-5 images using the JACop plugin in Fiji software.

For coculture experiments, 10^4 RAW 264.7 cells were seeded on coverslips in 12-well plates and induced for 48 h before being exposed to RhB-loaded NCs for 2 h, as performed for the monocultures. The media was removed and non-interacting NCs were removed by washing with PBS. Then, 100 µl of PBS containing 10^5 C1498 cells stained with CellTracker™ Green, as described prior at the "Internalization assays" section, were added onto the coverslips as a single drop and together with the NC-loaded RAW264.7 cells already adhered on it. After 30 min, fresh medium was added to each well and the cells were incubated for 4 h at 37 °C in humidified atmosphere with 5% CO_2. After incubation, the medium containing the NCs was removed, cells were washed three times with 1X PBS (pH 7.4) and incubated with 5 µg/ml of CellMask™ Deep Red plasma membrane stain for 5 min. At the end of the incubation period, cells were washed three times with 1X PBS, fixed with 3.7% paraformaldehyde for 10 min,

rewashed with PBS and blocked with 2 %(w/v) BSA for 15 min. The cells were rinsed three times with PBS prior to incubation with 0.1 µg/ml Hoechst 33342 for 10 min, rewashed with PBS and rinsed one time with ddH_2O. The coverslips were mounted with Fluoroshield medium. The images were processed using the Fiji software. Images were collected using three channels and excitation diode lasers 405 nm and 561 nm.

3.3.11 Cumulative release of rhodamine B from NCs from RAW 264.7

RAW 264.7 macrophages were seeded in 12-well plates at 10^5 cells per well and MØ, M(LPS) and M(C1498) phenotypes were induced for 48 h. The cells were exposed to (PLGA)COOH, (PLGA)PEG, and (PLGA)PEG-HA NCs loaded with RhB for 2 h, washed once with PBS pH 7.4 and incubated in 1 ml of fresh media without phenol at 37 °C. After 1, 4, 8, 12, 24 and 48 h, the medium was collected, centrifugated (25 °C, 500 g, 5 min), and supernatant fluorescence intensity was measured using a SpectraMax® M3 plate reader (Molecular Devices), controlled by SoftMax Pro software at 590 nm (exc: 480 nm). After sample collection, the cells were incubated again with 1 ml of fresh media under the same conditions.

The cumulative release (CR) values were obtained according to equation (2), with the percentage released (% released(t)) calculated by equation (3)

$$\%\, CR = \%\, released(t-1) + \%\, released(t) \quad (2)$$

$$\%\, released = \frac{\mathrm{FLU}_t}{FLU_{Total}} \cdot 100 \quad (3)$$

where FLUt is the fluorescence of at 590 nm of the sample at time t, and FLU_{Total} is the fluorescence of the NC-loaded RAW 264.7 cells at t=0. FLU_{total} was obtained by a control experiment in which the cells were destroyed by adding 1 ml of DMSO to each well right after exposure to the NCs loaded with RhB for 2 h and wash with PBS pH 7.4. The fluorescence intensity of the resultant solution was measured similarly to the samples collected.

3.3.12 Cell viability in monoculture and coculture models

Cell viability was assayed by the tetrazolium reduction colorimetric method and propidium iodide (PI) method, respectively. In tetrazolium reduction colorimetric assay, 3-(4,5-dimethylthiazol-2-yl)-2,5-diphenyltetrazolium bromide (MTT, #M2128) is reduced to

formazan by the action of NAD(P)H dependent oxidoreductases. Monoculture assays were performed in 96-well clear plates with flat bottom. 5 x10^3 C1498 cells were seeded per well and grown for 24 h before being exposed to the NCs for 24h. To assess cell viability of MØ, M(LPS) and M(C1498) macrophages, 5 x 10^3 MØ macrophages were seeded per well and induced with LPS or conditioned C1498 medium, or non-induced for 48 h before being exposed to ATO-loaded NCs for 24 h. For coculture experiments, the seeding and macrophage induction was performed as described for monoculture experiments. After, the media was removed and non-interacting NCs were removed by washing with PBS. 2.5 x 10^5 C1498 cells were added to each well together with the NC-loaded RAW264.7 cells and the plate was incubated for 24 h at 37 °C in humidified atmosphere with 5% CO_2. The C1498 non-adherent cells were removed together with media, placed on another 96-well plate and formazan was solubilized by 100 µl of isopropanol 4 mM HCl prior to the absorbance measurement. The macrophages remain adherent to the bottom of the plate, and it was added 100 µl of DMSO to the each well to solubilize the formazan prior to absorbance reading. The absorbance was measured using a SpectraMax® M3 plate reader (Molecular Devices), controlled by SoftMax Pro software at 570 and 630 nm, for mono and co-culture assays. (PLGA)COOH and (PLGA)PEG-HA NCs were tested at an ATO dosage of 1.2 µg ml^{-1}.

Propidium iodide (PI) is a red-fluorescent dye that binds to DNA by intercalating between the bases. Membranes of viable cells exclude PI, however, dead or damaged cells are permeable to PI. In a 12-well plate, 2.5 x 10^5 C1498 cells were seeded in each well and grown for 24 h. Also, 1 x 10^5 MØ macrophages were seeded per well in 12-well plates and induced with LPS, conditioned C1498 medium or non-induced for 48 h. The C1498 cells and macrophages were exposed to the NCs at 1.2 µg ml-1 of ATO (2.2 x 10^{10} (PLGA)COOH NCs/ml, 7.0 x 10^{10} (PLGA)PEG-HA NCs/ml and 2.5 x 10^{10} (PLGA)PEG NCs/ml) for 24 h. Culture medium was removed, the cells were detached from the plate with a cell scraper, collected and washed by centrifugation (4 °C, 500 g, 10 min) and, resuspended in 1X Annexin V Binding Buffer provided with the FITC Annexin V Apoptosis Detection Kit I. The samples were stained with 5 µl of PI staining solution per test and incubated protected from light for 15 min. For co-culture experiments, 1 x 10^5 RAW 264.7 cells were seeded in 12-well plates and polarized for 48 h before being exposed to ATO-loaded NCs for 2 h. After removing the medium and washing with PBS (pH 7.4) to remove non-interacting NCs, 5 x 10^4 C1498 cells stained with CellTracker™ Green were added to each well together with the NC-loaded Raw 264.7 cells. The cocultures were incubated for 24 h at 37 °C in humidified atmosphere with 5% CO_2. The macrophages were detached from the plate with a cell scraper and collected together with the

C1498 cells. The cells were washed by centrifugation (4 °C, 500 g, 10 min), resuspended in 100 µl of 1X Annexin V Binding Buffer and stained with 5 µl of PI staining solution provided in the kit and incubated in dark for 15 min. The measurements were performed immediately in a BD FACS Callibur™ Flow Cytometer equipped with one laser (488 nm). Emission was measured using FL1 (630/30) and data analysis was performed using FlowJo v10.

3.4 Results and Discussion

3.4.1 ATO-loaded NCs characterization

The hydrodynamic diameter of ATO-loaded (PLGA)COOH, (PLGA)PEG, and (PLGA)PEG-HA NCs measured by DLS and NTA showed a larger size for NCs containing HA on the surface when compared with the others NCs (Table 2 and Fig.6 a-c). The hydrodynamic radius of the 1430 ± 40 kDa HA fragment determined by size exclusion chromatography correspond to 81 ± 1 nm.[229] The increase in the hydrodynamic diameter of the (PLGA)PEG-HA NCs may be due to the hyaluronic acid molecules conjugated to the NCs (1500 – 1800 kDa) and the random coupling of HA chain to (PLGA)PEG-NH_2 NCs, since HA molecules have several carboxylic groups that can be activated by EDC/NHS.

The NCs were visualized by Cryo-EM microscopy (Fig. 6d, 6e and 6f). Zeta potential (ζ-potential) was also determined for all formulations (Table 2 and Fig. 6g) and was significantly lower for (PLGA)PEG-HA NCs than (PLGA)COOH and (PLGA)PEG NCs due to HA (negatively-charged molecule) conjugated on the surface of the NCs, in accordance with previous reports.[227, 230] On the other hand, PEG reduced the overall negative surface charge and increased the ζ-potential of (PLGA)PEG NCs compared to (PLGA)COOH and (PLGA)PEG-HA NCs. The particle yield – particles number per ml - was estimated using NTA and exhibited no significant difference between the NCs (Table 2 and Fig. 6h). Encapsulation efficiency (EE) of ATO in each NCs formulation was determined by ICP-MS (Table 2 and Fig. 6i). The EE was 4.4 ± 0.8 % for (PLGA)COOH NCs, 1.2 ± 0.2 % for (PLGA)PEG NCs and 4.9 ± 0.3 % for (PLGA)PEG-HA NCs, corresponding to 45 ± 4, 13 ± 2 and 49 ± 16 µM, respectively. ATO IC50 is in the range of 0.9, 0.5, 1.3 and 2.9 µM for acute promyelocytic leukemia NB4, acute lymphocytic leukemia CCRF-CEM, acute lymphoblastic leukemia SUP-B15 and acute promyelocytic leukemia HL-60 cell lines, respectively.[231-232] Thus, despite the low encapsulation efficiency, the amount of ATO into the NCs is relevant for leukemia treatment. RhB-loaded NCs used for NC-cellular interaction studies performed by flow cytometry were

also characterized and showed homogeneously distributed sizes (PdI < 0.2, Table S1) and size populations are represented in Fig S1a.

Table 2 - Characterization of ATO-loaded (PLGA)COOH, (PLGA)PEG, and (PLGA)PEG-HA nanocarriers. NTA size (diameter), Z-average (PdI), Cryo-EM size (diameter), ζ-potential, particle yield (number of NCs per ml), and ATO concentration of the NCs. Statistical analysis was performed using ANOVA with Tukey's post hoc test. Values represented are mean ± SD of independent syntheses (n=4). * Significantly different from (PLGA)PEG NCs with p-value < 0.05. # Significantly different from (PLGA)PEG-HA NCs with p-value < 0.05. & Significantly different from (PLGA)PEG-HA NCs with p-value < 0.05. $ Significantly different from (PLGA)PEG NCs with p-value < 0.05. @ Significantly different from (PLGA)PEG-HA NCs with p-value < 0.05. % Significantly different from (PLGA)PEG-HA NCs with p-value < 0.05. ** Significantly different from (PLGA)PEG NCs with p-value < 0.01. ## Significantly different from (PLGA)COOH NCs with p-value < 0.01. *** Significantly different from (PLGA)PEG NCs with p-value < 0.005. ### Significantly different from (PLGA)PEG-HA NCs with p-value < 0.005. &&& Significantly different from (PLGA)PEG-HA NCs with p-value < 0.005. $$$ Significantly different from (PLGA)PEG NCs with p-value < 0.005. @@@ Significantly different from (PLGA)PEG NCs with p-value < 0.005.

	NTA size (nm) (D90)	**Z-average (nm) (PdI)**	**Zeta potential (mV)**	**Particle yield (10^{12} NCs/ml)**	**EE (%)**
(PLGA)COOH NCs	183 ± 44 $^{\$}$ (244 ± 19)	181 ± 5 $^{**, \%}$ (0.06 $^{\$\$\$, \#\#\#}$)	-33.9 ± 0.8 $^{***, @}$	11 ± 5	4.4 ± 0.8 *
(PLGA)PEG NCs	127 ± 51 (176 ± 28)	143 ± 7 $^{\&}$ (0.19)	-15.2 ± 0.2 $^{\&\&\&}$	11 ± 1	1.2 ± 0.2 $^{\#}$
(PLGA)PEG-HA NCs	202 ± 70 $^{\#\#}$ (296 ± 36)	214 ± 5 (0.34$^{@@@}$)	-41 ± 2	7 ± 2	4.9± 0.3

Source: By the author

The conjugation of HA or PEG carboxylic acid terminated to (PLGA)PEH-NH_2 NCs was confirmed by an amide peak between δ 4.0 – 4.2 in the 1H-NMR spectrum of (PLGA)PEG-A and (PLGA)PEG NCs (Fig S4). Also, the mass of HA bounded to the surface of the (PLGA)PEG-AH NCs loaded to ATO and RhB were determined by the CTAB turbidimetric method, which indicated 3.4 ± 0.4 and 2.3 ± 0.6 μg (mean ± SD, n=6) of HA conjugated to the surface of NCs, resulting in 19.5 ± 2.3 molecules/NC and 13.1 ± 2.8 molecules/NC, respectively. The conjugation efficiency was equal to 68 ± 7 % and 46 ± 13% for the NCs loaded to ATO and RhB, respectively.

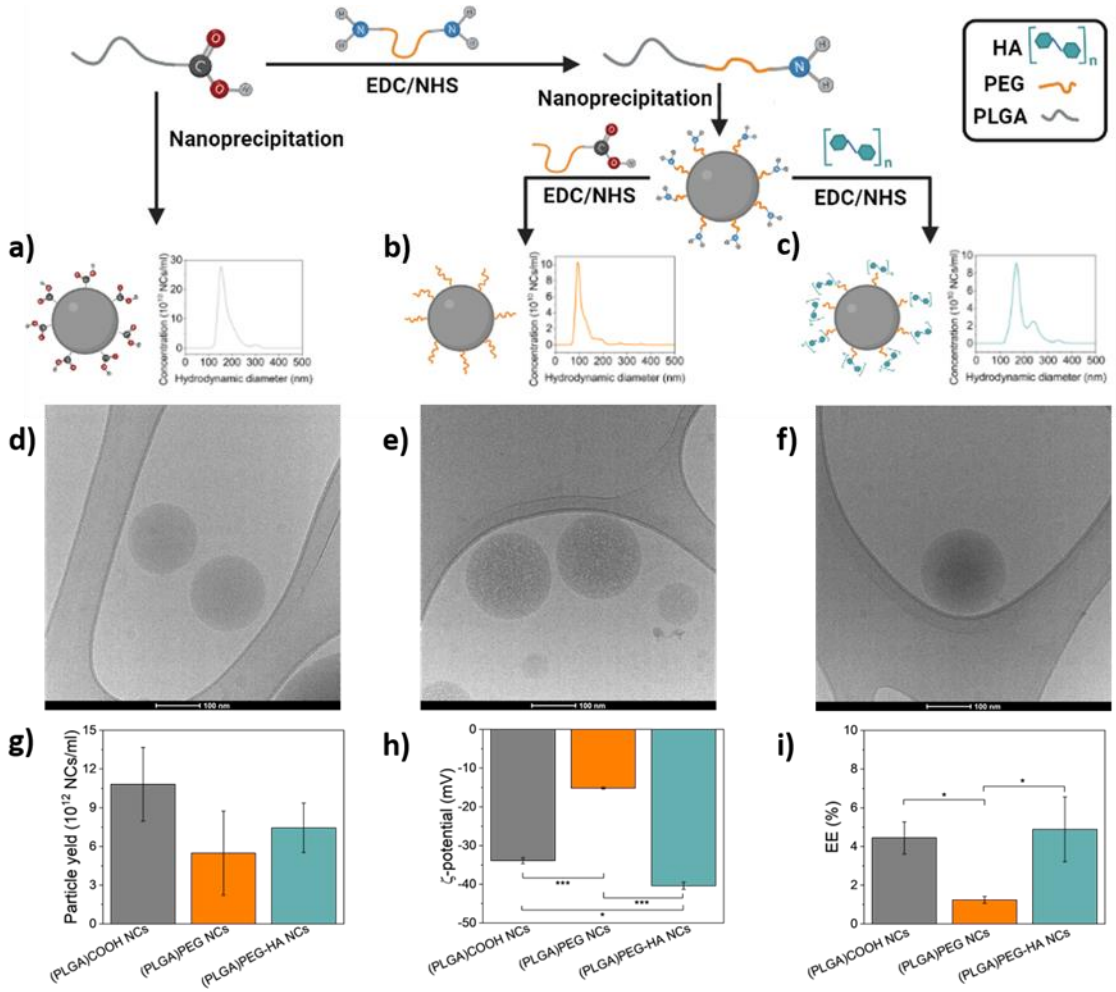

Figure 6 - Characterization of the (PLGA)COOH, (PLGA)PEG, (PLGA)PEG-HA NCs. NTA size distribution of a) (PLGA)COOH NCs, b) (PLGA)PEG NCs and c) (PLGA)PEG-HA NCs with respective representative Cryo-EM images in d), e) and f). g) Particle yield (number of NCs per ml), h) ζ-potential and, i) ATO encapsulation efficiency (EE). Statistical analysis was performed using ANOVA with Tukey's post hoc test. Values represented are mean ± SD of four batches (n=4). *p-value < 0.05, *** p-value < 0.001.

Source: By the author

3.4.2 Macrophages phenotype induced by conditioned medium from leukemia cells increases CD44 intensity and benefits interaction with PLGA(PEG)-HA NCs

Macrophages are highly plastic cells that respond to extracellular cues by adopting different functional phenotypes that differ in terms of receptor expression, cytokine production, effector function, and repertoire of chemokines. RAW264.7 macrophages were stimulated with LPS (M(LPS)) or conditioned medium from C1498 (M(C1498)) for 48 h to simulate two phenotypes, pro- and anti-inflammatory, followed by quantification of the phenotypic markers

CD80, CD206 and Arg-1, and CD44 receptor by flow cytometry. LPS exposure increased CD80 intensity probably due upregulation of CD80 expression, a standard marker of pro-inflammatory M1-like phenotype (Fig. 7a). Pro-inflammatory macrophages are effector cells responsible for detection, phagocytosis and destruction of microorganisms and cancer cells, and are characterized by an increase in expression of markers such as CD80, CD86 or CD38. In leukemia, M1-like macrophages exhibit anti-leukemia and immunostimulatory functions, reducing cancer drug resistance.[102] The macrophages exposed to conditioned medium from C1498 cells (M(C1498)) showed increased intensity of CD206 and Arg-1, associated markers for anti-inflammatory M2-like phenotype (Fig. 7c). *In vitro*, *in vivo* and clinical models reported that macrophages polarized by AML blasts have upregulated CD206 expression, and have leukemia supporting and immunosuppressive properties.[121, 125-126] Also, infiltration of anti-inflammatory macrophages into BM is related to drug resistance in AML patients.[125] CD44 is an adhesion molecule involved in the regulation of adhesion and homing to BM, mobilization of leukemia-initiating cells, and its expression level in BM correlates with worse prognosis in leukemias.[117,133] CD44 is also expressed in leukemic stem cells (LSCs) and plays an important role in homing and engraftment of LSCs within the osteoblast-rich area of the bone marrow, retaining their ability to initiate and maintain the leukemic clonal hierarchy and favouring drug resistance and AML relapse.[85,118] Administration of monoclonal antibody directed to CD44 prevent AML-LSCs interaction with stem cell–supportive microenvironmental niches, leading to AML eradication.[85] In macrophages, CD44 regulates macrophage migration and $CD44^{-}$ macrophages are less sensitivite to chemoattractants.[133] Thus, CD44 intensities were determined for non-activated (MØ), M(LPS) and M(C1498) macrophages (Fig. 7b). M(C1498) phenotype showed increased CD44 intensity while M(LPS) macrophages CD44 intensity remains at the same level as non-induced macrophages. Previous observations by Rios de la Rosa *et al*. suggest that CD44 was downregulated in M2-like THP-1 macrophages.[131]Macrophage activation exists on a spectrum and different stimuli may lead to various phenotypes.[233] Some authors, subdivide M2 macrophage into M2a, M2b, M2c, and M2d phenotypes, which differ from each other in polarizing cytokines, protein expression and function.[234] IL-4 and IL-13 cytokines induce M2a macrophages, a wound-healing phenotype, while TAMs are known to be M2d macrophages.[234] Growth factor independence 1 (Gfi1) is crucial for the induction of M2 macrophage phenotype by C1498GFP AML cells *in vitro* and *in vivo*.[121] Gfi-1 induced macrophages presented a $Ly6C^{-}CD206^{+}$ M2-Like phenotype and differs from macrophages induced by IL-4, that showed an enhanced differentiation into $Ly6C^{+}CD206^{+}$ and $Ly6C^{+}CD206^{-}$ phenotypes.[121] Rios de la Rosa et al. induced M2-like THP-

1 macrophages by exposing the cells to IL-4 and IL-13 for 24 h, which may result in a different receptor expression pattern or phenotype subtype than M(C1498) phenotype, induced by conditioned medium from leukemic cells.

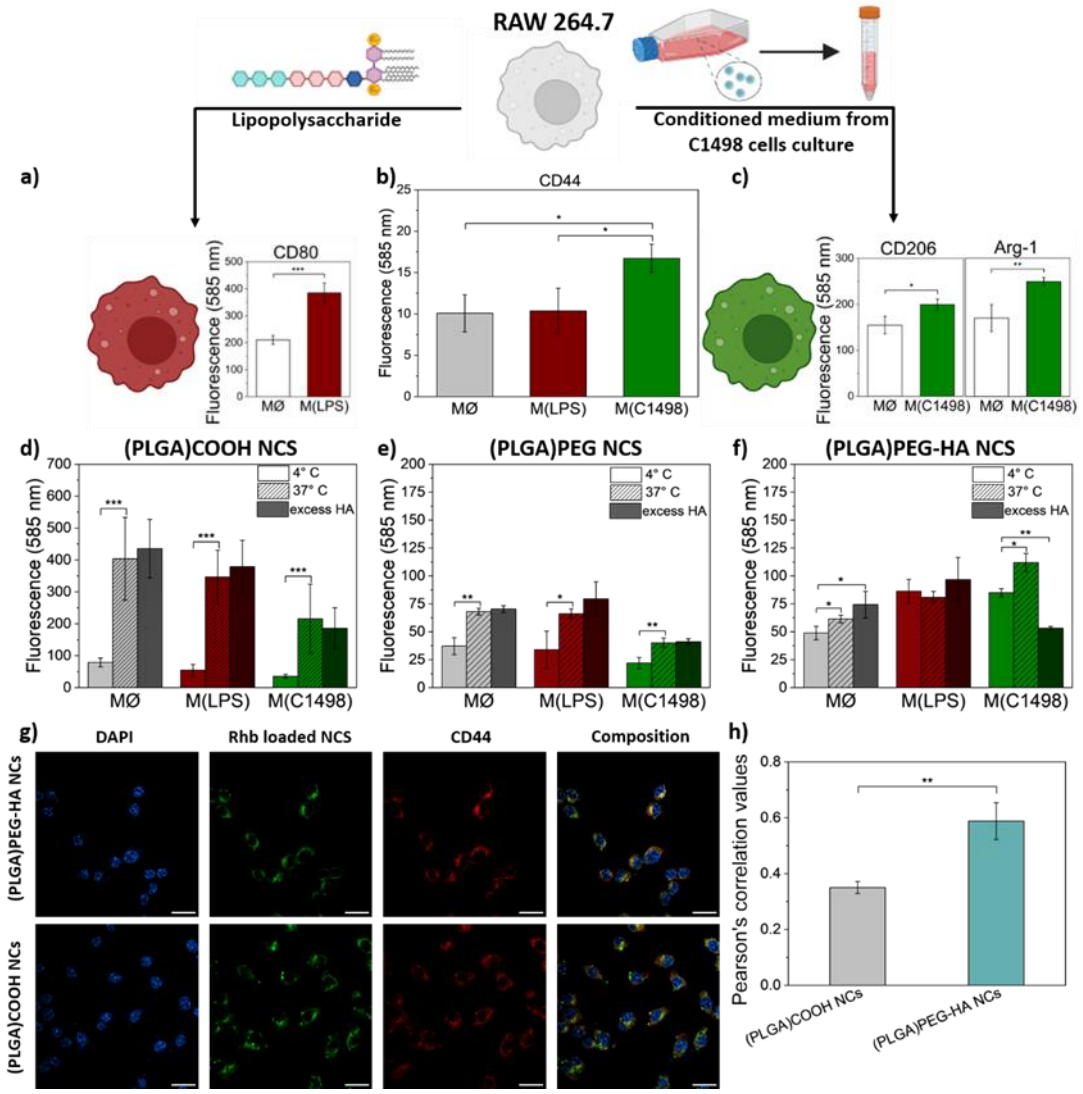

Figure 7 - RAW 264.7 phenotypes protein intensity and interaction with (PLGA)COOH, (PLGA-PEG and (PLGA)PEG-HA NCs. The intensity of a) CD80, b) CD44, c) Arg-1 and CD206 on MØ, M(LPS) and M(C1498) RAW 264.7 macrophages were evaluated via flow cytometry using fluorescent-labelled primary antibodies. In vitro cell-NC interaction study between d) (PLGA)COOH, e) (PLGA)PEG and f) (PLGA)PEG-HA NCs and RAW 264.7 macrophages at 4° C, 37° C and excess HA via flow cytometry. g) Confocal microscopy of M(C1498) RAW 264.7 macrophages incubated with RhB-loaded (PLGA)COOH and (PLGA)PEG-HA NCs for 2 h at 37 °C. Scale bar: 15 µm. h) Pearson's correlation value of RhB-loaded NCs and anti-CD44 labeled with PE-Cy7. The experiment was performed at 37, 4 °C and in the absence of HA or with media containing 50 µg of HA. Values represented are mean ± SD (n=4). *p-value < 0.05, ** p-value < 0.01, *** p-value < 0.001.

Source: By the author

To evaluate whether the CD44 intensity levels affect NCs interaction with the macrophages phenotypes, macrophages were exposed to RhB-loaded (PLGA)COOH (Fig. 7d), (PLGA)PEG (Fig. 7e) and (PLGA)PEG-HA NCs (Fig. 7f) for 2 h at 4 and 37 °C (in medium

without HA or with excess of HA, 50 µg/ml,) and interaction was evaluated by flow cytometry. At 4 °C, the active energy-mediated processes of the cells are paralyzed, thus energy-dependent endocytosis is ceased. (PLGA)COOH NCs had a great interaction with all phenotypes at 37 °C, but without specifically targeting any of the phenotypes (Fig. 7d). Interaction was markedly reduced at 4 °C, indicating that (PLGA)COOH NCs are highly internalized by the cells but do not adhere to a great extent to cell surface. (PLGA)PEG NCs had little interaction with macrophages at 37 and 4 °C (Fig. 7e). PEG provides a steric barrier to the surface of NCs by reducing opsonization and preventing recognition of NCs by macrophages, thus preventing NCs from being detected, phagocytosed and, destroyed.[235] Competition with free HA did not affect the interaction between PLGA(COOH) or (PLGA)PEG NCs and any of the macrophages phenotypes, suggesting CD44-independent endocytosis. However, (PLGA)PEG-HA NCs interaction with M(C1498), was evidently reduced by competitive inhibition with free HA (Fig. 7f), suggesting receptor-mediated adhesion and endocytosis and, at 37 °C, (PLGA)PEG-HA NCs associated fluorescence was higher in M(C1498) than in MØ and M(LPS) phenotypes (Fig. 7f), which correlates with CD44 increased intensity in the pro-leukemia phenotype, M(C1498). HA coated NCs have already been reported to target anti-inflammatory macrophages associated to breast cancer and glioma.[222,236] At 4 °C, macrophages interaction with (PLGA)PEG-HA NCs (Fig. 7f) was greater than with (PLGA)COOH (Fig. 7d) and (PLGA)PEG NCs (Fig. 7e), suggesting that cell interaction with (PLGA)PEG-HA NCs occurs mainly through adhesion. Considering the experiment at 37° C as 100 % of the NC-cell interaction (adhesion and uptake), the *in vitro* cellular adhesion/interaction rate (A/I%) is calculated by the equation $A/I\% = \frac{FLU_{4\,°C}}{Flu_{\,37\,°C}} \times 100$ (Supp Fig S7). (PLGA)PEG-HA NCs adhesion corresponds to 76 ± 9% (mean ± SD, n=4) of NC-cell interaction with M(C1498), while the adhesion of (PLGA)COOH and (PLGA)PEG NCs correspond to 20 ± 11% and 47 ± 9% of the NC-cell interaction with M(C1498), respectively. The greater adhesion/interaction rate of (PLGA)PEG-HA NCs in C1498 macrophages agrees with the upregulation of CD44 in M(C1498) phenotype. In accordance, CD44 expression by human THP-1 macrophages correlates positively with adhesion of HA-based NCs.[131] However, increasing levels of CD44 expression reduces the amount of internalized HA material, indicating that CD44 may capture the HA-based NCs and prevent its interaction with other receptors that triggers uptake.[131] Thus, the HA-coated NCs adhere to M(C1498) phenotype surface rather than be internalized by this phenotypes due to increased CD44 expression.

Confocal laser scanning microscopy images of M(C1498) macrophages incubated for 2 h with the NCs were obtained (Fig. 7g) and the co-localization of anti-CD44 and (PLGA)COOH or (PLGA)PEG-HA NCs were assessed by calculating the Pearson's correlation values (r) (Fig. 7h). (PLGA)PEG-HA NCs showed a strong positive correlation (r = 0.59 ± 0,06) with anti-CD44, corroborating with the competitive inhibition with free HA results. Together, these results provide evidence that (PLGA)PEG-HA NCs interact with the M(C1498) cells via CD44 receptor. It has already been reported that HA-based NCs uptake by human macrophages (THP-1) is triggered by NC-CD44 interaction.[131] CD44 is also overexpressed in several cancer cells and has been shown to mediate HA-conjugated NCs uptake in human lung carcinoma epithelial cells (A549), human breast cancer cells (MDA-MB-231 and MCF7) and human glioblastoma cells (A172, U251 and U87MG).[51,237-238] HA-decorated NCs loaded with doxorubicin and irinotecan were reported to effectively target CD44 expressed by cancer stem cells, reduce drug efflux from cancer stem cells and reduced drug resistance by inhibiting the activity of topoisomerases I and II.[49] (PLGA)COOH NCs presented mild correlation with anti-CD44 (r = 0.35 ± 0,02) justifying the NC-cell interaction non affected by competitive inhibition with free HA (Fig. 7d).

3.4.3 Leukemia associated anti-inflammatory macrophages effectively deliver HA decorated NCs to AML cells

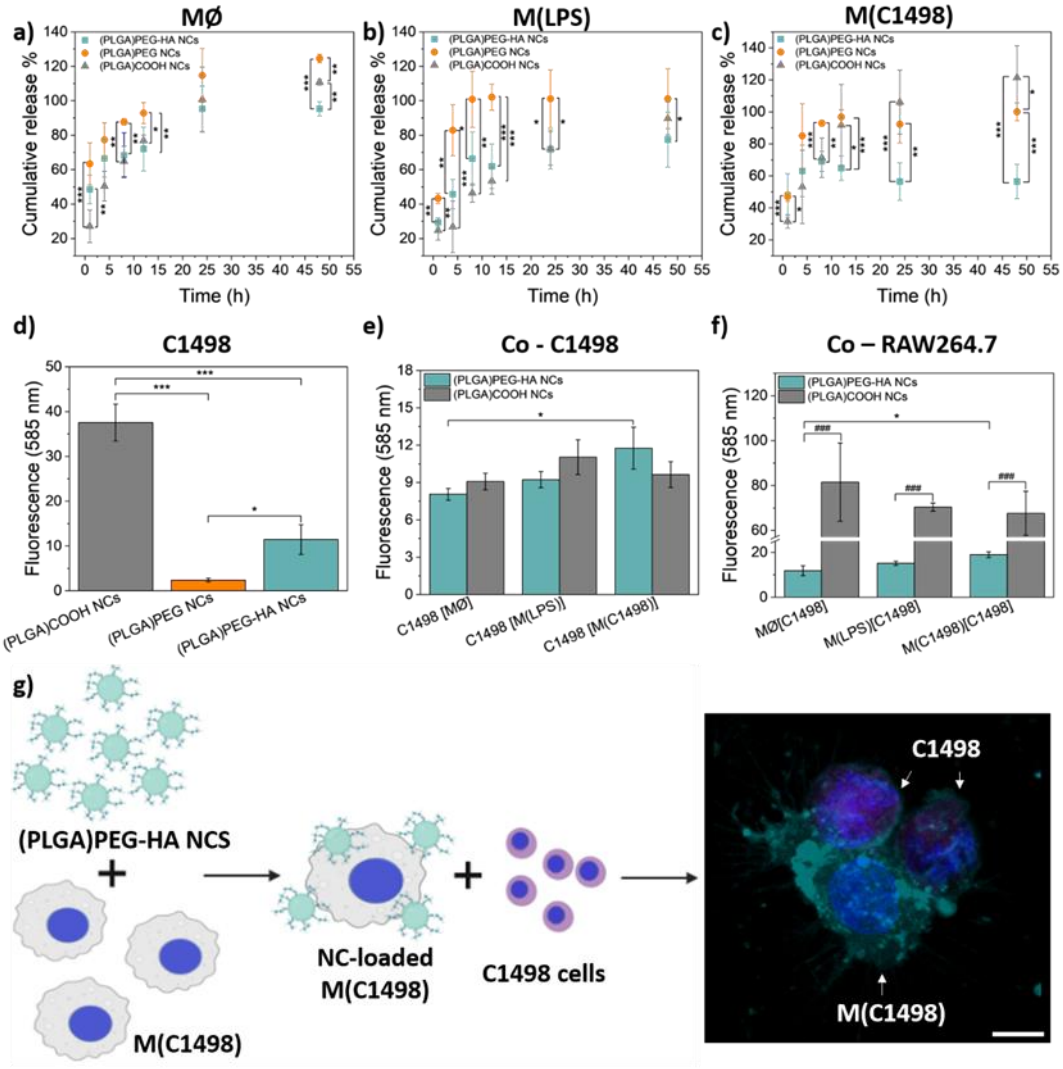

Figure 8 - Studies of RAW 264.7 macrophages as carriers of (PLGA)COOH, (PLGA)PEG and (PLGA)PEG-HA NCs. Cumulative release of (PLGA)COOH, (PLGA)PEG and (PLGA)PEG-HA NCs loaded with RhB from a) MØ, b) M(LPS) and c) M(C1498) RAW 264.7 macrophages. d) In vitro cellular interaction at 37° C of (PLGA)COOH, (PLGA)PEG and (PLGA)PEG-HA NCs with C1498 cells. e) In vitro cellular interaction of (PLGA)COOH and (PLGA)PEG-HA NCs with C1498 cells after 4 h of co-culture with NC-loaded macrophages. f) Remaining NC-cell interaction of NC-loaded RAW 264.7 macrophages after 4 h of co-culture with C1498 cells. g) M(C1498) macrophage prior loaded with (PLGA)PEG-HA NCs (cyan) delivering them to C1498 cells (magenta) after 4 h pf co-culture. Nuclei represented in blue. Scale bar: 15 µm. Statistical analysis comparing phenotypes was performed using ANOVA with Tukey's post-hoc test and statistical analysis comparing the NCs was performed using Student t-test. Values represented are mean ± SD (n=4). *p-value < 0.05, ** p-value < 0.01, *** p-value < 0.001, ### p-value < 0.001.

Source: By the author

MØ, M(LPS) and M(C1498) macrophages were exposed to RhB-loaded (PLGA)COOH, (PLGA)PEG and (PLGA)PEG-HA NCs for 2 h. The release of RhB from (PLGA)PEG-HA NCs was slower in all phenotypes compared to the other NCs (Fig. 8a-c) and, it did not reach 100% release after 48 h with M(LPS) (Fig. 8b) and M(C1498) (Fig. 8c) macrophage phenotypes. For M(LPS) and M(C1498) phenotypes, interaction with HA-modified NCs occurs mostly through adhesion (Fig. S7), which prevents the NCs from being degraded by the lysosomes after endocytosis and release RhB. In addition, NCs enter the cells through different endocytic pathways and not all the pathways lead to the lysosomes, for example, some pathways end up recycling the cargo to the cell surface.[180] CD44 enters cells via a clathrin-independent pathway and avoids the degradative lysosomal pathway, [239] however it was not tested whether CD44 trafficking route can influence the fate of nanoparticles containing HA. HA-liposome uptake positively correlates with CD44 receptor density and occurs via lipid raft-mediated endocytosis, ending up at primarily endosomes and lysosomes of the human lung carcinoma epithelial cell line A549 after 2 h treatment.[237] Although, HA hydrogels nanoparticles are shown to enter the A549 cells through CD44-mediated endocytosis and co-located with endosomes and lysosomes after 2 h incubation, the HA hydrogel particles also escape to the cytoplasm of A549 cells after 4 h of treatment.[240] CD44-mediated uptake also led to HA-conjugated liposome lysosomal evasion in GBM cells, while increasing lysosome co-localization in astrocytes and microglia cells.[51]

To assess the macrophages' ability to effectively deliver the NCs to C1498, we studied the uptake of the (PLGA)COOH and (PLGA)PEG-HA NCs loaded with RhB in C1498 co-culture with MØ, M(LPS) and M(C1498) macrophages. The macrophages were exposed to the NCs for 2 h, washed with PBS and C1498 cells were incubated with the NC-loaded macrophages for 4 h. After co-culture, C1498 and MØ, M(LPS), and M(C1498) interaction with NCs were studied using flow cytometry. (PLGA)COOH NCs were similarly delivered to C1498 by all macrophage phenotypes, consecution of its high uptake by all phenotypes and C1498 cells. On the other hand, M(C1498) delivered a greater amount of (PLGA)PEG-HA NCs to C1498 cells than MØ macrophages probably due to their greater adhesion on M(C1498) surface.

To visualize the interaction of NC-loaded macrophages and leukemic cells, confocal microscopy images of co-cultures of M(C1498) macrophages prior to load with (PLGA)PEG-HA NCs and C1498 cells were obtained (Fig. 8g). Despite not having been exposed directly to NCs, it is possible to observe that there are (PLGA)PEG-HA NCs interacting with C1498 cells,

restating M(C1498) macrophages ability to delivery (PLGA)PEG-HA NCs to C1498 cells. Also, cell-to-cell interaction of M(C1498) and C1498 cells shown in Fig. 8g suggests that macrophages deliver the NCs to C1498 cells mainly by cell contact instead of releasing the NCs on the medium. M1 RAW 264.7 macrophages delivery doxorubicin to human ovarian cancer cell line SKOV3 through the cell-to-cell tunneling nanotube pathways, leading to ovarian carcinoma cell death.[150] In AML, cell-to-cell interaction of macrophages and AML blasts occurs, inducing macrophage polarization to a leukemia-supporting phenotype and activating pro-survival pathways and inhibition of apoptosis in AML blasts.[102]

3.4.4 Macrophage-mediated delivery of (PLGA)PEG-HA NCs to AML cells is more effective than the free NCs

To study the toxicity of the NCs in monocultures of MØ, M(LPS), M(C1498) (Fig. S8) and C1498 (Fig. 9a) cells were incubated with (PLGA)COOH and (PLGA)PEG-HA NCs loaded with ATO at 37 °C for 24 h. ATO dosage was 1.2 μg ml^{-1}. Incubation with (PLGA)PEG-HA NCs reduced M(C1498) macrophages viability assessed by MTT (Fig. S8a) and increased the amount of PI positive (PI^+) cells (Fig. S8c), indicating that (PLGA)PEG-HA NCs induce greater toxicity in M(C1498) than in MØ and M(LPS) phenotypes. This result correlates with the *in vitro* cellular interaction studies that showed an increased NC-cell interaction of (PLGA)PEG-HA NCs with this macrophage phenotype. However, despite the high uptake of PLGA(COOH) NCs by all macrophage phenotypes (Fig. 7d), treatment with (PLGA)COOH NCs did not reduce cellular viability assessed by MTT assays compared to (PLGA)PEG-HA NCs (Fig. S8a). In monocultures of M(C1498), (PLGA)COOH NCs treatment also led to a lower percentage of PI^+ cells than (PLGA)PEG-HA NCs (Fig. S8c). As indicated before (Fig. 7f and S7), (PLGA)PEG-HA NCs interact with M(C1498) phenotype mainly through adhesion, while (PLGA)COOH NCs are mostly internalized (only 20 ± 11% of adhesion), suggesting an extracellular source of membrane damage that may be associated with the (PLGA)PEG-HA NCs adhesion. In addition, other mechanisms of damage such oxidative stress may affect cell viability even at low uptake levels, as reported for PLGA NCs prepared with 5 %(w/v) of dextran as subtilizing agent that led to oxidative membrane damage and increase of early apoptotic events although having reduced cell uptake.[241] To assess the efficacy of the NCs in co-culture, C1498 cells were co-incubated with NC-preloaded macrophages (2 h exposure) for 24 h. M(C1498) loaded with (PLGA)PEG-HA NCs significantly reduced C1498 viability and increased the percentage of PI^+ cells compared with macrophages loaded with (PLGA)COOH

NCs (Fig 9a and d). Also, MTT assay indicates that M(C1498) phenotype loaded with (PLGA)PEG-HA NCs was more effective against C1498 cells than MØ and M(LPS) phenotypes exposed to the same formulation and initial concentration of NCs, explained by the favored M(C1498)-mediated delivery of the NCs to C1498 cells (Fig. 8e) and enhanced adhesion of (PLGA)PEG-HA NCs to M(C1498) surface (Fig S7). In addition, M(Ø) and M(C1498) macrophages loaded with (PLGA)PEG-HA NCs were more toxic to C1498 cells than (PLGA)COOH NC-loaded macrophages even though their delivery to C1498 is comparable. Thus, although (PLGA)COOH NCs are also delivered to AML cells by the macrophages, (PLGA)PEG-HA NCs target pro-leukemic macrophages and their therapeutic efficacy against AML is improved when delivered by macrophages. M(LPS) phenotype was more affected by the (PLGA)COOH NCs than by the NCs modified with HA in co-culture with C1498 cells, presenting a larger population of PI^+ cells (Fig. 9e). Besides the greater interaction of (PLGA)COOH NCs with M(LPS) (Fig. 7d), the adhesion of (PLGA)COOH NCS to M(LPS) surface is quite reduced when compared with the adhesion of (PLGA)PEG-HA NCs (Fig. S7), which may minimize the NCs effect on M(LPS) macrophages. One of the challenges of cell-based drug delivery is to prevent the payloads from interacting with the carrier cell. NCs adhered to the cell surface are promising solutions for this problem and were previously reported to effectively deliver payloads to target sites. [9,139-140,143,242-51] Other authors have also shown improvement in the anti-cancer effect of drugs delivered by macrophages to tumor tissues.[7,148,150]

Advances in targeted drug delivery have brought new perspectives to leukemia treatment. In 2019, FDA approved Vyxeos, a liposomal formulation of daunorubicin and cytarabine, for the treatment of high-risk AML.[243] Despite recent advances, AML patient survival remains dismally poor. Cell-based delivery systems may overcome some shortcomings of nanoparticle carriers such as rapid clearance and immunogenicity while increasing biodistribution and passing biological barriers by taking advantage of native cells' properties. Cell-based delivery systems have brought new perspectives to leukemia treatment. L-asparaginase delivered by red blood cells (RBC) relapsed Acute Lymphoblastic Leukemia in phase III trial[141] and mesenchymal stromal cells (MSC) loaded with paclitaxel improved the survival BDF1-mice-bearing L1210.[142] The paclitaxel-loaded MSC were able to attract and kill leukemic cells as well as inhibit angiogenesis.[142] Also, C1498 cells treated with liquid nitrogen to eliminate pathogenicity were used to deliver doxorubicin to the bone marrow of AML

mice.[144] AML cryo-shocked cell remains capable of home at the bone marrow by the interaction of CD44 and CXCR4 receptors with endogenous HA. [144]

Because of CD44 increased intensity, (PLGA)-PEG-HA NCs preferentially adhere to the membrane of pro-leukemic macrophages. Also, (PLGA)-PEG-HA NCs loaded to macrophages have their delivery to AML blasts tuned by cell-to-cell interaction, accumulating into the leukemic cell and increasing cancer cell death. In addition, (PLGA)-PEG-HA NCs may also reduce AML relapse by targeting AML- leukemic stem cells that express the CD44 receptor.[118] Our results suggest that macrophage-based delivery of (PLGA)PEG-HA NCs loaded with ATO are a promising platform to treat AML as they can improve targetability by adhering to AML-related macrophages and reduce AML blasts viability *in vitro*.

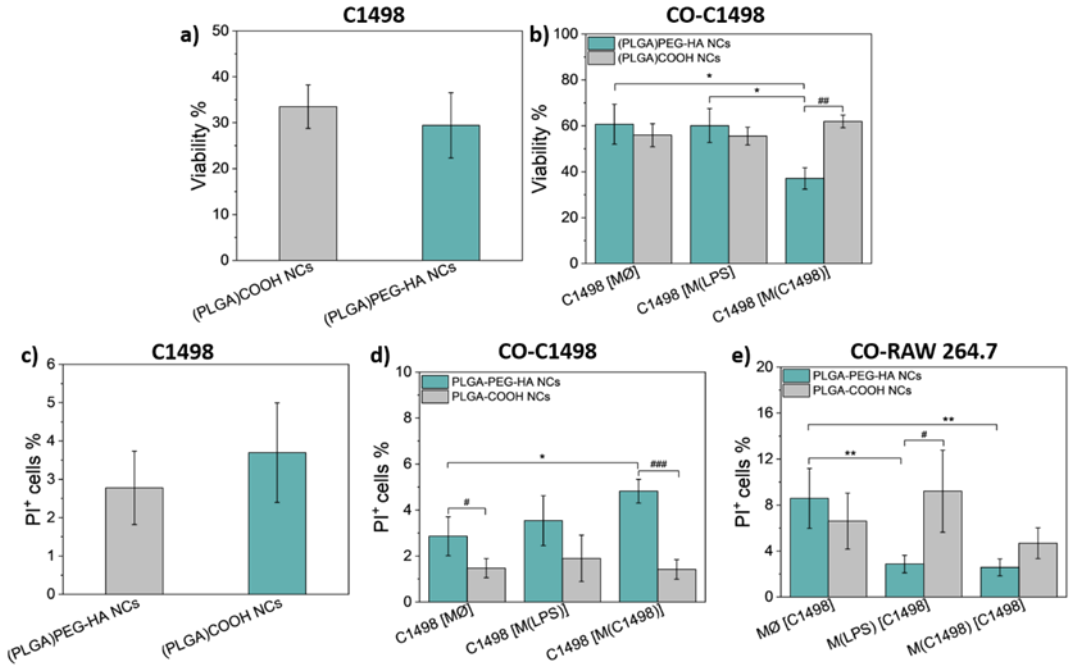

Figure 9 - Evaluation of cellular viability by MTT and PI assay for (PLGA)COOH and (PLGA)PEG-HA NCs. Viability of a) C1498 cells monocultures assessed by MTT after incubation with (PLGA)COOH and (PLGA)PEG-HA NCs for 24 h at 37 °C. b) Viability of C1498 cells after 24 h of co-culture with NC-loaded macrophages assessed by MTT. Percentage of PI-positive cells (PI^+ %) of c) C1498 cells monocultures exposed to (PLGA)COOH and (PLGA)PEG-HA NCs for 24 h, d) C1498 cells after 24 h of co-culture with NC-loaded macrophages and e) NC-loaded RAW 264.7 macrophages after 24 h of co-culture with C1498 cells. ATO dosage was the same for all experimental groups (1.2 µg/ml) and all experiment were carried at 37 °C. Statistical analysis comparing phenotypes was performed using ANOVA with Tukey's post-hoc test and statistical analysis comparing the NCs was performed using student t-test. Values represented are mean ± SD (n=4). * p-value < 0.05, # p-value < 0.05, ## p-value < 0.01, ### p-value < 0.001.

Source: By the author

3.5 Conclusion

(PLGA)PEG-HA NCs showed higher interaction with AML-related macrophages than with non-induced or LPS-induced macrophage phenotypes. NC interaction with pro-leukemic phenotype was markedly reduced by competitive inhibition with free HA, corroborating with CD44 increased intensity in the phenotype suggesting a receptor-mediated interaction. In addition, (PLGA)PEG-HA NCs interact with macrophages mostly through adhesion to the cell surface, preventing NCs degradation by lysosomes after endocytosis.

To assess the pro-leukemic macrophages' (M(C1498)) ability to effectively deliver the NCs to AML blasts, we studied the uptake of (PLGA)COOH and (PLGA)PEG-HA NCs by C1498 co-cultured with MØ, M(LPS) and M(C1498) macrophages pre-exposed to the NCs. All macrophage polarizations similarly delivered (PLGA)COOH NCs to C1498 due to its high uptake by all macrophage phenotypes and C1498 cells. However, the enhanced uptake hampered (PLGA)COOH NCs macrophage delivery to C1498 cells, reducing its therapeutic efficacy. (PLGA)PEG-HA NCs showed higher adhesion carried by macrophages and boosted (PLGA)PEG-HA NCs delivery to C1498 cells. M(C1498) macrophages were the most efficient (PLGA)PEG-HA NCs carriers, due to elevated CD44 expression by the phenotype and consequent HA-decorated NCs greater adhesion to the cell surface. This behavior reflected in therapeutic efficacy as pro-leukemic macrophages carrying (PLGA)PEG-HA NCs loaded with ATO led to a higher cell death for AML cells, here represented by C1498 cells, than the other macrophage phenotypes were capable to trigger as carriers. The results provide early evidence that macrophage-based delivery of (PLGA)PEG-HA NCs loaded with ATO is a promising strategy to treat AML by specifically targeting and adhering to AML-associated macrophages, as well as effectively reducing AML blasts viability.

4 Overall Conclusions

Polymeric nanocarriers (NCs) are promising vehicles to delivery therapeutics to cancer. However, an in-depth investigation of the NCs' interaction with biological systems is pivotal to ensure the safety of the NCs as well as to guide the improvements of its targetability and effect against cancer cells. Polysaccharides have been applied in nanomedicine as stabilizing and coating agents to increase systemic circulation times, promote bioadhesive or actively target cancer cells by receptor-mediated endocytosis. In this dissertation we investigate how does polysaccharides affect the interactions between nanomaterials and cancer cells, as well as cancer-associated cells.

In **Chapter 1** we showed that control over the amount of Dex added as stabilizing agent to the formulation of DOX-loaded PLGA NCs NCs impacts their interaction with non-phagocytic cells due to the decrease of protein adsorption (protein corona formation) with the increase of dextran amount. NCs prepared with 5 %(w/v) of Dex induced greater oxidative membrane damage and increase of early apoptotic events in myocardial and breast adenocarcinoma cells. Since irreversible cardiomyopathy and heart failure are mainly induced by oxidative stress, NCs prepared with 5 %(w/v) of Dex may contribute more to the long-term adverse effects than formulations with lower Dex concentrations or without Dex.

In **Chapter 2** we reported that AML-related macrophages can effectively deliver PLGA NCs decorated with HA to AML cells via CD44-targeting. (PLGA)-PEG-HA NCs adhered to the membrane of pro-leukemic macrophages through CD44-mediated interaction and were delivered to AML blasts by cell-to-cell interaction, accumulating into the leukemic cell. This behavior reflected in therapeutic efficacy as pro-leukemic macrophages carrying HA-decorated NCs loaded with ATO led to a higher cell death for AML cells. The results provide early evidence that macrophage-based delivery of (PLGA)PEG-HA NCs loaded with ATO is a promising strategy to treat AML.

REFERENCES

1 SUNG, H. *et al*. Global cancer statistics 2020: GLOBOCAN estimates of incidence and mortality worldwide for 36 cancers in 185 countries. **CA:** a cancer journal for clinicians, v. 71, n. 3, p. 209–249, 2021. DOI: 10.3322/caac.21660

2 MITCHELL, M. J. *et al*. Engineering precision nanoparticles for drug delivery. **Nature Reviews Drug Discovery**, v. 20, n. 2, p. 101–124, 2021. DOI: 10.1038/s41573-020-0090-8

3 ZERRILLO, L. *et al*. PLGA nanoparticles grafted with hyaluronic acid to improve site-specificity and drug dose delivery in osteoarthritis nanotherapy. **Nanomaterials**, v. 12, n. 13, p. 2248, 2022. DOI: 10.3390/nano12132248

4 SANEJA, A. *et al*. CD44 targeted PLGA nanomedicines for cancer chemotherapy. **European Journal of Pharmaceutical Sciences**, v. 121, p. 47–58, 2018. DOI: 10.1016/j.ejps.2018.05.012. DOI: 10.1016/j.ejps.2018.05.012

5 WANG, X. *et al*. Intelligent biomimetic nanoplatform for systemic treatment of metastatic triple-negative breast cancer via enhanced EGFR-targeted therapy and immunotherapy. **ACS Applied Materials and Interfaces**, v. 14, n. 20, p. 23152–23163, 2022. DOI: 10.1021/acsami.2c02925

6 KUCUKSAYAN, E. *et al*. A new combination strategy to enhance apoptosis in cancer cells by using nanoparticles as biocompatible drug delivery carriers. **Scientific Reports**, v. 11, n. 1, p. 1–19, 2021. DOI: 10.1038/s41598-021-92447-x

7 EVANS, M. A. *et al*. Macrophage-mediated delivery of hypoxia-activated prodrug nanoparticles. **Advanced Therapeutics**, v. 3, n. 2, p. 1900162, 2020. DOI: 10.1002/adtp.201900162

8 AMBROGIO, M. W. *et al*. Poly(lactic- co-glycolic acid) nanoparticles as delivery systems for the improved administration of radiotherapeutic anticancer agents. **ACS Applied Nano Materials**, v. 3, n. 11, p. 10565–10570, 2020. DOI: 10.1021/acsanm.0c02350

9 WYATT SHIELDS, C. *et al*. Cellular backpacks for macrophage immunotherapy. **Science Advances**, v. 6, n. 18, p. 1–12, 2020. DOI: 10.1126/sciadv.aaz6579

10 LANGER, R.; FOLKMAN, J. Polymers for the sustained release of proteins and other macromolecules. **Nature**, v. 263, n. 5580, p. 797–800, 1976. DOI: 10.1038/263797a0

11 GU, Z. *et al*. The effect of size and polymer architecture of doxorubicin–poly(ethylene) glycol conjugate nanocarriers on breast duct retention, potency and toxicity. **European Journal of Pharmaceutical Sciences**, v. 121, n. 1, p. 118-125, 2018. DOI: 10.1016/j.ejps.2018.04.033

12 ZHONG, Y. *et al*. Ligand-directed active tumor-targeting polymeric nanoparticles for cancer chemotherapy. **Biomacromolecules**, v. 15, n. 6, p. 1955–1969, 2014. DOI: 10.1021/bm5003009

13 ESSA, D. *et al*. The design of Poly(lactide-co-glycolide) nanocarriers for medical applications. **Frontiers in Bioengineering and Biotechnology**, v. 8, p. 1–20, 2020. DOI: 10.3389/fbioe.2020.00048.

14 CHARIOU, P. L.; ORTEGA-RIVERA, O. A.; STEINMETZ, N. F. Nanocarriers for the delivery of medical, veterinary, and agricultural active ingredients. **ACS Nano**, v. 14, n. 3, p. 2678–2701, 2020. DOI: 10.1021/acsnano.0c00173.

15 DECUZZI, P. *et al*. Size and shape effects in the biodistribution of intravascularly injected particles. **Journal of Controlled Release**, v. 141, n. 3, p. 320–327, 2010. DOI: 10.1016/j.jconrel.2009.10.014.

16 GRATTON, S. E. A. *et al*. The effect of particle design on cellular internalization pathways. **Proceedings of the National Academy of Sciences of the United States of America**, v. 105, n. 33, p. 11613–11618, 2008. DOI: 10.1073/pnas.0801763105.

17 ZHANG, D. *et al*. The morphology and surface charge-dependent cellular uptake efficiency of upconversion nanostructures revealed by single-particle optical microscopy. **Chemical Science**, v. 9, n. 23, p. 5260–5269, 2018. DOI: 10.1039/C8SC01828F.

18 HE, C. *et al*. Effects of particle size and surface charge on cellular uptake and biodistribution of polymeric nanoparticles. **Biomaterials**, v. 31, n. 13, p. 3657–3666, 2010. DOI: 10.1016/j.biomaterials.2010.01.065.

19 ENGINEER, C.; PARIKH, J.; RAVAL, A. Review on hydrolytic degradation behavior of biodegradable polymers from controlled drug delivery system. **Trends in Biomaterials and Artificial Organs**, v. 25, n. 2, p. 79–85, 2011.

20 CHEVALIER, M. T.; GONZALEZ, J.; ALVAREZ, V. Biodegradable polymeric microparticles as drug delivery devices. **IFMBE Proceedings**, v. 49, p. 187–190, 2015. DOI: 10.1007/978-3-319-13117-7_49.

21 KUMARI, A.; YADAV, S. K.; YADAV, S. C. Biodegradable polymeric nanoparticles based drug delivery systems. **Colloids and Surfaces B:** biointerfaces, v. 75, n. 1, p. 1–18, 2010. DOI: doi: 10.1016/j.colsurfb.2009.09.001.

22 ZHANG, Y.; CHAN, H. F.; LEONG, K. W. Advanced materials and processing for drug delivery: The past and the future. **Advanced Drug Delivery Reviews**, v. 65, n. 1, p. 104–120, 2013. DOI: 10.1016/j.addr.2012.10.003

23 COHEN-SELA, E. *et al*. A new double emulsion solvent diffusion technique for encapsulating hydrophilic molecules in PLGA nanoparticles. **Journal of Controlled Release**, v. 133, n. 2, p. 90–95, 2009. DOI: 10.1016/j.jconrel.2008.09.073

24 PRIMAVESSY, D.; GÜNDAY TÜRELI, N.; SCHNEIDER, M. Influence of different stabilizers on the encapsulation of desmopressin acetate into PLGA nanoparticles. **European Journal of Pharmaceutics and Biopharmaceutics**, v. 118, p. 48–55, 2017. DOI: 10.1016/j.ejpb.2016.12.003.

25 YEREDLA, N. *et al*. Aqueous two phase system assisted self-assembled PLGA

microparticles. **Scientific Reports**, v. 6, p. 27736, 2016. DOI: 10.1038/srep27736.

26 DING, D.; ZHU, Q. Recent advances of PLGA micro/nanoparticles for the delivery of biomacromolecular therapeutics. **Materials Science and Engineering C**, v. 92, p. 1041–1060, 2018. DOI: 10.1016/j.msec.2017.12.036.

27 HINES, D. J.; KAPLAN, D. L. Poly(lactic-co-glycolic) acid-controlled-release systems: Experimental and modeling insights. **Critical Reviews in Therapeutic Drug Carrier Systems**, v. 30, n. 3, p. 257–276, 2013. DOI: 10.1615/critrevtherdrugcarriersyst.2013006475.

28 MITTAL, G. *et al*. Estradiol loaded PLGA nanoparticles for oral administration: effect of polymer molecular weight and copolymer composition on release behavior in vitro and in vivo. **Journal of Controlled Release**, v. 119, n. 1, p. 77–85, 2007. DOI: 10.1016/j.jconrel.2007.01.016.

29 FONSECA, C.; SIMÕES, S.; GASPAR, R. Paclitaxel-loaded PLGA nanoparticles: Preparation, physicochemical characterization and in vitro anti-tumoral activity. **Journal of Controlled Release**, v. 83, n. 2, p. 273–286, 2002. DOI: 10.1016/s0168-3659(02)00212-2.

30 DANHIER, F. *et al*. PLGA-based nanoparticles: An overview of biomedical applications. **Journal of Controlled Release**, v. 161, n. 2, p. 505–522, 2012. DOI: 10.1016/j.jconrel.2012.01.043.

31 KAPADIA, C. H.; IOELE, S. A.; DAY, E. S. Layer-by-layer assembled PLGA nanoparticles carrying miR-34a cargo inhibit the proliferation and cell cycle progression of triple-negative breast cancer cells. **Journal of Biomedical Materials Research A**, v. 108, n. 3, p. 601–613, 2020. DOI: 10.1002/jbm.a.36840.

32 CHEN, Q. *et al.* Biodegradable nanoparticles decorated with different carbohydrates for efficient macrophage-targeted gene therapy. **Journal of Controlled Release**, v. 323, p. 179–190, 2020. DOI: 10.1016/j.jconrel.2020.03.044. DOI: 10.1002/jbm.a.36840.

33 JIANG, G. *et al*. Intracellular delivery of anti-BCR/ABL antibody by PLGA nanoparticles suppresses the oncogenesis of chronic myeloid leukemia cells. **Journal of Hematology and Oncology**, v. 14, n. 1, p. 1–18, 2021. DOI: 10.1186/s13045-021-01150-x.

34 LIU, Y. *et al.* Systemic delivery of CRISPR/Cas9 with PEG-PLGA nanoparticles for chronic myeloid leukemia targeted therapy. **Biomaterials Science**, v. 6, n. 6, p. 1592–1603, 2018. DOI: 10.1039/c8bm00263k.

35 HARRIS, J. C.; STERIN, E. H.; DAY, E. S. Membrane-wrapped nanoparticles for enhanced chemotherapy of acute myeloid leukemia. **ACS Biomaterials Science & Engineering**, v. 8, n. 10, p. 4439–4448, 2022. DOI: 10.1021/acsbiomaterials.2c00832.

36 BIN LIANG, N. *et al*. B-Poly (L -Lactide-Co-Glycolide) nanoparticles for enhancing cellular uptake and promoting antileukemia activity. **International Journal of Nanomedicine**, v. 14, p. 543–556, 2019. DOI: 10.2147/IJN.s190027.

37 YADAV, K. S. *et al.* Long circulating PEGylated PLGA nanoparticles of cytarabine for targeting leukemia. **Journal of Microencapsulation**, v. 28, n. 8, p. 729–742, 2011. DOI:

10.3109/02652048.2011.615949.

38 BAO, W. *et al*. Applications of daunorubicin-loaded PLGA-PLL-PEG-Tf nanoparticles in hematologic malignancies: an in vitro and in vivo evaluation. **Drug Design, Development and Therapy**, v. 13, p. 1107–1115, 2019. DOI: 10.2147/DDDT.S195832.

39 DANQUAH, M. K.; ZHANG, X. A.; MAHATO, R. I. Extravasation of polymeric nanomedicines across tumor vasculature. **Advanced Drug Delivery Reviews**, v. 63, n. 8, p. 623–639, 2011. DOI: 10.1016/j.addr.2010.11.005.

40 WEIS, S. M.; CHERESH, D. A. Tumor angiogenesis: molecular pathways and therapeutic targets. **Nature Medicine**, v. 17, n. 11, p. 1359–1370, 2011. DOI: 10.1038/nm.2537.

41 CARMELIET, P.; JAIN, R. K. Angiogenesis in cancer and other diseases. **Nature**, v. 407, n. 6801, p. 249–257, 2000. DOI: 10.1038/35025220.

42 SINDHWANI, S. *et al*. The entry of nanoparticles into solid tumours. **Nature Materials**, v. 19, n. 5, p. 566–575, 2020. DOI: 10.1038/s41563-019-0566-2.

43 WILHELM, S. *et al*. Analysis of nanoparticle delivery to tumours. **Nature Reviews Materials**, v. 16, n. 3, p. 13–17, 2016. DOI: 10.1038/natrevmats.2016.14.

44 PRICE, L. S. L. *et al*. A reanalysis of nanoparticle tumor delivery using classical pharmacokinetic metrics. **Science Advances**, v. 6, n. 29, p. 1–9, 2020. DOI: 10.1126/sciadv.aay9249.

45 KAMALY, N. *et al*. Targeted polymeric therapeutic nanoparticles: design, development and clinical translation. **Chemical Society reviews**, v. 41, n. 7, p. 2971-3010, 2012. DOI: 10.1039/c2cs15344k

46 FENTON, O. S. *et al*. Advances in biomaterials for drug delivery. **Advanced Materials**, v. 30, n. 29, p. 1–29, 2018. DOI: 10.1002/adma.201705328.

47 DANHIER, F.; FERON, O.; PRÉAT, V. To exploit the tumor microenvironment: Passive and active tumor targeting of nanocarriers for anti-cancer drug delivery. **Journal of Controlled Release**, v. 148, n. 2, p. 135–146, 2010. DOI: 10.1016/j.jconrel.2010.08.027.

48 AHMAD, A. *et al*. Precision cancer nanotherapy: evolving role of multifunctional nanoparticles for cancer active targeting. **Journal of Medicinal Chemistry**, v. 62, n. 23, p. 10475–10496, 2019. DOI: 10.1021/acs.jmedchem.9b00511.

49 WANG, H. *et al*. Hyaluronic acid-decorated dual responsive nanoparticles of Pluronic F127, PLGA, and chitosan for targeted co-delivery of doxorubicin and irinotecan to eliminate cancer stem-like cells. **Biomaterials**, v. 72, p. 74–89, 2015. DOI: 10.1016/j.biomaterials.2015.08.048.

50 ALMEIDA, P. V. *et al.* Amine-modified hyaluronic acid-functionalized porous silicon nanoparticles for targeting breast cancer tumors. **Nanoscale**, v. 6, n. 17, p. 10377–10387, 2014ax. DOI: 10.1039/C4NR02187H

51 HAYWARD, S. L.; WILSON, C. L.; KIDAMBI, S. Hyaluronic acid-conjugated liposome

nanoparticles for targeted delivery to CD44 overexpressing glioblastoma cells. **Oncotarget**, v. 7, n. 23, p. 34158–34171, 2016. DOI: 10.18632/oncotarget.8926.

52 VANGARA, K. K.; LIU, J. L.; PALAKURTHI, S. Hyaluronic acid-decorated PLGA-PEG nanoparticles for targeted delivery of SN-38 to ovarian cancer. **Anticancer Research**, v. 33, n. 6, p. 2425–2434, 2013.

53 ALBERTI, D. *et al*. Theranostic nanoparticles loaded with imaging probes and rubrocurcumin for combined cancer therapy by folate receptor targeting. **ChemMedChem**, v. 12, n. 7, p. 502–509, 2017. DOI: 10.1002/cmdc.201700039.

54 ALIBOLANDI, M. *et al*. Folate receptor-targeted multimodal polymersomes for delivery of quantum dots and doxorubicin to breast adenocarcinoma: in vitro and in vivo evaluation. **International Journal of Pharmaceutics**, v. 500, n. 1–2, p. 162–178, 2016. DOI: 10.1016/j.ijpharm.2016.01.040.

55 FASEHEE, H. *et al*. Delivery of disulfiram into breast cancer cells using folate-receptor-targeted PLGA-PEG nanoparticles: In vitro and in vivo investigations. **Journal of Nanobiotechnology**, v. 14, n. 1, p. 1–18, 2016. DOI: 10.1186/s12951-016-0183-z.

56 REZVANTALAB, S. *et al*. PLGA-based nanoparticles in cancer treatment. **Frontiers in Pharmacology**, v. 9, p. 1260, 2018. DOI: 10.3389/fphar.2018.01260.

57 LEMARCHAND, C.; GREF, R.; COUVREUR, P. Polysaccharide-decorated nanoparticles. **European Journal of Pharmaceutics and Biopharmaceutics**, v. 58, n. 2, p. 327–341, 2004. DOI: 10.1016/j.ejpb.2004.02.016.

58 PENG, P. *et al*. Polysaccharide nanoparticles for targeted cancer therapies. **Current Drug Metabolism**, v. 19, n. 9, p. 781–792, 2018. DOI: 10.1016/j.bioactmat.2021.03.008.

59 RANJBARI, J. *et al*. Anti-cancer drug delivery using carbohydrate-based polymers. **Current Pharmaceutical Design**, v. 23, n. 39, p. 6019–6032, 2017. DOI: 10.2174/1381612823666170505124927.

60 SWIERCZEWSKA, M. *et al*. Polysaccharide-based nanoparticles for theranostic nanomedicine. **Advanced Drug Delivery Reviews**, v. 99, p. 70–84, 2016. DOI: 10.1016/j.addr.2015.11.015.

61 KANG, B. *et al*. Carbohydrate nanocarriers in biomedical applications: Functionalization and construction. **Chemical Society Reviews**, v. 44, n. 22, p. 8301–8325, 2015. DOI: 10.1039/C5CS00092K.

62 XIE, Y. L.; WANG, M. J.; YAO, S. J. Preparation and characterization of biocompatible microcapsules of sodium cellulose sulfate/chitosan by means of layer-by-layer self-assembly. **Langmuir**, v. 25, n. 16, p. 8999–9005, 2009. DOI: 10.1021/la9014338.

63 LIU, Z. *et al*. Polysaccharides-based nanoparticles as drug delivery systems. **Advanced Drug Delivery Reviews**, v. 60, n. 15, p. 1650–1662, 2008. DOI: 10.1016/j.addr.2008.09.001.

64 MARRADI, M. *et al*. Glyconanoparticles as multifunctional and multimodal carbohydrate

systems. **Chemical Society Reviews**, v. 42, n. 11, p. 4728–4745, 2013. DOI: 10.1039/C2CS35420A.

65 ADAK, A. K.; LI, B. Y.; LIN, C. C. Advances in multifunctional glycosylated nanomaterials: preparation and applications in glycoscience. **Carbohydrate Research**, v. 405, p. 2–12, 2015. DOI: 10.1016/j.carres.2014.07.026.

66 BLOISE, N. *et al*. Targeting the "sweet side" of tumor with glycan-binding molecules conjugated-nanoparticles: Implications in cancer therapy and diagnosis. **Nanomaterials**, v. 11, n. 2, p. 1–19, 2021. DOI: 10.3390/nano11020289.

67 DOH, K. O.; YEO, Y. Application of polysaccharides for surface modification of nanomedicines. **Therapeutic Delivery**, v. 3, n. 12, p. 1447–1456, 2012. DOI: 10.4155/tde.12.105.

68 VARSHOSAZ, J. Dextran conjugates in drug delivery. **Expert Opinion on Drug Delivery**, v. 9, n. 5, p. 509–523, 2012. DOI: 10.1517/17425247.2012.673580.
.
69 QIAN, C. *et al*. Suppression of pancreatic tumor growth by targeted arsenic delivery with anti-CD44v6 single chain antibody conjugated nanoparticles. **Biomaterials**, v. 34, n. 26, p. 6175–6184, 2013. DOI: 10.1016/j.biomaterials.2013.04.056.

70 ALHARETH, K. *et al*. Conformation of surface-decorating dextran chains affects the pharmacokinetics and biodistribution of doxorubicin-loaded nanoparticles. **European Journal of Pharmaceutics and Biopharmaceutics**, v. 81, n. 2, p. 453–457, 2012. DOI: 10.1016/j.ejpb.2012.03.009.

71 MA, W. *et al*. Evaluation of blood circulation of polysaccharide surface-decorated PLA nanoparticles. **Carbohydrate Polymers**, v. 72, n. 1, p. 75–81, 2008. DOI: 10.1016/j.carbpol.2007.07.033.

72 REICHARDT, N. C.; MARTÍN-LOMAS, M.; PENADÉS, S. Opportunities for glyconanomaterials in personalized medicine. **Chemical Communications**, v. 52, n. 92, p. 13430–13439, 2016. DOI: 10.1039/C6CC04445J.

73 HARDWICKE, J. *et al*. Dextrin-rhEGF conjugates as bioresponsive nanomedicines for wound repair. **Journal of Controlled Release**, v. 130, n. 3, p. 275–283, 2008. DOI: 10.1016/j.jconrel.2008.07.023.

74 SAGNELLA, S. M. *et al.* Dextran-based doxorubicin nanocarriers with improved tumor penetration. **Biomacromolecules**, v. 15, n. 1, p. 262–275, 2014. DOI: 10.1021/bm401526d.

75 FERGUSON, E. L.; DUNCAN, R. Dextrin-phospholipase A2: Synthesis and evaluation as a bioresponsive anticancer conjugate. **Biomacromolecules**, v. 10, n. 6, p. 1358–1364, 2009. DOI: 10.1021/bm8013022.

76 FRASER, J. R. E.; LAURENT, T. C.; LAURENT, U. B. G. Hyaluronan: its nature, distribution, functions and turnover. **Journal of Internal Medicine**, v. 242, n. 1, p. 27–33, 1997. DOI: 10.1046/j.1365-2796.1997.00170.x.

77 KIM, H. *et al*. Hyaluronic acid-based extracellular matrix triggers spontaneous M2-like polarity of monocyte/macrophage. **Biomaterials Science**, v. 7, n. 6, p. 2264–2271, 2019. DOI: 10.1039/C9BM00155G.

78 JURJ, A. *et al*. The extracellular matrix alteration, implication in modulation of drug resistance mechanism: friends or foes? **Journal of Experimental and Clinical Cancer Research**, v. 41, n. 1, p. 1–21, 2022. DOI: 10.1186/s13046-022-02484-1.

79 TAKASUGI, M. *et al*. Naked mole-rat very-high-molecular-mass hyaluronan exhibits superior cytoprotective properties. **Nature Communications**, v. 11, n. 1, p. 1–10, 2020. DOI: 10.1038/s41467-020-16050-w.

80 SNETKOV, P. *et al*. Hyaluronic acid: the influence of molecular weight and degradable properties of biopolymer. **Polymers**, v. 12, n. 8, p. 1800, 2020. DOI: 10.3390/polym12081800.

81 ARUFFO, A. *et al*. CD44 is the principal cell surface receptor for hyaluronate. **Cell**, v. 61, n. 7, p. 1303–1313, 1990. DOI: 10.1016/0092-8674(90)90694-a.

82 ORIAN-ROUSSEAU, V. CD44, a therapeutic target for metastasising tumours. **European Journal of Cancer**, v. 46, n. 7, p. 1271–1277, 2010. DOI: 10.1016/j.ejca.2010.02.024.

83 GHOSH, S. C. *et al*. CD44 : a validated target for improved delivery of cancer therapeutics. **Expert Opinion on Therapeutic Targets**, v.16, n. 7, p. 635–650, 2015. DOI: 10.1517/14728222.2012.687374.

84 AUZENNE, E. *et al*. Hyaluronic acid-paclitaxel: antitumor efficacy against CD44(+) human ovarian carcinoma xenografts. **Neoplasia**, v. 9, n. 6, p. 479–486, 2007. DOI: 10.1593/neo.07229.

85 JIN, L. *et al*. Targeting of CD44 eradicates human acute myeloid leukemic stem cells. **Nature Medicine**, v. 12, n. 10, p. 1167–1174, 2006. DOI: 10.1038/nm1483.

86 PEER, D.; MARGALIT, R. Tumor-targeted hyaluronan nanoliposomes increase the antitumor activity of liposomal doxorubicin in syngeneic and human xenograft mouse tumor models. **Neoplasia**, v. 6, n. 4, p. 343–353, 2004. DOI: 10.1593/neo.03460.

87 TENZER, S. *et al*. Rapid formation of plasma protein corona critically affects nanoparticle pathophysiology. **Nature Nanotechnology**, v. 8, n. 10, p. 772–781, 2013. DOI: 10.1038/nnano.2013.181.

88 XIAO, W. *et al*. The protein corona hampers the transcytosis of transferrin-modified nanoparticles through blood–brain barrier and attenuates their targeting ability to brain tumor. **Biomaterials**, v. 274, p. 120888, 2021. DOI: 10.1016/j.biomaterials.2021.120888.

89 SALVATI, A. *et al*. Transferrin-functionalized nanoparticles lose their targeting capabilities when a biomolecule corona adsorbs on the surface. **Nature Nanotechnology**, v. 8, n. 2, p. 137–143, 2013. DOI: 10.1038/nnano.2012.237.

90 FRANCIA, V. *et al.* Corona composition can affect the mechanisms cells use to internalize nanoparticles. **ACS Nano**, v. 13, n. 10, p. 11107–11121, 2019. DOI: 10.1021/acsnano.9b03824.

91 RITZ, S. *et al*. Protein corona of nanoparticles: distinct proteins regulate the cellular uptake. **Biomacromolecules**, v. 16, n. 4, p. 1311–1321, 2015. DOI: 10.1021/acs.biomac.5b00108.

92 TEKIE, F. S. M. *et al*. Controlling evolution of protein corona: a prosperous approach to improve chitosan-based nanoparticle biodistribution and half-life. **Scientific Reports**, v. 10, n. 1, p. 9664, 2020. DOI: 10.1038/s41598-020-66572-y.

93 PEIGNEUX, A. *et al*. Protein corona formation and its influence on biomimetic magnetite nanoparticles. **Journal of Materials Chemistry B**, v. 8, n. 22, p. 4870–4882, 2020. DOI: 10.1039/C9TB02480H.

94 MICELI, E. *et al*. Understanding the elusive protein corona of thermoresponsive nanogels. **Nanomedicine**, v. 13, n. 20, p. 2657–2667, 2018. DOI: 10.2217/nnm-2018-0217.

95 OBST, K. *et al*. Protein corona formation on colloidal polymeric nanoparticles and polymeric nanogels: impact on cellular uptake, toxicity, immunogenicity, and drug release properties. **Biomacromolecules**, v. 18, n. 6, p. 1762–1771, 2017. DOI: 10.1021/acs.biomac.7b00158.

96 WALKEY, C. D. *et al*. Nanoparticle size and surface chemistry determine serum protein adsorption and macrophage uptake. **Journal of the American Chemical Society**, v. 134, n. 4, p. 2139–2147, 2012. DOI: 10.1021/ja2084338.

97 VROMAN, L. Effect of adsorbed proteins on the wettability of hydrophilic and hydrophobic solids. **Nature**, v. 196, p. 476–477, 1962. DOI: 10.1038/196476a0.

98 GUPTA, M. N.; ROY, I. How corona formation impacts nanomaterials as drug carriers. **Molecular Pharmaceutics**, v. 17, n. 3, p. 725–737, 2020. DOI: 10.1021/acs.molpharmaceut.9b01111.

99 SHI, L. *et al*. Effects of polyethylene glycol on the surface of nanoparticles for targeted drug delivery. **Nanoscale**, v. 13, n. 24, p. 10748–10764, 2021. DOI: 10.1039/D1NR02065J.

100 DUARTE, D.; HAWKINS, E. D.; LO CELSO, C. The interplay of leukemia cells and the bone marrow microenvironment. **Blood**, v. 131, n. 14, p. 1507–1511, 2018. DOI: 10.1182/blood-2017-12-784132.

101 MENTER, T.; TZANKOV, A. Tumor microenvironment in acute myeloid leukemia: adjusting niches. **Frontiers in Immunology**, v. 13, p. 1–11, 2022. DOI: 10.3389/fimmu.2022.811144.

102 MIARI, K. E. *et al*. Macrophages in acute myeloid leukaemia: significant players in therapy resistance and patient outcomes. **Frontiers in Cell and Developmental Biology**, v. 9, p. 1–14, 2021. DOI: 10.3389/fcell.2021.692800.

103 BOUTIN, L. *et al*. Mesenchymal stromal cells confer chemoresistance to myeloid leukemia blasts through Side Population functionality and ABC transporter activation. **Haematologica**, v. 105, n. 4, p. 987–998, 2020. DOI: 10.3324/haematol.2018.214379.

104 BARYAWNO, N. *et al*. A cellular taxonomy of the bone marrow Stroma in homeostasis and leukemia. **Cell**, v. 177, n. 7, p. 1915- 1932.e16, 2019. DOI: 10.1016/j.cell.2019.04.040.

105 TIKHONOVA, A. N. *et al*. The bone marrow microenvironment at single-cell resolution. **Nature**, v. 569, n. 7755, p. 222–228, 2019. DOI: 10.1038/s41586-019-1104-8

106 LADIKOU, E. E. *et al*. Acute myeloid leukaemia in its niche: the bone marrow microenvironment in acute myeloid leukaemia. **Current Oncology Reports**, v. 22, n. 3, p. 1–9, 2020. DOI: 10.1007/s11912-020-0885-0

107 KHOURY, J.D. *et al*. The 5th edition of the World Health Organization Classification of Haematolymphoid Tumours: Myeloid and Histiocytic/Dendritic Neoplasms. **Leukemia**, v. 36, p. 1703–1719, 2022. DOI: 10.1038/s41375-022-01613-1

108 KANTARJIAN, H. *et al.* Acute myeloid leukemia : current progress and future directions. **Blood Cancer Journal**, v. 11, p. 41, 2021. DOI: 10.1038/s41408-021-00425-3.

109 RAAIJMAKERS, M. H. G. P. *et al*. Bone progenitor dysfunction induces myelodysplasia and secondary leukaemia. **Nature**, v. 464, n. 7290, p. 852–857, 2010. DOI: 10.1038/nature08851.

110 KODE, A. *et al.* Leukaemogenesis induced by an activating β-catenin mutation in osteoblasts. **Nature**, v. 506, n. 7487, p. 240–244, 2014. DOI: 10.1038/nature12883.

111 DONG, L. *et al*. Leukaemogenic effects of Ptpn11 activating mutations in the stem cell microenvironment. **Nature**, v. 539, n. 7628, p. 304–308, 2016. DOI: 10.1038/nature20131.

112 ABDUL-AZIZ, A. M. *et al*. HIF1α drives chemokine factor pro-tumoral signaling pathways in acute myeloid leukemia. **Oncogene**, v. 37, n. 20, p. 2676–2686, 2018. DOI: 10.1038/s41388-018-0151-1.

113 JENSEN, P. O. *et al*. Increased cellular hypoxia and reduced proliferation of both normal and leukaemic cells during progression of acute myeloid leukaemia in rats. **Cell Proliferation**, v. 33, n. 6, p. 381–395, 2000. DOI: 10.1046/j.1365-2184.2000.00183.x.

114 ZHANG, H. *et al*. HIF1α is required for survival maintenance of chronic myeloid leukemia stem cells. **Blood**, v. 119, n. 11, p. 2595–2607, 2012. DOI: 10.1182/blood-2011-10-387381.

115 CHELONI, G. *et al*. The leukemic stem cell niche: adaptation to hypoxia versus Oncogene addiction. **Stem Cells International**, v. 2017, 2017. DOI: 10.1155/2017/4979474.

116 KREVVATA, M. *et al*. Inhibition of leukemia cell engraftment and disease progression in mice by osteoblasts. **Blood**, v. 124, n. 18, p. 2834–2846, 2014. DOI: 10.1182/blood-2013-07-517219.

117 ZÖLLER, M. CD44, hyaluronan, the hematopoietic stem cell, and leukemia-initiating cells. **Frontiers in Immunology**, v. 6, p. 235, 2015. DOI: 10.3389/fimmu.2015.00235.

118 ISHIKAWA, F. *et al*. Chemotherapy-resistant human AML stem cells home to and engraft within the bone-marrow endosteal region. **Nature Biotechnology**, v. 25, n. 11, p. 1315–1321,

2007. DOI: 10.1038/nbt1350.

119 CIVINI, S. *et al*. Leukemia cells induce changes in human bone marrow stromal cells. **Journal of Translational Medicine**, v. 11, n. 1, p. 1–14, 2013. DOI: 10.1186/1479-5876-11-298.

120 ZHAI, Y. *et al*. Growth differentiation factor 15 contributes to cancer-associated fibroblasts-mediated chemo-protection of AML cells. **Journal of Experimental and Clinical Cancer Research**, v. 35, n. 1, p. 1–12, 2016. DOI: 10.1186/s13046-016-0405-0.

121 AL-MATARY, Y. S. *et al*. Acute myeloid leukemia cells polarize macrophages towards a leukemia supporting state in a growth factor independence 1 dependent manner. **Haematologica**, v. 101, n. 10, p. 1216–1227, 2016. DOI: 10.3324/haematol.2016.143180.

122 YANG, X. *et al.* Repolarizing heterogeneous leukemia-associated macrophages with more M1 characteristics eliminates their pro-leukemic effects. **Oncoimmunology**, v. 7, n. 4, p. e1412910, 2017. DOI: 10.1080/2162402X.2017.1412910.

123 WANG, L.; ZHENG, G. Macrophages in leukemia microenvironment. **Blood Science**, v. 1, n. 1, p. 29–33, 2019. DOI: 10.1097/BS9.0000000000000014.

124 BRÜCK, O. *et al*. Immune profiles in acute myeloid leukemia bone marrow associate with patient age, T-cell receptor clonality, and survival. **Blood Advances**, v. 4, n. 2, p. 274–286, 2020. DOI: 10.1182/bloodadvances.2019000792.

125 XU, Z. J. *et al.* The M2 macrophage marker CD206: a novel prognostic indicator for acute myeloid leukemia. **Oncoimmunology**, v. 9, n. 1, p. 1683347, 2020. DOI: 10.1080/2162402X.2019.1683347.

126 MUSSAI, F. *et al*. Acute myeloid leukemia creates an arginase-dependent immunosuppressive microenvironment. **Blood**, v. 122, n. 5, p. 749–758, 2013. DOI: 10.1182/blood-2013-01-480129.

127 PONCE, L. P. *et al*. SIRPα-antibody fusion proteins stimulate phagocytosis and promote elimination of acute myeloid leukemia cells. **Oncotarget**, v. 8, n. 7, p. 11284–11301, 2017. DOI: 10.18632/oncotarget.14500.

128 VACHON, E. *et al.* CD44 is a phagocytic receptor. **Blood**, v. 107, n. 10, p. 4149–4159, 2019. DOI: 10.1182/blood-2005-09-3808.

129 BENDALL, L. J.; BRADSTOCK, K. F.; GOTTLIEB, D. J. Expression of CD44 variant exons in acute myeloid leukemia is more common and more complex than that observed in normal blood, bone marrow or CD34+ cells. **Leukemia**, v. 14, n. 7, p. 1239–1246, 2000. DOI: 10.1038/sj.leu.2401830.

130 FLORIAN, S. *et al*. Detection of molecular targets on the surface of CD34+/CD38- Stem cells in various myeloid malignancies. **Leukemia and Lymphoma**, v. 47, n. 2, p. 207–222, 2006. DOI: 10.1080/10428190500272507.

131 RIOS DE LA ROSA, J. M. *et al*. The CD44-mediated uptake of hyaluronic acid-based

carriers in macrophages. **Advanced Healthcare Materials**, v. 6, n. 4, p. 1–11, 2017. DOI: 10.1002/adhm.201601012.

132 GEE, K. *et al*. Differential regulation of CD44 expression by lipopolysaccharide (LPS) and TNF-α in human monocytic cells: distinct involvement of c-Jun N-terminal kinase in LPS-induced CD44 expression. **Journal of Immunology**, v. 169, n. 10, p. 5660–5672, 2002. DOI: 10.4049/jimmunol.169.10.5660.

133 HERTWECK, M. K.; ERDFELDER, F.; KREUZER, K. A. CD44 in hematological neoplasias. **Annals of Hematology**, v. 90, n. 5, p. 493–508, 2011. DOI: 10.1007/s00277-011-1161-z.

134 GABIZON, A. A.; DE ROSALES, R. T. M.; LA-BECK, N. M. Translational considerations in nanomedicine: the oncology perspective. **Advanced Drug Delivery Reviews**, v. 158, p. 140–157, 2020. DOI: 10.1016/j.addr.2020.05.012.

135 ISHIDA, T. *et al*. PEGylated liposomes elicit an anti-PEG IgM response in a T cell-independent manner. **Journal of Controlled Release**, v. 122, n. 3, p. 349–355, 2007. DOI: 10.1016/j.jconrel.2007.05.015.

136 YANG, L. *et al*. Cell-based drug delivery systems and their in vivo fate. **Advanced Drug Delivery Reviews**, v. 187, p. 114394, 2022. DOI: 10.1016/j.addr.2022.114394.

137 DONG, H. *et al*. Advances in living cell-based anticancer therapeutics. **Biomaterials Science**, v. 8, n. 9, p. 2344–2365, 2020. DOI: 10.1039/D0BM00036A.

138 LI, Z. *et al*. Cell-based delivery systems: emerging carriers for immunotherapy. **Advanced Functional Materials**, v. 31, n. 23, p. 1–32, 2021. DOI: 10.1002/adfm.202100088.

139 ZHAO, Z. *et al*. Red blood cell anchoring enables targeted transduction and re-administration of AAV-mediated gene therapy. v. 19, n. 24, p. 2201293, 2022. DOI: 10.1002/advs.202201293.

140 BRENNER, J. S. *et al*. Red blood cell-hitchhiking boosts delivery of nanocarriers to chosen organs by orders of magnitude. **Nature Communications**, v. 9, n. 1, p. 2684, 2018. DOI: 10.1038/s41467-018-05079-7.

141 BARUCHEL, A. *et al*. Updated clinical activity of graspa versus native l-asparaginase in combination with cooprall regimen in phase 3 randomized trial in patients with relapsed acute lymphoblastic leukemia (NCT01518517). **Blood**, v. 126, n. 23, p. 3723–3723, 2015. DOI: 10.1182/blood.V126.23.3723.3723.

142 PESSINA, A. *et al*. Mesenchymal stromal cells primed with Paclitaxel attract and kill leukaemia cells, inhibit angiogenesis and improve survival of leukaemia-bearing mice. **British Journal of Haematology**, v. 160, n. 6, p. 766–778, 2013. DOI: 10.1111/bjh.12196.

143 ANSELMO, A. C. *et al*. Monocyte-mediated delivery of polymeric backpacks to inflamed tissues: a generalized strategy to deliver drugs to treat inflammation. **Journal of Controlled Release**, v. 199, p. 29–36, 2015. DOI: 10.1016/j.jconrel.2014.11.027.

144 CI, T. *et al*. Cryo-shocked cancer cells for targeted drug delivery and vaccination. **Science Advances**, v. 6, n. 50, p. 3–10, 2020. DOI: 10.1126/sciadv.abc3013.

145 LI, S. *et al*. Nanomedicine engulfed by macrophages for targeted tumor therapy. **International Journal of Nanomedicine**, v. 11, p. 4107–4124, 2016. DOI: 10.2147/IJN.S110146.

146 XIA, Y. *et al*. Engineering macrophages for cancer immunotherapy and drug delivery. **Advanced Materials**, v. 32, n. 40, p. 1–20, 2020. DOI: 10.1002/adma.202002054.

147 KEECH, T.; WINKLER, I.; LEVESQUE, J.-P. Macrophage involvement in the response of acute myeloid leukaemia to chemotherapy. **Experimental Hematology**, v. 76, p. S70, 2019. DOI: 10.1016/j.exphem.2019.06.375.

148 FU, J. *et al*. Macrophage mediated biomimetic delivery system for the treatment of lung metastasis of breast cancer. **Journal of Controlled Release**, v. 204, p. 11–19, 2015. DOI: 10.1016/j.jconrel.2015.01.039.

149 PANG, L. *et al*. Exploiting macrophages as targeted carrier to guide nanoparticles into glioma. **Oncotarget**, v. 7, n. 24, p. 37081–37091, 2016. DOI: 10.18632/oncotarget.9464.

150 GUO, L. *et al*. Tunneling nanotubular expressways for ultrafast and accurate m1 macrophage delivery of anticancer drugs to metastatic ovarian carcinoma. **ACS Nano**, v. 13, n. 2, p. 1078–1096, 2019. DOI: 10.1021/acsnano.8b08872.

151 THORN, C. F. *et al*. Doxorubicin pathways. **Pharmacogenetics and Genomics**, v. 21, n. 7, p. 440–446, 2011. DOI: 10.1097/FPC.0b013e32833ffb56.

152 ZHAO, N. *et al*. Advances in delivery systems for doxorubicin. **Journal of nanomedicine & nanotechnology**, v. 9, n. 5, p. 519, 2018. DOI: 10.4172/2157-7439.1000519.

153 PELAZ, B. *et al*. Surface functionalization of nanoparticles with polyethylene glycol: effects on protein adsorption and cellular uptake. **ACS Nano**, v. 9, n. 7, p. 6996–7008, 2015. DOI: 10.1021/acsnano.5b01326.

154 BADMAN, R. P. *et al*. Dextran-coated iron oxide nanoparticle-induced nanotoxicity in neuron cultures. **Scientific Reports**, v. 10, n. 1, p. 1–14, 2020. DOI: 10.1038/s41598-020-67724-w.

155 SEO, D. Y. *et al*. Investigation of the genetic toxicity by dextran-coated superparamagnetic iron oxide nanoparticles (SPION) in HepG2 cells using the comet assay and cytokinesis-block micronucleus assay. **Toxicology and Environmental Health Sciences**, v. 9, n. 1, p. 23–29, 2017. DOI: 10.1007/s13530-017-0299-z.

156 SIES, H.; BERNDT, C.; JONES, D. P. Oxidative stress. **Annual Review of Biochemistry**, v. 86, p. 715–48, 2017. DOI: 10.1146/annurev-biochem-061516-045037.

157 STARK, G. Topical review functional consequences of oxidative membrane damage. **Journal of Membrane Biology**, v. 205, n. 1, p. 1–16, 2005. DOI: 10.1007/s00232-005-0753-8.

158 MANKE, A.; WANG, L.; ROJANASAKUL, Y. Mechanisms of nanoparticle-induced oxidative stress and toxicity. **BioMed Research International**, v. 2013, p. 15, 2013. DOI: 10.1155/2013/942916.

159 FRESTA, C.G. *et al.* Non-toxic engineered carbon nanodiamond concentrations induce oxidative/nitrosative stress, imbalance of energy metabolism, and mitochondrial dysfunction in microglial and alveolar basal epithelial cells article. **Cell Death and Disease**, v. 9, n. 2, p. 245, 2018. DOI: 10.1038/s41419-018-0280-z.

160 PIEPER, S.; LANGER, K. Doxorubicin-loaded PLGA nanoparticles - a systematic evaluation of preparation techniques and parameters. **Materials Today:** proceedings, v. 4, Suppl. 2, p. S188–S192, 2017. DOI: 10.1016/j.matpr.2017.09.185.

161 MORA-HUERTAS, C. E.; FESSI, H.; ELAISSARI, A. Polymer-based nanocapsules for drug delivery. **International Journal of Pharmaceutics**, v. 385, n. 1–2, p. 113–142, 2010. DOI: 10.1016/j.ijpharm.2009.10.018.

162 KHOEE, S.; YAGHOOBIAN, M. An investigation into the role of surfactants in controlling particle size of polymeric nanocapsules containing penicillin-G in double emulsion. **European Journal of Medicinal Chemistry**, v. 44, n. 6, p. 2392–2399, 2009. DOI: 10.1016/j.ejmech.2008.09.045.

163 GIL, E. C. *et al*. Subcoating with Kollidon VA 64 as water barrier in a new combined native dextran/HPMC-cetyl alcohol controlled release tablet. **European Journal of Pharmaceutics and Biopharmaceutics**, v. 69, n. 1, p. 303–311, 2008. DOI: 10.1016/j.ejpb.2007.10.012.

164 YANG, L. *et al*. Swelling and diffusion model of a hydrophilic film coating on controlled-release urea particles. **Particuology**, v. 30, p. 73–82, 2017. DOI: 10.1016/j.partic.2016.03.005.

165 LIN, S. Y.; LI, M. J.; LIN, K. H. Hydrophilic excipients modulate the time lag of time-controlled disintegrating press-coated tablets. **AAPS PharmSciTech**, v. 5, n. 4, p. 2–6, 2004. DOI: 10.1208/pt050454.

166 MA, L. *et al.* Efficient targeting of adipose tissue macrophages in obesity with polysaccharide nanocarriers. **ACS Nano**, v. 10, n. 7, p. 6952–6962, 2016. DOI: 10.1021/acsnano.6b02878.

167 ZANGANEH, S. *et al*. Iron oxide nanoparticles inhibit tumour growth by inducing pro-inflammatory macrophage polarization polarization in tumour tissues. **Nature Nanotechnology**, v. 11, n. 11, p. 986–994, 2016. DOI: 10.1038/nnano.2016.168.

168 KANG, Y. S. *et al*. The C-type lectin SIGN-R1 mediates uptake of the capsular polysaccharide of Streptococcus pneumoniae in the marginal zone of mouse spleen. **Proceedings of the National Academy of Sciences of the United States of America**, v. 101, n. 1, p. 215–220, 2004. DOI: 10.1073/pnas.0307124101.

169 KANG, Y. S. *et al*. SIGN-R1, a novel C-type lectin expressed by marginal zone macrophages in spleen, mediates uptake of the polysaccharide dextran. **International Immunology**, v. 15, n. 2, p. 177–186, 2003. DOI: 10.1093/intimm/dxg019.

170 UNTERWEGER, H. *et al*. Non-immunogenic dextran-coated superparamagnetic iron oxide nanoparticles: a biocompatible, size-tunable contrast agent for magnetic resonance imaging. **International Journal of Nanomedicine**, v. 12, p. 5223–5238, 2017. DOI: 10.2147/IJN.S138108.

171 BREIDING, M. J. Targeting the C-type lectins-mediated host-pathogen interactions with dextran. **Physiology & Behavior**, v. 63, n. 8, p. 1–18, 2014. DOI: 10.18433/j3n590.

172 DERTINGER, T. *et al.* Role of carbohydrate receptors in the macrophage uptake of dextran-coated iron oxide nanoparticles. *In*: ZAHAVY, E. *et al*. (ed.). **Nano-biotechnology for biomedical and diagnostic research**. Berlin: Springer, 2012. p. 17–21. DOI: 10.1007/978-94-007-2555-3_11.

173 JÓZEFOWSKI, S. *et al*. Scavenger receptors and β-glucan receptors participate in the recognition of yeasts by murine macrophages. **Inflammation Research**, v. 61, n. 2, p. 113–126, 2012. DOI: 10.1007/s00011-011-0395-5.

174 SIMON, J. *et al*. Protein corona mediated stealth properties of biocompatible carbohydrate-based nanocarriers. **Israel Journal of Chemistry**, v. 58, n. 12, p. 1363–1372, 2018. DOI: 10.1002/ijch.201800166.

175 LEMARCHAND, C. *et al.* Influence of polysaccharide coating on the interactions of nanoparticles with biological systems. **Biomaterials**, v. 27, n. 1, p. 108–118, 2006. DOI: 10.1016/j.biomaterials.2005.04.041.

176 VIGOR, K. L. *et al*. Nanoparticles functionalised with recombinant single chain Fv antibody fragments (scFv) for the magnetic resonance imaging of cancer cells. **Biomaterials**, v. 31, n. 6, p. 1307–1315, 2010. DOI: 10.1016/j.biomaterials.2009.10.036.

177 SAKULKHU, U. *et al*. Protein corona composition of superparamagnetic iron oxide nanoparticles with various physico-chemical properties and coatings. **Scientific Reports**, v. 4, p. 1–9, 2014. DOI: 10.1038/srep05020.

178 MIRSHAFIEE, V. *et al*. Impact of protein pre-coating on the protein corona composition and nanoparticle cellular uptake. **Biomaterials**, v. 75, p. 295–304, 2016. DOI: 10.1016/j.biomaterials.2015.10.019.

179 CORBO, C. *et al*. Unveiling the in vivo protein corona of circulating leukocyte-like carriers. **ACS Nano**, v. 11, n. 3, p. 3262–3273, 2017. DOI: 10.1021/acsnano.7b00376.

180 RENNICK, J. J.; JOHNSTON, A. P. R.; PARTON, R. G. Key principles and methods for studying the endocytosis of biological and nanoparticle therapeutics. **Nature Nanotechnology**, v. 16, n. 3, p. 266–276, 2021. DOI: 10.1038/s41565-021-00858-8.

181 COMMISSO, C.; FLINN, R. J.; BAR-SAGI, D. Determining the macropinocytic index of cells through a quantitative image-based assay. **Nature Protocols**, v. 9, n. 1, p. 182–192, 2014. DOI: 10.1038/nprot.2014.004.

182 LI, L. *et al*. The effect of the size of fluorescent dextran on its endocytic pathway. **Cell**

Biology International, v. 39, n. 5, p. 531–539, 2015. DOI: 10.1002/cbin.10424.
183 SAGNELLA, S. M. *et al*. Dextran-based doxorubicin nanocarriers with improved tumor penetration. **Biomacromolecules**, v. 15, n. 1, p. 262–275, 2014. DOI: 10.1021/bm401526d.

184 BERRY, C. C. *et al*. Cell response to dextran-derivatised iron oxide nanoparticles post internalisation. **Biomaterials**, v. 25, n. 23, p. 5405–5413, 2004. DOI: 10.1016/j.biomaterials.2003.12.046.

185 WILHELM, C. *et al*. Intracellular uptake of anionic superparamagnetic nanoparticles as a function of their surface coating. **Biomaterials**, v. 24, n. 6, p. 1001–1011, 2003. DOI: 10.1016/S0142-9612(02)00440-4.

186 SAGNELLA, S. M. *et al*. Dextran-based doxorubicin nanocarriers with improved tumor penetration. **Biomacromolecules**, v. 15, n. 1, p. 262–275, 2014. DOI: 10.1021/bm401526d.

187 JOSHI, B. S.; ZUHORN, I. S. Heparan sulfate proteoglycan-mediated dynamin-dependent transport of neural stem cell exosomes in an in vitro blood–brain barrier model. **European Journal of Neuroscience**, v. 53, n. 3, p. 706–719, 2021. DOI: 10.1111/ejn.14974

188 CHRISTIANSON, H. C.; BELTING, M. Heparan sulfate proteoglycan as a cell-surface endocytosis receptor. **Matrix Biology**, v. 35, p. 51–55, 2014. DOI: 10.1016/j.matbio.2013.10.004.

189 MOORE, A.; WEISSLEDER, R.; BOGDANOV, A. Uptake of dextran-coated monocrystalline iron oxides in tumor cells and macrophages. **Journal of Magnetic Resonance Imaging**, v. 7, n. 6, p. 1140–1145, 1997. DOI: 10.1002/jmri.1880070629.

190 MASSIA, S. P.; STARK, J.; LETBETTER, D. S. Surface-immobilized dextran limits cell adhesion and spreading. **Biomaterials**, v. 21, n. 22, p. 2253–2261, 2000. DOI: 10.1016/s0142-9612(00)00151-4.

191 SRITHARAN, S.; SIVALINGAM, N. A comprehensive review on time-tested anticancer drug doxorubicin. **Life Sciences**, v. 278, p. 119527, 2021. DOI: 10.1016/j.lfs.2021.119527.

192 COLDWELL, K. E. *et al*. Detection of Adriamycin-DNA adducts by accelerator mass spectrometry at clinically relevant Adriamycin concentrations. **Nucleic Acids Research**, v. 36, n. 16, p. e100, 2008. DOI: 10.1093/nar/gkn439.

193 MICKUVIENE, I.; KIRVELIENE, V.; JUODKA, B. Experimental survey of non-clonogenic viability assays for adherent cells in vitro. **Toxicology in Vitro**, v. 18, n. 5, p. 639–648, 2004. DOI: 10.1016/j.tiv.2004.02.001.

194 MONTEIRO-RIVIERE, N. A.; INMAN, A. O.; ZHANG, L. W. Limitations and relative utility of screening assays to assess engineered nanoparticle toxicity in a human cell line. **Toxicology and Applied Pharmacology**, v. 234, n. 2, p. 222–235, 2009. DOI: 10.1016/j.taap.2008.09.030.

195 ASSAYS, C. B. *et al*. Detection of apoptosis using the BD annexin V FITC assay on the BD FACSVerse™ System. **BD Biosciences**, v. 8, p. 1–2, 2016.

196 ASLANTÜRK, Ö. S. In vitro cytotoxicity and cell viability assays: principles, advantages, and disadvantages. **Genotoxicity -** a predictable risk to our actual world, p. 1–18, 2018. DOI: 10.5772/intechopen.71923.

197 CARNEIRO, B. A.; EL-DEIRY, W. S. Targeting apoptosis in cancer therapy. **Nature Reviews Clinical Oncology**, v. 17, n. 7, p. 395–417, 2020. DOI: 10.1038/s41571-020-0341-y.

198 FULDA, S. Tumor resistance to apoptosis. **International Journal of Cancer**, v. 124, n. 3, p. 511–515, 2009. DOI: 10.1038/sj.cdd.4402305.

199 ZEMBRUSKI, N. C. L. *et al*. 7-Aminoactinomycin D for apoptosis staining in flow cytometry. **Analytical Biochemistry**, v. 429, n. 1, p. 79–81, 2012. DOI: 10.1016/j.ab.2012.07.005.

200 PULAKKAT, S. *et al*. Surface engineered protein nanoparticles with hyaluronic acid based multilayers for targeted delivery of anticancer agents. **ACS Applied Materials and Interfaces**, v. 8, n. 36, p. 23437–23449, 2016. DOI: 10.1021/acsami.6b04179.

201 ANGIUS, F.; FLORIS, A. Liposomes and MTT cell viability assay: an incompatible affair. **Toxicology in Vitro**, v. 29, n. 2, p. 314–319, 2015. DOI: 10.1016/j.tiv.2014.11.009.

202 STEPANENKO, A. A.; DMITRENKO, V. V. Pitfalls of the MTT assay: direct and off-target effects of inhibitors can result in over/underestimation of cell viability. **Gene**, v. 574, n. 2, p. 193–203, 2015. DOI: 10.1016/j.gene.2015.08.009.

203 PARK, M. V. D. Z. *et al*. The status of in vitro toxicity studies in the risk assessment of nanomaterials. **Nanomedicine**, v. 4, n. 6, p. 669–685, 2009. DOI: 10.2217/nnm.09.40.

204 WANG, S.; YU, H.; WICKLIFFE, J. K. Limitation of the MTT and XTT assays for measuring cell viability due to superoxide formation induced by nano-scale TiO 2. **Toxicology in Vitro**, v. 25, n. 8, p. 2147–2151, 2011. DOI: 10.1016/j.tiv.2011.07.007.

205 WÖRLE-KNIRSCH, J. M.; PULSKAMP, K.; KRUG, H. F. Oops they did it again! carbon nanotubes hoax scientists in viability assays. **Nano Letters**, v. 6, n. 6, p. 1261–1268, 2006. DOI: 10.1021/nl060177c

206 FISICHELLA, M. *et al*. Mesoporous silica nanoparticles enhance MTT formazan exocytosis in HeLa cells and astrocytes. **Toxicology in Vitro**, v. 23, n. 4, p. 697–703, 2009. DOI: 10.1016/j.tiv.2009.02.007.

207 BELYANSKAYA, L. *et al*. The reliability and limits of the MTT reduction assay for carbon nanotubes-cell interaction. **Carbon**, v. 45, n. 13, p. 2643–2648, 2007. DOI: 10.1016/j.carbon.2007.08.010.

208 HOLDER, A. L. *et al*. Particle-induced artifacts in the MTT and LDH viability assays. **Chemical Research in Toxicology**, v. 25, n. 9, p. 1885–1892, 2012. DOI: 10.1021/tx3001708

209 GORMLEY, A. J.; GHANDEHARI, H. Evaluation of Toxicity of nanostructures in biological systems. *In*: SAHU, S. C.; CASCIANO, D. A. (ed.). **Nanotoxicity**: from in vivo and in vitro models to health risks. Hoboken: John Wiley, 2009. DOI: 10.1002/9780470747803.ch7.

210 KROLL, A. *et al*. Interference of engineered nanoparticles with in vitro toxicity assays. **Archives of Toxicology**, v. 86, n. 7, p. 1123–1136, 2012. DOI: 10.1007/s00204-012-0837-z.

211 DANIELI, P. P.; RONCHI, B.; ROSSI, C. Assessing the in vitro viability of bovine peripheral blood mononuclear cells (PBMCs): a comparison between the MTT (or XTT) and Trypan Blue Exclusion (TBE) test. **Acta Naturalis Scientia**, v. 1, n. 2, p. 58–61, 2014.

212 MADESH, M.; BALASUBRAMANIAN, K. A. Microtiter plate assay for superoxide dismutase using MTT reduction by superoxide. **Indian Journal of Biochemistry and Biophysics**, v. 35, n. 3, p. 184–188, 1998.

213 SOEIRO, V. C. *et al*. Dextran: influence of molecular weight in antioxidant properties and immunomodulatory potential. **International Journal of Molecular Sciences**, v. 17, n. 8, p. 1–15, 2016. DOI: 10.3390/ijms17081340.

214 MOHAMMADI, M. R. *et al*. PEG/Dextran double layer influences Fe ion release and colloidal stability of iron oxide nanoparticles. **Scientific Reports**, v. 8, n. 1, p. 1–11, 2018. DOI: 10.1038/s41598-018-22644-8.

215 YU, M. *et al*. Dextran and polymer polyethylene glycol (PEG) coating reduce both 5 and 30 nm iron oxide nanoparticle cytotoxicity in 2D and 3D cell culture. **International Journal of Molecular Sciences**, v. 13, n. 5, p. 5554–5570, 2012. DOI: 10.3390/ijms13055554

216 FADEEL, B.; KAGAN, V. E. Apoptosis and macrophage clearance of neutrophils: Regulation by reactive oxygen species. **Redox Report**, v. 8, n. 3, p. 143–150, 2003. DOI: 10.1179/135100003225001511.

217 KAREN LIN, K.-Y.; SIRIN, O.; GOODELL, M. Hematopoietic progenitor cells. **Gene and Cell Therapy**, v. 322, p. 1861–1866, 2008. DOI: 10.1038/s41576-020-00298-5.

218 ÇELIK, H. et al. Highly multiplexed proteomic assessment of human bone marrow in acute myeloid leukemia. **Blood Advances**, v. 4, n. 2, p. 367–379, 2020. DOI: 10.1182/bloodadvances.2019001124.

219 RAYAHIN, J. E. *et al*. High and low molecular weight hyaluronic acid differentially influence macrophage activation. **ACS Biomaterials Science and Engineering**, v. 1, n. 7, p. 481–493, 2015. DOI: 10.1021/acsbiomaterials.5b00181.

220 RODRIGO, O. J. *et al.* Effects of CCL2/CCR2 blockade in acute myeloid leukemia. **Blood**, v. 126, n. 23, p. 1348, 2015. DOI: 10.1182/blood.V126.23.1348.1348.

221 PIETSCH, E. C. *et al*. Anti-leukemic activity and tolerability of anti-human CD47 monoclonal antibodies. **Blood Cancer Journal**, v. 7, n. 2, 2017. DOI: 10.1038/bcj.2017.7.

222 YANG, L. *et al.* Development a hyaluronic acid ion-pairing liposomal nanoparticle for enhancing anti-glioma efficacy by modulating glioma microenvironment. **Drug Delivery**, v. 25, n. 1, p. 388–397, 2018. DOI: 10.1080/10717544.2018.1431979.

223 ALMALIK, A. *et al*. Hyaluronic acid (HA) presentation as a tool to modulate and control

the receptor-mediated uptake of HA-coated nanoparticleHyaluronic acid (HA) presentation as a tool to modulate and control the receptor-mediated uptake of HA-coated nanoparticless. **Biomaterials**, v. 34, n. 21, p. 5369–5380, 2013. DOI: 10.1016/j.biomaterials.2013.03.065.

224 FARAJZADEH, R. *et al*. Macrophage repolarization using CD44-targeting hyaluronic acid–polylactide nanoparticles containing curcumin. **Artificial Cells, Nanomedicine and Biotechnology**, v. 46, n. 8, p. 2013–2021, 2018. DOI: 10.1080/21691401.2017.1408116.

225 TRAN, T. H. *et al*. Modulation of macrophage functional polarity towards anti-inflammatory phenotype with plasmid DNA delivery in CD44 targeting hyaluronic acid nanoparticles. **Scientific Reports**, v. 5, p. 1–15, 2015. DOI: 10.1038/srep16632.

226 PARAYATH, N. N.; PARIKH, A.; AMIJI, M. M. Repolarization of tumor-associated macrophages in a genetically engineered nonsmall cell lung cancer model by intraperitoneal administration of hyaluronic acid-based nanoparticles encapsulating MicroRNA-125b. **Nano Letters**, v. 18, n. 6, p. 3571–3579, 2018. DOI: 10.1021/acs.nanolett.8b00689.

227 SANEJA, A. *et al*. Development and mechanistic insight into enhanced cytotoxic potential of hyaluronic acid conjugated nanoparticles in CD44 overexpressing cancer cells. **European Journal of Pharmaceutical Sciences**, v. 97, p. 79–91, 2017. DOI: 10.1016/j.ejps.2016.10.028.

228 SONG, J. M. *et al.* A simple method for hyaluronic acid quantification in culture broth. **Carbohydrate Polymers**, v. 78, n. 3, p. 633–634, 2009. DOI: 10.1016/j.carbpol.2009.04.033.

229 GATTA, A. *et al*. A complete hyaluronan hydrodynamic characterization using a size exclusion chromatography – triple detector array system during in vitro enzymatic degradation. **Analytical Biochemistry**, v. 404, n. 1, p. 21–29, 2010. DOI: 10.1016/j.ab.2010.04.014.

230 PRADHAN, R. *et al*. Hyaluronic acid-decorated poly(lactic-co-glycolic acid) nanoparticles for combined delivery of docetaxel and tanespimycin. **Carbohydrate Polymers**, v. 123, p. 313–323, 2015. DOI: 10.1016/j.carbpol.2015.01.064.

231 ALEX, A. A. *et al*. Arsenic trioxide enhances the NK cell cytotoxicity against acute promyelocytic leukemia while simultaneously inhibiting its Bio-genesis. **Frontiers in Immunology**, v. 9, p. 1–13, 2018. DOI: 10.3389/fimmu.2018.01357.

232 CHENDAMARAI, E. *et al.* Comparison of newly diagnosed and relapsed patients with acute promyelocytic leukemia treated with arsenic trioxide: insight into mechanisms of resistance. **PLoS ONE**, v. 10, n. 3, p. 1–15, 2015. DOI: 10.1371/journal.pone.0121912.

233 MURRAY, P. J. *et al.* Macrophage activation and polarization: nomenclature and experimental guidelines. **Immunity**, v. 41, n. 1, p. 14–20, 2014. DOI: 10.1016/j.immuni.2014.06.008.

234 WANG, L. *et al*. M2b macrophage polarization and its roles in diseases. **Journal of Leukocyte Biology**, v. 106, n. 2, p. 345–358, 2019. DOI: 10.1002/JLB.3RU1018-378RR.

235 LI, Y. P. *et al.* PEGylated PLGA nanoparticles as protein carriers: Synthesis, preparation and biodistribution in rats. **Journal of Controlled Release**, v. 71, n. 2, p. 203–211, 2001. DOI: 10.1016/s0168-3659(01)00218-8.

236 SONG, M. *et al*. Bioconjugated manganese dioxide nanoparticles enhance chemotherapy response by priming tumor-Associated macrophages toward m1-like phenotype and attenuating tumor hypoxia. **ACS Nano**, v. 10, n. 1, p. 633–647, 2016. DOI: 10.1021/acsnano.5b06779.

237 QHATTAL, H. S. S.; LIU, X. Characterization of CD44-mediated cancer cell uptake and intracellular distribution of hyaluronan-grafted liposomes. **Molecular Pharmaceutics**, v. 8, n. 4, p. 1233–1246, 2011. DOI: 10.1021/mp2000428.

238 YOUM, I. *et al*. Uptake and cytotoxicity of docetaxel-loaded hyaluronic acid-grafted oily core nanocapsules in MDA-MB 231 cancer cells. **Pharmaceutical Research**, v. 31, n. 9, p. 2439–2452, 2014. DOI: 10.1007/s11095-014-1339-x.

239 MALDONADO-BÁEZ, L. *et al*. Microtubule-dependent endosomal sorting of clathrin-independent cargo by Hook1. **Journal of Cell Biology**, v. 201, n. 2, p. 233–247, 2013. DOI: 10.1083/jcb.201208172.

240 FU, Y. *et al*. Hypoxia-responsive hyaluronic acid nanogels with improved endo/lysosomal escape ability for tumor-targeted cytochrome c delivery. **European Polymer Journal**, v. 173, 2022. DOI: 10.1016/j.eurpolymj.2022.111259.

241 ANTONIO, L. C. *et al*. The amount of dextran in PLGA nanocarriers modulates protein corona and promotes cell membrane damage. **Journal of Materials Chemistry B**, v. 10, n. 40, p. 8282–8294, 2022. DOI: 10.1039/D2TB01296K.

242 DOSHI, N. *et al.* Cell-based drug delivery devices using phagocytosis-resistant backpacks. **Advanced Materials**, v. 23, n. 12, p. H105-H109, 2011. DOI: 10.1002/adma.201004074.

243 KRAUSS, A. C. *et al*. FDA approval summary: (daunorubicin and cytarabine) liposome for injection for the treatment of adults with high-risk acute myeloid leukemia. **Clinical Cancer Research**, v. 25, n. 9, p. 2685–2690, 2019. DOI: 10.1158/1078-0432.ccr-18-2990.

APPENDICES

Appendix A - Supporting Information: the amount of Dextran in PLGA nanocarriers modulates protein corona and promotes cell membrane damage

Characterization of the PLGA-DOX, Dex1/PLGA-DOX and Dex5/PLGA NCs by Fourier transform infrared spectroscopy (FTIR)

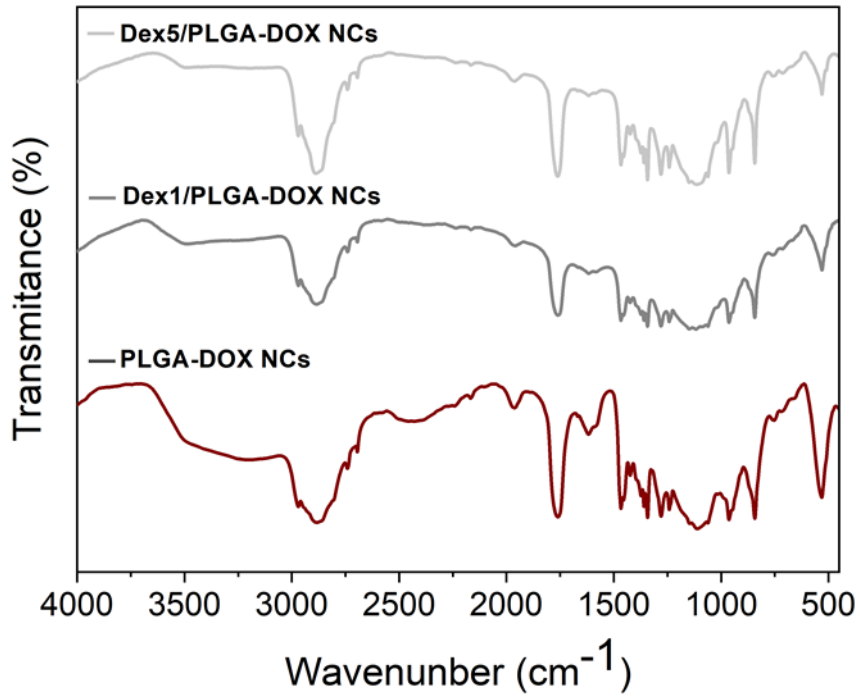

Figure S 1 - Infrared spectra of PLGA-DOX, Dex1/PLGA-DOX and Dex5/PLGA NCs obtained by FTIR. Samples were prepared by drop-casting 20 µl of the samples diluted in *deionized water in silicon wafers* and dried under reduced atmosphere. The spectrum was collected using an Infrared spectrometer Nicolet 6700/GRAMS Suite, with 128 scans per sample with 4 cm^{-1} resolution from 4000 to 400 cm^{-1}.

Source: By the author

Infrared spectra of the NCs were obtained by Fourier transform infrared spectroscopy (FTIR). In all spectra there are a band at 1750 cm^{-1} and less intense bands between 1050 and 1300 cm^{-1} that confirm the formation of ester bonds (O-C-O). The strong band at 2850 cm^{-1} corresponds to alkane aldehyde stretching, which is present in the chemical structure of PLGA. The 3410 cm^{-1} band presented in the FTIR spectrum of the NCs corresponds to the stretching vibration of O-H bonds.

DOX calibration curve

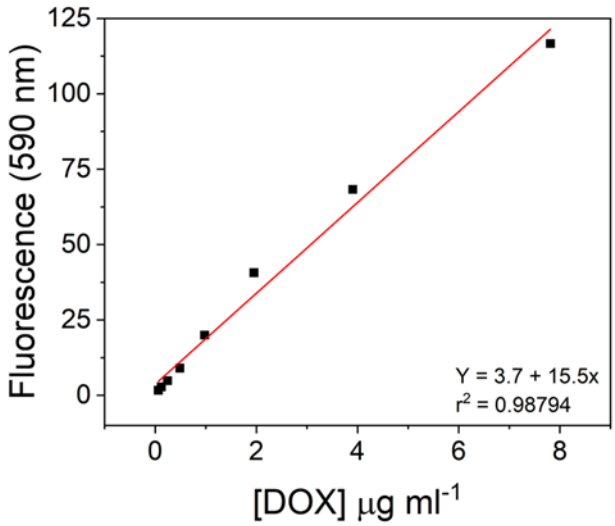

Figure S 2 - Calibration curve of DOX in ddH_2O (ex: 480 nm; ems: 590 nm). The linear regression equation was used to calculate the amount of DOX released from the NCs in the cumulative release studies.

Source: By the author

The calibration curve of DOX in Fig. S2 was employed to determine the concentration of DOX in the samples collect for the characterization of the drug released from the nanocarriers, where Y is fluorescence and x the concentration of DOX in µg ml^{-1}.

Cell viability after 24 h of incubation with the NCs

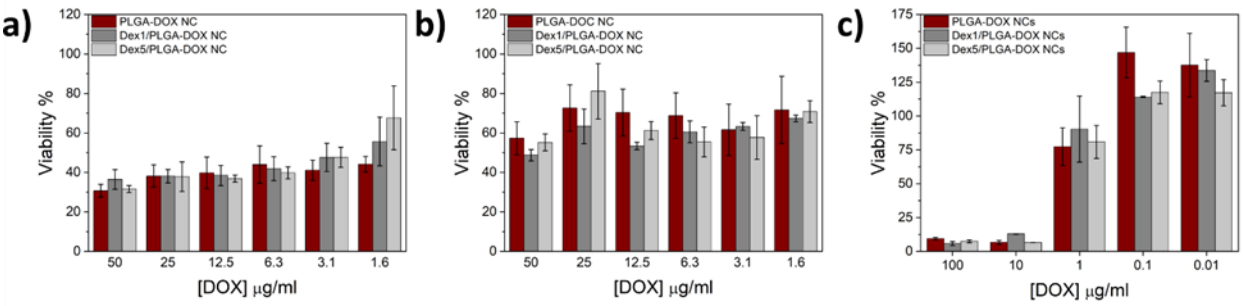

Figure S 3 - Evaluation of cellular viability by MTT assay for nanocarriers prepared in the presence and absence of dextran 40. Viability of a) MCF-7, b) H9C2 and c) RAW 264.7 incubated for 24 h at 37 °C with PLGA-DOX, Dex1/PLGA-DOX and Dex5/PLGA NCs. Statistical analysis was performed using ANOVA with Tukey's post-hoc test. Values represented are mean±SD (n=4).

Source: By the author

NCs prepared with and without dextran equally affect cell viability of the three cell lines after 24 h of incubation in all DOX concentrations tested. For RAW 264.7 cells, it is possible

to observe a dose-dependence response, which is in accordance with DOX mechanism of toxicity in this cell line.[1-2]

Gate strategy for *in vitro* cellular uptake studies

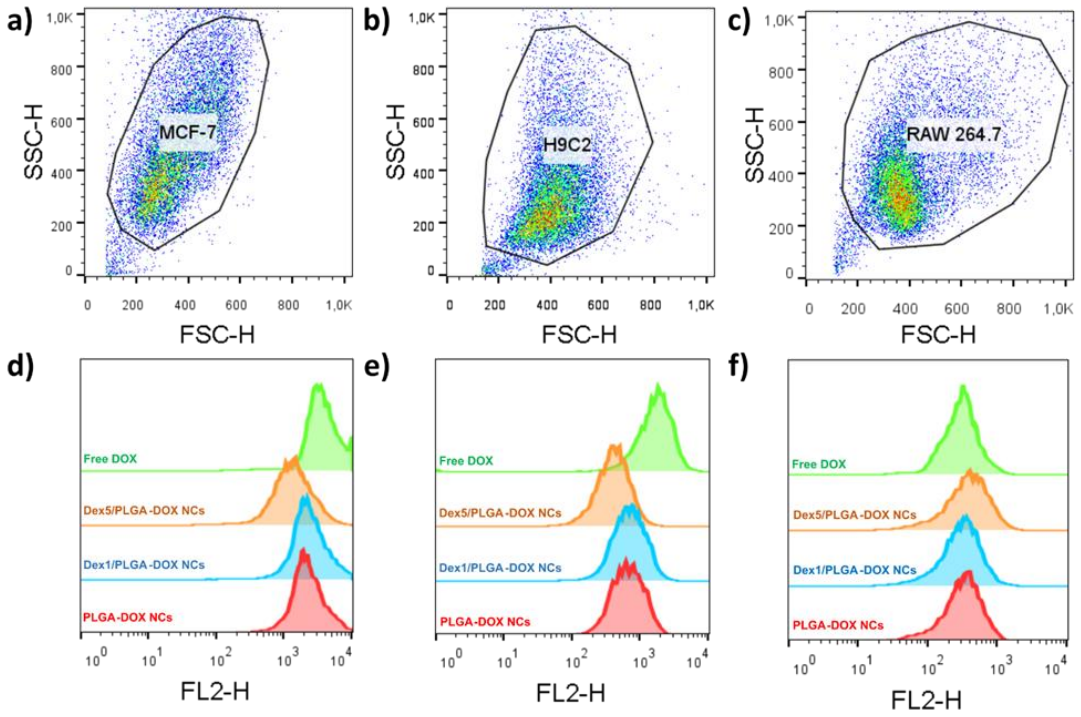

Figure S 4 - In vitro cellular uptake of PLGA-DOX, Dex1/PLGA-DOX and Dex5/PLGA NCs by flow cytometry analysis. Gating strategy for a) MCF-7, b) H9C2 and c) RAW264.7. Representative histograms of flow cytometry of d) MCF-7 and e) H9C2 incubated for 4 h at 37 °C with DOX, PLGA-DOX, Dex1/PLGA-DOX and Dex5/PLGA NCs and f) RAW 264.7 incubated for 2 h at 37 °C with DOX, PLGA-DOX, Dex1/PLGA-DOX and Dex5/PLGA NCs. Excitation was measured using FL2 (590/30) and data analysis were performed using FlowJo v10 Software.

Source: By the author

NCs uptake by RAW 264.7 after 4 h of incubation and inhibition studies

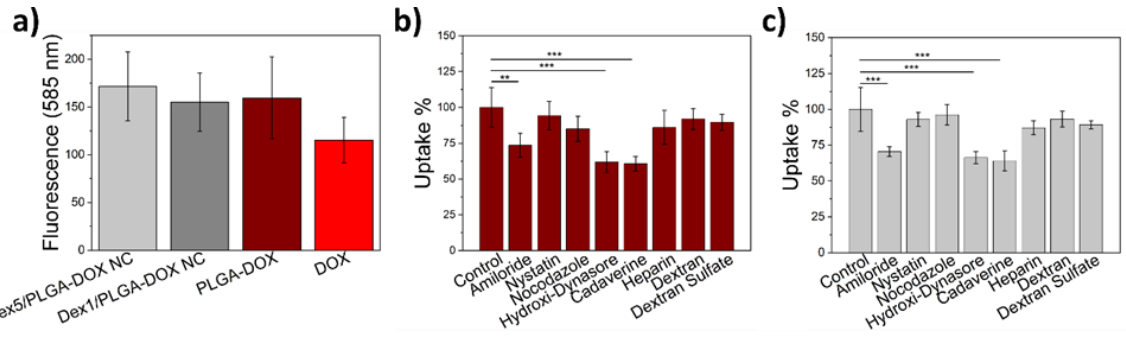

Figure S 5 - In vitro cellular uptake of PLGA-DOX, Dex1/PLGA-DOX and Dex5/PLGA NCs by flow cytometry analysis. Comparison of cell fluorescence of a) RAW 264.7 incubated for 4 h at 37 °C with DOX, PLGA-DOX, Dex1/PLGA-DOX and Dex5/PLGA NCs. Inhibition studies to evaluate the mechanism involved in the uptake of b) PLGA-DOX and c) Dex5/PLGA NCs by MCF-7. The cells were incubated for 30 minutes with amiloride, nystatin, nocodazole, hydroxi-dynasore, cadaverine, heparin, dextran and dextran sulfate (100 µg ml^{-1}, 40 µg ml^{-1}, 10 µg ml^{-1}, 100 µmol l^{-1}, 100 µmol l^{-1}, 10 units ml^{-1}, 2 mg ml^{-1} and 5 µg ml^{-1}, respectively) prior exposure to the NCs. DOX dosage was 12.5 µg ml^{-1} for all analysis. Statistical analysis was performed using ANOVA with Tukey's post hoc test. Values represented are mean ± SD (n=3/4).

Source: By the author

Gate strategy for in vitro annexin V binding assay

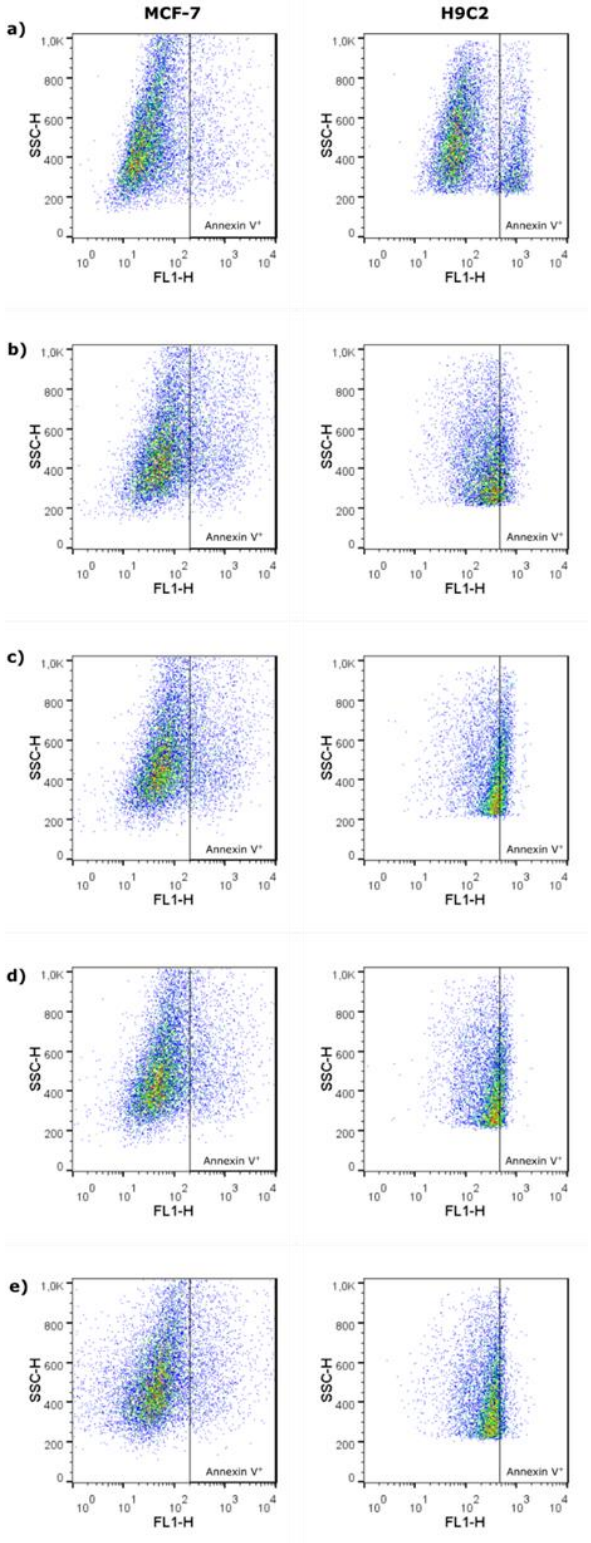

Figure S 6 - In vitro evaluation of cellular viability by annexin V binding assay. Gating strategy for a) live cells control and cells incubated for 24 h at 37 °C with b) Dex5/PLGA NCs, c) Dex1/PLGA-DOX, d) PLGA-DOX and e) DOX. Excitation was measured using FL1 (530/30) and data analysis were performed using FlowJo v10 Software.

Source: By the author

Raw image of SDS-PAGE gel of the proteins recovered from protein corona

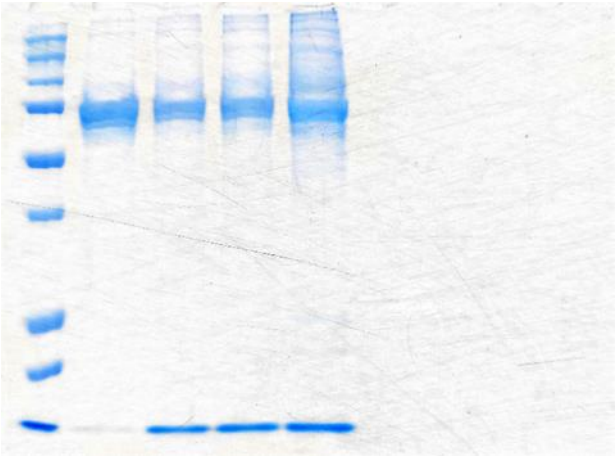

Figure S 7 - Raw image for SDS-PAGE gel image in Fig. 2h of the proteins recovered from protein corona formed on PLGA-DOX, Dex1/PLGA-DOX and Dex5/PLGA-DOX NCs.

Source: By the author

NMR spectrum of PLGA-DOX, Dex1/PLGA-DOX and Dex5/PLGA-DOX NCs

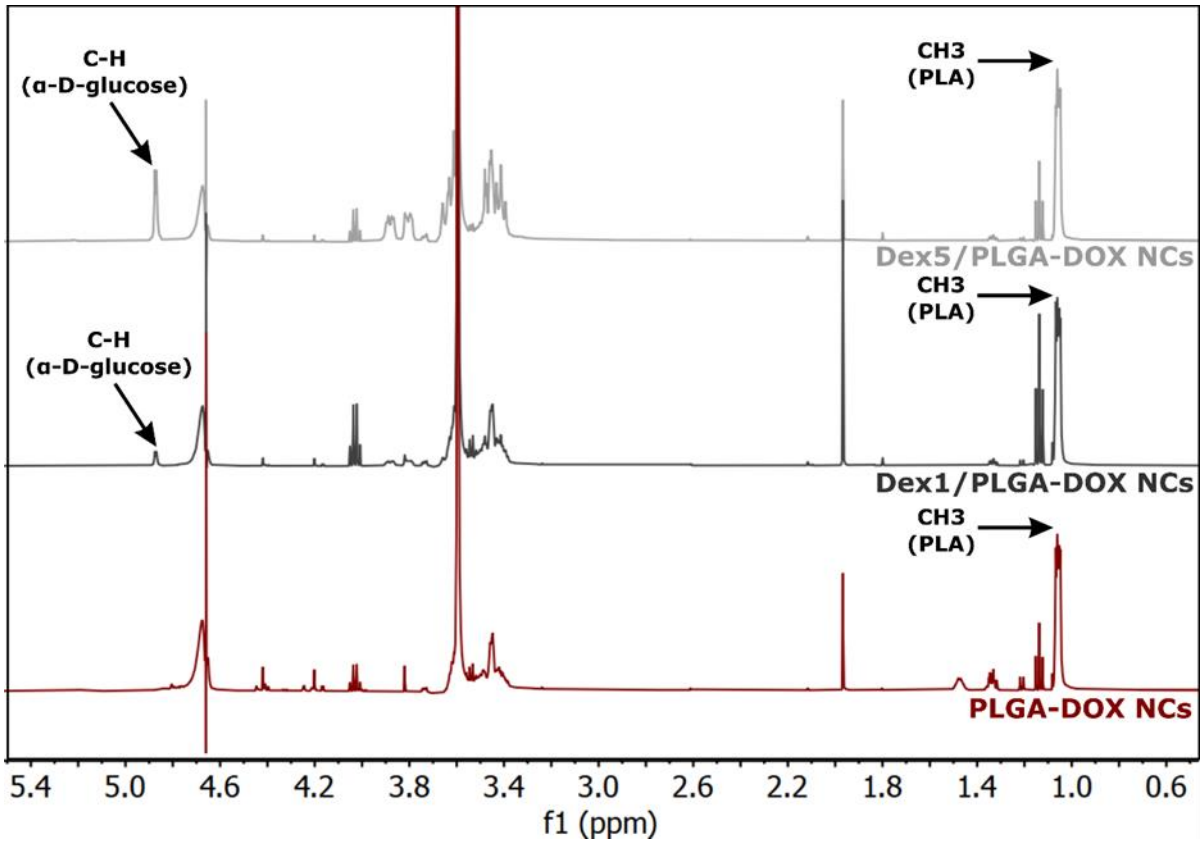

Figure S 8 - NMR spectra of PLGA-DOX, Dex1/PLGA-DOX and Dex5/PLGA-DOX NCs The ^{1}H-NMR spectra of PLGA-DOX, Dex1/LGA-DOX and Dex5/PLGA-DOX NCs show peaks at δ 1.20 ppm, assigned to the methyl groups of lactic acid monomers, and δ 4.88 ppm, corresponding to CH of (1→6)-α-D-glucose monomers of dextran molecule. The molar ration of (1→6)-α-D-glucose monomers and

PLA monomers calculated by equation 1 was 8,2 and 1,7 % for Dex5/PLGA-DOX and PLGA-DOX NCs, respectively.

Source: By the author

REFERENCES

1 HASSAN, F. *et al*. Lipopolysaccharide prevents doxorubicin-induced apoptosis in RAW 264.7 macrophage cells by inhibiting p53 activation. **Molecular Cancer Research**, v. 3, n. 7, p. 373–379, 2005.

2 LIAO, Z. S. *et al*. Self-assembled pH-responsive polymeric micelles for highly efficient, noncytotoxic delivery of doxorubicin chemotherapy to inhibit macrophage activation: in vitro investigation. **Biomacromolecules**, v. 19, n. 7, p. 2772–2781, 2018.

Appendix B - Supporting Information: pro-leukemic macrophage-based delivery of nanotherapeutics to acute myeloid leukemia

Characterization of the PLGA-PEG-NH_2 copolymer

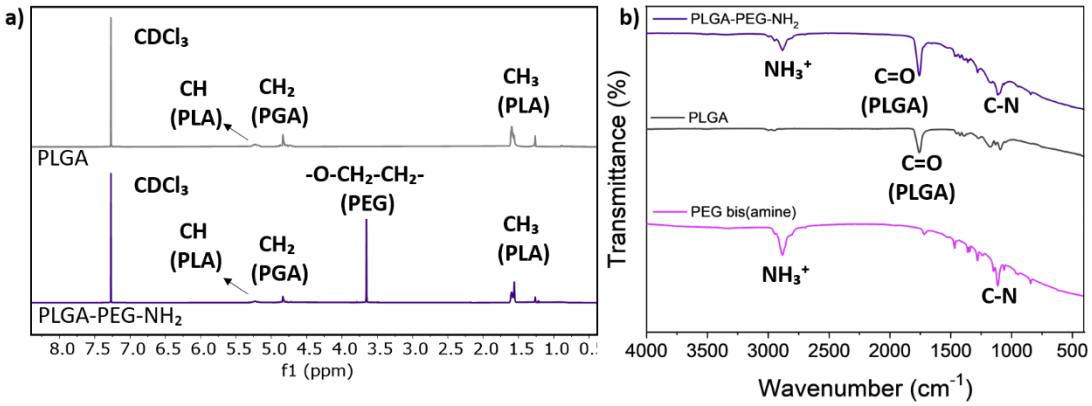

Figure S1 - a) 1H-NMR spectra (400 MHz) of PLGA and PLGA-PEG-NH2 collected using an Agilent nuclear magnetic resonance spectrometer Technologies, model 400/54 premium shielded. The samples were prepared by adding 15 mg of copolymer in 750 µl deuterated chloroform, CDCl3. a) FTIR spectra of PLGA, diamino-PEG and PLGA-PEG-NH2. Samples were prepared by drop-casting 20 µl of the samples diluted in *deionized water in silicon wafers* and dried under reduced atmosphere. The spectrum was collected using an Infrared spectrometer Nicolet 6700/GRAMS Suite, with 128 scans per sample with 4 cm^{-1} resolution from 4000 to 400 cm^{-1}.
Source: By the author

The ^{1}H-NMR spectra of PLGA and PLGA-PEG-NH_2 copolymers show peaks between δ 1.20 – 1.60 ppm assigned to the methyl groups of lactic acid monomers. The multiplets between δ 5.10 – 5.30 and δ 4.75 – 4.85 ppm correspond to CH groups of lactic acid monomers and CH_2 groups of glycolic acid monomers, respectively. In the spectrum of the PLGA-PEG-NH_2 copolymer there is a peak at δ 3.66 ppm corresponding to the –O-CH_2-CH_2- group of PEG. The FTIR spectra of PLGA and PLGA-PEG-NH_2 copolymers show a band at 1758 cm^{-1} corresponding to C=O stretch, present in PLGA monomers. The spectra of PEG bis(amino) and PLGA-PEG-NH_2 it is possible to observe bands at 2884 cm–1 and 1279 cm–1 that correspond, respectively, to NH_3^+ and to C-N stretching. Together, FTIR and ^{1}H-NMR spectra confirm PLGA-PEG-NH_2 copolymer synthesis.

The synthesis yield was calculated through the ratio between the real yield and the theoretical yield and the value obtained was 67 ± 21% (mean ± standard deviation of 3 syntheses).

Characterization of the NCs loaded with rhodamine B

Table 1 - Characterization of rhodamine B-loaded (PLGA)COOH, (PLGA)PEG, and (PLGA)PEG-HA nanocarriers. NTA size (diameter), Z-average (PdI), ζ-potential and particle yield (number of NCs per ml). Statistical analysis was performed using ANOVA with Tukey's post hoc test. Values represented are mean ± SD of independent syntheses (n=3).

	NTA size (nm)	Z-average (nm) (PdI)	Zeta potencial (mV)	Particle yeld (10^{12} NCs/ml)
(PLGA)COOH NCs	156 ± 51	144 ± 55 (0.06)	-29 ± 5	12.4 ± 1.2
(PLGA)PEG-NH2	128 ± 48	230 ± 35 (0.12)	-23 ± 1	13.5 ± 0.8
(PLGA)PEG NCs	165 ± 52	250 ± 34 (0.10)	-34 ± 2	11.6 ± 1.9
(PLGA)PEG-HA NCs	171 ± 47	253 ± 37 (0.14)	-34.0 ± 0.3	1.14 ± 0.09

Source: By the author

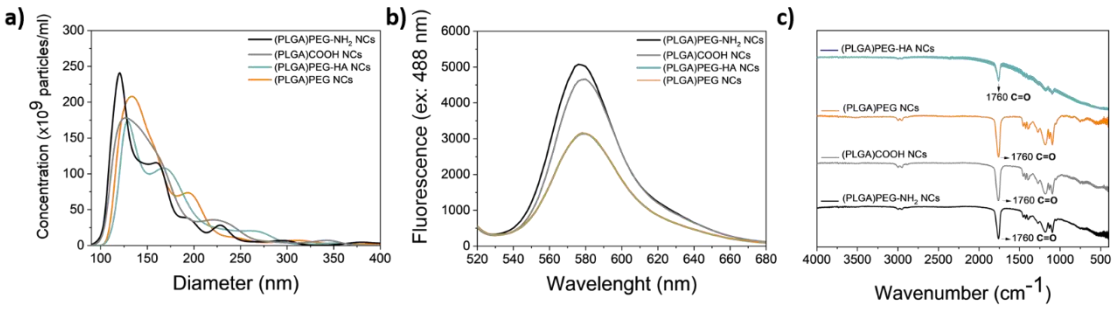

Figure S2 - Characterization of the (PLGA)PEG, (PLGA)COOH, (PLGA)PEG, (PLGA)PEG-HA NCs loaded with RhB. a) NTA size distribution of (PLGA)PEG-NH_2 NCs, (PLGA)COOH NCs, (PLGA)PEG NCs and (PLGA)PEG-HA NCs. b) Fluorescence spectrum of (PLGA)PEG-NH_2, (PLGA)COOH, (PLGA)PEG, (PLGA)PEG-HA NCs loaded with rhodamine B (excitation: 488 nm). C) Infrared spectra of (PLGA)PEG-NH_2, (PLGA)COOH, (PLGA)PEG, (PLGA)PEG-HA NCs obtained by FTIR. Samples were prepared by drop-casting 20 µl of the samples diluted in *deionized water in silicon wafers* and dried under reduced atmosphere. The spectrum was collected using an Infrared spectrometer Nicolet 6700/GRAMS Suite, with 128 scans per sample with 4 cm^{-1} resolution from 4000 to 400 cm^{-1}.

Source: By the author

Also, the mass of HA bounded to the surface of the (PLGA)PEG-AH NCs loaded with rhodamine B was determined by the CTAB turbidimetric method, which indicated 2.3 ± 0.6 mg (mean ± SD, n=3) of HA conjugated to the surface of NCs, conjugation efficiency equal to 46 ± 13 %.

Characterization of the (PLGA)PEG-NH_2 NCs loaded with arsenic trioxide

Table 2 - Characterization of ATO-loaded (PLGA)PEG-NH_2 NCs nanocarriers. NTA size (diameter), Z-average (PdI), ζ-potential and particle yield (number of NCs per ml), and ATO concentration of the NCs.

	NTA size (nm) (D90)	**Z-average (nm) (PdI)**	**Zeta potencial (mV)**	**Concentration (10^{12} NCs/ml)**	**EE (%)**
(PLGA)PEG-NH_2 NCs	200 ± 70 (252 ± 57)	169 ± 21 (0.12)	3.6 ± 1.3	7.5 ± 3.3	2.9 ± 0,3

Source: By the author

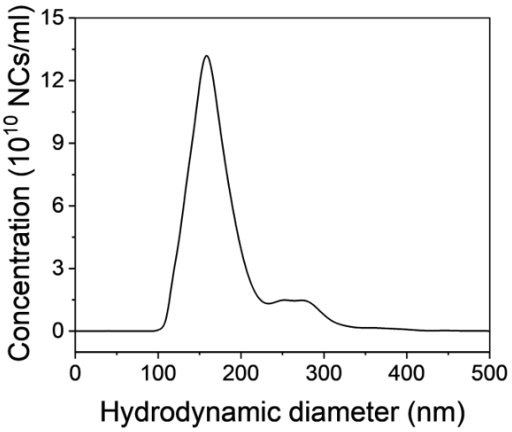

Figure S3 - NTA size distribution of (PLGA)PEG-NH_2 NCs loaded with arsenic trioxide.

Source: By the author

1H-NMR of the NCs loaded with ATO

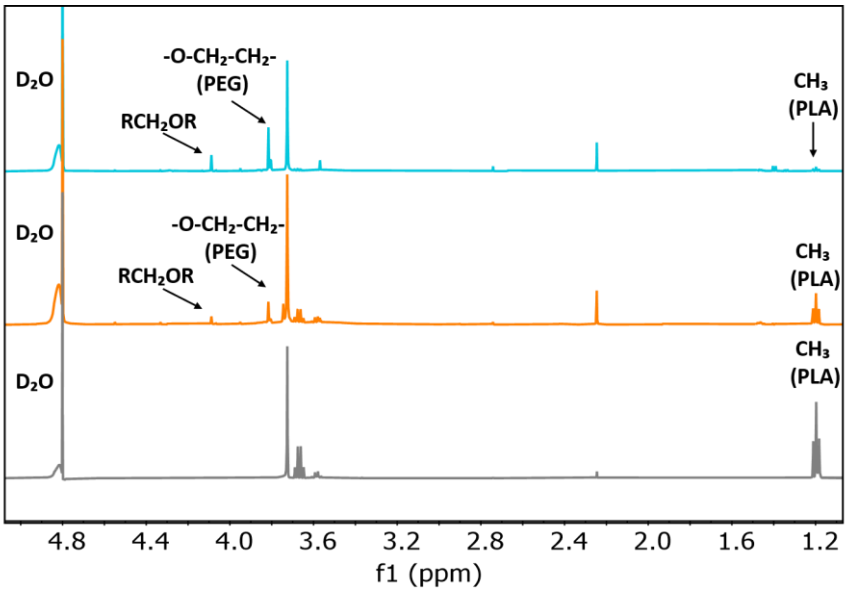

Figure S4 - 1H-NMR spectra (400 MHz) of (PLGA)PEG-HA, (PLGA)PEG and (PLGA)COOH NCs collected using an Agilent nuclear magnetic resonance spectrometer Technologies, model 400/54 premium shielded. The samples were prepared by adding 5 mg of freeze dried NCs in 750 µl deuterated water, D_2O.

Source: By the author

The ^{1}H-NMR spectra of (PLGA)-PEG-HA, (PLGA)PEG and (PLGA)COOH NCs show peaks between δ 1.20 – 1.40 ppm assigned to the methyl groups of lactic acid monomers. In the spectrum of (PLGA)-PEG-HA and (PLGA)PEG NCs there is a peak at δ 3.66 ppm corresponding to the –O-CH_2-CH_2- group of PEG and as amide peak between δ 4.0 – 4.2 ppm that confirms the conjugation of hyaluronic acid or polyethylene glycol carboxylic acid terminated to (PLGA)PEH-NH_2 NCs.

HA calibration curve obtained using the CTAB turbidimetric method

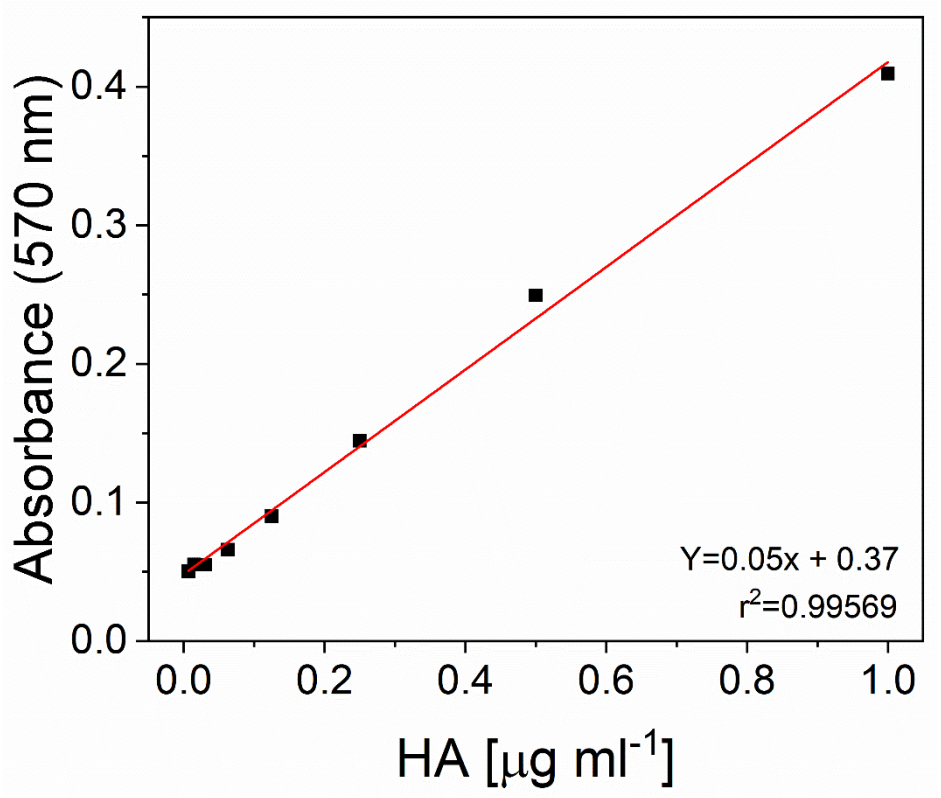

Figure S5 - Calibration curve of HA (0.005 – 1 μg ml⁻¹) in ddH₂O obtained using the turbidimetric method of hexadecyltrimethylammonium bromide (CTAB). The linear regression equation was used to calculate the amount of HA on the surface of the NCs.
Source: By the author

The calibration curve of HA in Fig. S5 was employed to determine the mass of conjugated HA on the surface of the NCs, where Y is absorbance and x the concentration of HA in μg ml^{-1}. The mass of HA conjugated to the surface of the NCs was estimated by subtracting the amount present in the supernatant from the initial amount of HA used in the conjugation reaction.

Uptake and adhesion kinetics of nanocarriers loaded with rhodamine B

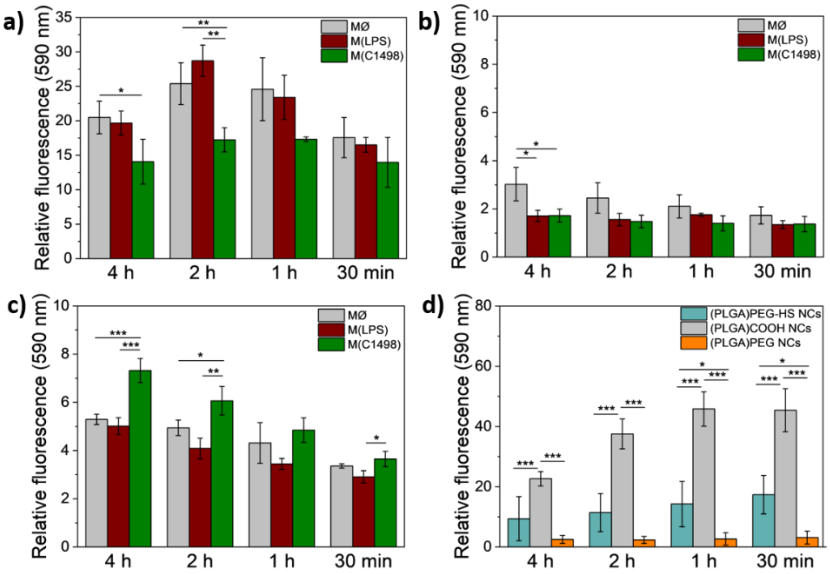

Figure S6 - *In vitro* cellular uptake and adhesion kinetics studies of (PLGA)COOH, e) (PLGA)PEG and f) (PLGA)PEG-HA NCs by RAW 264.7 macrophages and C1498 cells via flow cytometry. Cell fluorescence of a) MØ, b) M(LPS) and c) M(C1498) RAW 264.7 macrophages and d) C1498 cells exposed for 2h to (PLGA)COOH, (PLGA)PEG and (PLGA)PEG-HA NCs. Values represented are mean ± SD (n=4). *p-value < 0.05, ** p-value < 0.01, *** p-value < 0.001.

Source: By the author

Adhesion/interaction rate nanocarriers loaded with rhodamine B

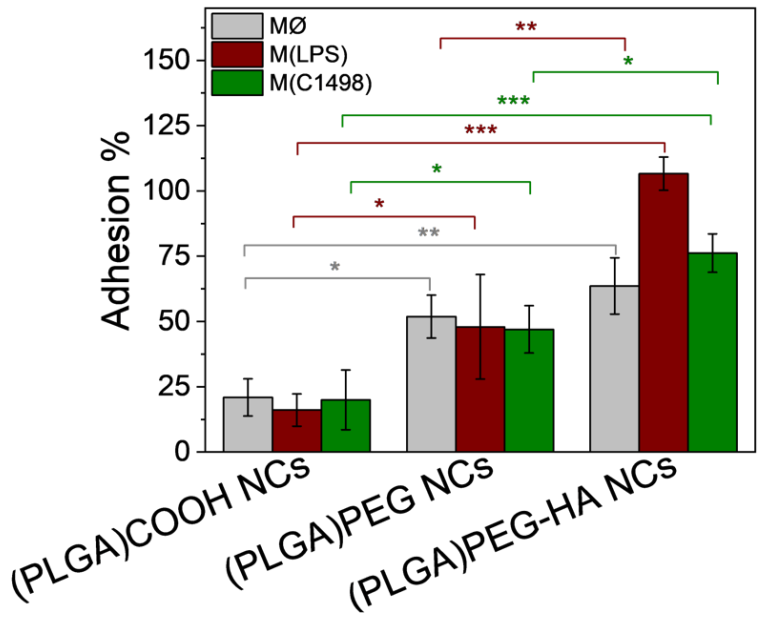

Figure S7 - *In vitro* cellular adhesion/interaction rate of (PLGA)COOH, e) (PLGA)PEG and f) (PLGA)PEG-HA NCs by RAW 264.7 macrophages and C1498 cells. Percentage was calculated by $A/I\% = \frac{FLU_{4\,°C}}{Flu_{37\,°C}} \times 100$ equation. Values represented are mean ± SD (n=4). *p-value < 0.05, ** p-value < 0.01, *** p-value < 0.001.

Source: By the author

Viability of RAW 264.7 macrophages after exposure to ATO-loaded NCs

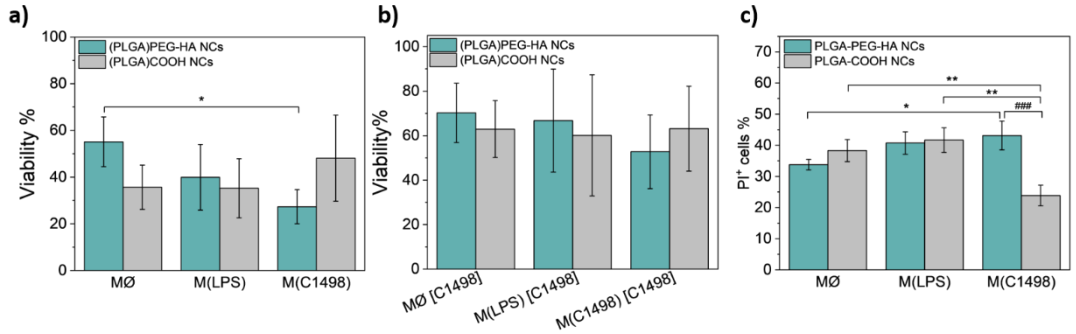

Figure S8 - Evaluation of cellular viability by MTT and PI assay for (PLGA)COOH and (PLGA)PEG-HA NCs. Viability of a) RAW 264.7 macrophages cells monocultures assessed by MTT after incubation with (PLGA)COOH and (PLGA)PEG-HA NCs for 24 h at 37 °C. b) Viability of NC-loaded RAW 264.7 macrophages after 24 h of co-culture with C1498 cells assessed by MTT. Percentage of PI-positive cells (PI^+ %) of c) RAW 264.7 macrophages monocultures exposed to (PLGA)COOH and (PLGA)PEG-HA NCs for 24 h at 37 °C. ATO dosage was the same for all experimental groups (1.2 µg/ml). Statistical analysis comparing between phenotypes was performed using ANOVA with Tukey's post-hoc test and statistical analysis comparing between the NCs was performed using student t-test. Values represented are mean ± SD (n=4). * p-value < 0.05, # p-value < 0.05, ## p-value < 0.01, ### p-value < 0.001,

Source: By the author

Gate strategy for *in vitro* cellular co-culture studies

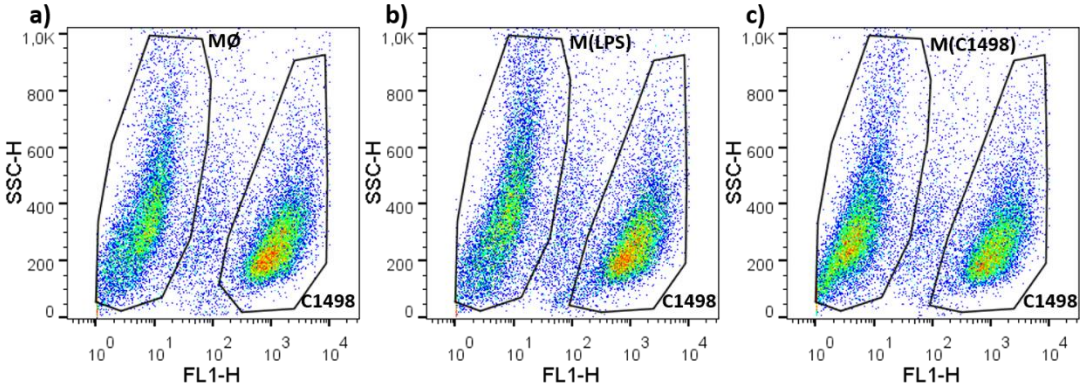

Figure S9 - Gating strategy for a) MØ, b) M(LPS) and c) M(C1498) macrophages co-cultured with C1498 cells stained with CellTracker™ Green. Excitation was measured using FL1 (530/30) and data analysis were performed using FlowJo v10 Software.

Source: By the author

Gate strategy for in vitro PI assay

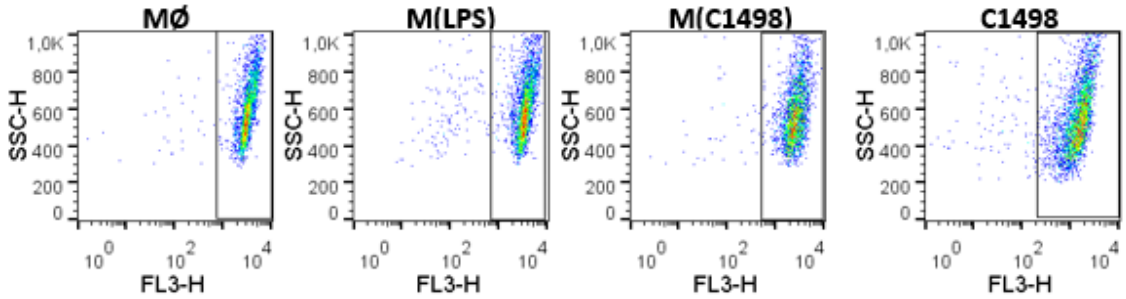

Figure S10 - *In vitro* evaluation of cellular viability by PI assay. Gating strategy for dead cells control. Excitation was measured using FL3 (630/30) and data analysis were performed using FlowJo v10 Software.
Source: By the author